ISSN: 2376-2136 (Print)
ISSN: 2376-2144 (Online)

Trends in Renewable Energy

Volume 9, Issue 2, December 2023

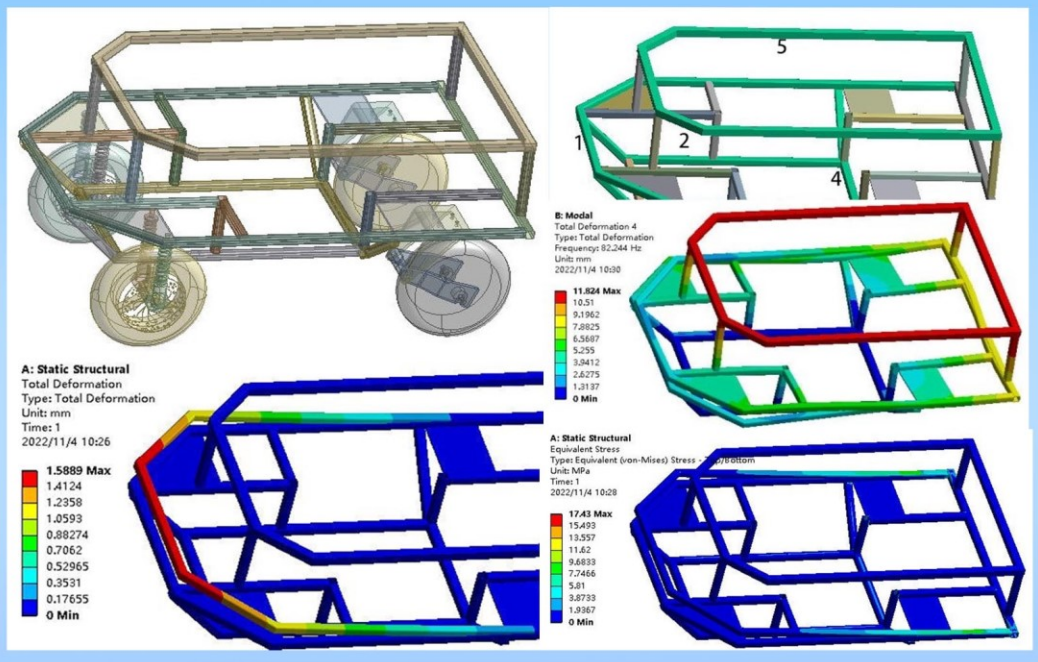

Cover image: Optimized Lightweight Frame for Intelligent New-energy Vehicles, see article by Wu in this issue

ISSN 2376-2136
9 772376 213001 23

futureenergysp.com
thefutureenergy.org

Trends in Renewable Energy

ISSN: 2376-2136 (Print) ISSN: 2376-2144 (Online)

http://futureenergysp.com/

Trends in Renewable Energy is an open accessed, peer-reviewed semi-annual journal publishing reviews and research papers in the field of renewable energy technology and science.

The aim of this journal is to provide a communication platform that is run exclusively by scientists working in the renewable energy field. Scope of the journal covers: Bioenergy, Biofuel, Biomass, Bioprocessing, Biorefinery, Biological waste treatment, Catalysis for energy generation, Energy conservation, Energy delivery, Energy resources, Energy storage, Energy transformation, Environmental impact, Feedstock utilization, Future energy development, Green chemistry, Green energy, Microbial products, Physico-chemical process for Biomass, Policy, Pollution, Renewable energy, Smart grid, Thermo-chemical processes for biomass, etc.

The Trends in Renewable Energy publishes the following article types: peer-reviewed reviews, mini-reviews, technical notes, short-form research papers, and original research papers.

The article processing charge (APC), also known as a publication fee, is fully waived for the Trends in Renewable Energy.

Editorial Team of Trends in Renewable Energy

Dr. Muhammad Mujtaba Asad	Faculty of Technical and Vocational Education, Universiti Tun Hussein Onn Malaysia, Malaysia
Dr. Afzal Sikander	Department of Instrumentation and Control Engineering, Dr. B. R. Ambedkar National Institute of Technology, India
Dr. Padmanabh Thakur	Professor and Head, Department of Electrical Engineering, Graphic Era University, India
Dr. K. DHAYALINI	Professor, Department of Electrical and Electronics Engineering, K. Ramakrishnan College of Engineering, Tamilnadu, India
Shangxian Xie	Texas A&M University, United States
Dr. Tanmoy Dutta	Sandia National Laboratories, United States
Dr. Efstathios Stefos	Pontifical Catholic University of Ecuador, Faculty of Exact and Natural Sciences, School of Physical Sciences and Mathematics, Ecuador
Dr. Xin Wang	Miami University, United States
Dr. Rami El-Emam	Assist. Prof., Faculty of Engineering, Mansoura University, Egypt
Dr. Rameshprabu Ramaraj	School of Renewable Energy, Maejo University, Thailand
Dr. ZAFER ÖMER ÖZDEMİR	Kirklareli University, Technology Faculty, Turkey
Dr. Vijay Yeul	Chandrapur Super Thermal Power Station, India
Dr. Mohanakrishna Gunda	VITO - Flemish Institute for Technological Research, Belgium
Dr. Shuai Tan	Georgia Institute of Technology, United States
Shahabaldin Rezania	Universiti Teknologi Malaysia (UTM), Malaysia
Dr. Madhu Sabnis	Contek Solutions LLC, Texas, United States
Dr. Qiangu Yan	Mississippi State University, United States
Dr. Mustafa Tolga BALTA	Associate Prof., Department of Mechanical Engineering, Faculty of Engineering, Aksaray University, Turkey
Dr. María González Alriols	Associate Prof., Chemical and Environmental Engineering Department, University of the Basque Country, Spain
Dr. Nattaporn Chaiyat	Assist. Prof., School of Renewable Energy, Maejo University, Thailand
Dr. Nguyen Duc Luong	Institute of Environmental Science and Engineering, National University of Civil Engineering, Vietnam
Mohd Lias Bin Kamal	Faculty of Applied Science, Universiti Teknologi MARA, Malaysia
Dr. N.L. Panwar	Assistant Prof., Department of Renewable Energy Engineering, College of Technology and Engineering, Maharana Pratap University of Agriculture and Technology, India
Dr. Caio Fortes	BASF, Brazil
Dr. Flavio Prattico	Department of Methods and Models for Economics, Territory and Finance, Sapienza University of Rome, Italy
Dr. Wennan ZHANG	Docent (Associate Prof.) and Senior Lecturer in Energy Engineering, Mid Sweden University, Sweden
Dr. Ing. Stamatis S. Kalligeros	Associate Prof., Hellenic Naval Academy, Greece
Carlos Rolz	Director of the Biochemical Engineering Center, Research Institute at Universidad del Valle, Guatemala
Ms. Lilias Makashini	Copperbelt University, Zambia
Dr. Ali Mostafaeipour	Associate Prof., Industrial Engineering Department, Yazd University, Iran
Dr. Camila da Silva	Prof., Maringá State University, Brazil
Dr. Anna Skorek-Osikowska	Silesian University of Technology, Poland
Dr. Shek Atiqure Rahman	Sustainable and Renewable Energy Engineering, College of Engineering, University of Sharjah, Bangladesh
Dr. Emad J Elnajjar	Associate Prof., Department of Mechanical Engineering, United Arab Emirates University, United Arab Emirates
Dr. Seyed Soheil Mousavi Ajarostaghi	Babol Noshirvani University of Technology, Babol, Iran
Dr. Dinesh K. Sharma	National Ecology and Environment Foundation, India
Dr. Lakshmana Kumar Ramasamy	Department of Corporate relations, Hindusthan College of Engineering and Technology, India
Dr. S. Venkata Ramana	SUSU/National Research University, Russian Federation
Dr. Priyanka Marathey	Department of Solar Energy, Pandit Deendayal Petroleum University, India
Osamah Siddiqui	University of Ontario Institute of Technology, Canada
Dr. Rupendra Kumar Pachauri	Assistant Prof., Electrical and Electronics Engineering Department, University

	of Petroleum and Energy Studies, India
Dr. Jun Mei	School of Chemistry and Physics, Science and Engineering Faculty, Queensland University of Technology, Australia
Dr. Valeria Di Sarli	Institute for Research on Combustion, National Research Council of Italy, Italy
Dr. Utkucan Şahin	Assistant Prof., Department of Energy Systems Engineering, Faculty of Technology, Muğla Sıtkı Koçman University, Turkey
Dr. ALIASHIM ALBANI	School of Ocean Engineering, Universiti Malaysia Terengganu, Malaysia
Dr. Ashwini Kumar	Assistant Prof., College of Engineering, HSBPVT's Parikrama Group of Institutions, India
Dr. Hasan AYDOGAN	Associate Prof., Mechanical Engineering Department, Selcuk University, Turkey
Dr. Jiekang Wu	Professor, School of Automation, Guangdong University of Technology, China
Dr. Ong Huei Ruey	DRB-HICOM University of Automotive, Malaysia
Dr. Miguel Ángel Reyes Belmonte	IMDEA Energy Institute, Spain
Dr. Chitra Venugopal	Associate Professor in Electrical Engineering, University of Trinidad and Tobago, Trinidad
Dr. Amit Kumar Singh	Assistant Prof., Instrumentation & Control Engineering Department, Dr. B.R.A. National Institute of Technology, India
Dr. Suvanjan Bhattacharyya	University of Pretoria, South Africa
Dr. Karunesh Tiwari	Babu Banarasi Das University, India
Dr. Sharadrao A. Vhanalkar	Karmaveer Hire Arts, Science, Commerce and Education College, India
Dr. Prasenjit Chatterjee	Assistant Prof. and Head, MCKV Institute of Engineering, India
Dr. S. Balamurugan	Mindnotix Technologies, India
Dr. Mohammad Nurunnabi	University of Oxford, United Kingdom
Dr. Kenneth Okedu	Caledonian College of Engineering, Oman
Dr. Cheng Zhang	Sr. Materials Engineer, Medtronic, Inc., United States
Dr. Chandani Sharma	Assistant Prof., Department of Electrical Engineering, Graphic Era University, India
Dr. Kashif Irshad	Assistant Prof., Mechanical Engineering Department, King Khalid University, Saudi Arabia
Dr. Abhijit Bhagavatula	Principal Lead Engineer, Southern Company Services, United States
Dr. S. Sathish	Associate Prof., Department of Mechanical Engineering, Hindustan University, India
Mr. A. Avinash	Assistant Prof., KPR Institute of Engineering & Technology, India
Dr. Bindeshwar Singh	Assistant Prof., Kamla Nehru Institute of Technology, India
Dr. Yashar Hashemi	Tehran Regional Electric Company, Iran
Dr. Navanietha Krishnaraj R	South Dakota School of Mines and Technology, United States
Dr. SANDEEP GUPTA	JECRC University, India
Dr. Shwetank Avikal	Graphic Era Hill University, India
Dr. Xianglin Zhai	Poochon Scientific LLC, United States
Dr. Rui Li	Associate Prof., College of Engineering, China Agricultural University, China
Dr. Adam Elhag Ahmed	National Nutrition Policy Chair, Department of Community Services, College of Applied Medical Sciences, King Saud University, Saudi Arabia
Dr. Jingbo Li	Massachusetts Institute of Technology, United States
Dr. Srikanth Mutnuri	Associate Prof., Department of Biological Sciences, Associate Dean for International Programmes and Collaboration, Birla Institute of Technology & Science, India
Dr. Bashar Malkawi	Global Professor of Practice in Law, James E. Rogers College of Law, University of Arizona, United States
Dr. Simona Silvia Merola	Istituto Motori - National Research Council of Naples, Italy
Dr. Hakan Caliskan	Faculty of Engineering, Department of Mechanical Engineering, Usak University, Turkey
Dr. Umashankar Subramaniam	Associate Prof., College of Engineering, Prince Sultan University, Saudi Arabia
Dr. Tayfun GÜNDOĞDU	Faculty of Electrical and Electronic Engineering, Department of Electrical Engineering, Istanbul Technical University, Turkey
Dr. Yukesh Kannah R	Department of Civil Engineering, Anna University Regional Campus, India
Jean Bosco Mugiraneza	University of Rwanda, Rwanda

Dr. R. Parameshwaran	Assistant Prof., Dept. of Mechanical Engineering, Birla Institute of Technology & Science (BITS-Pilani), India
Dr. Endong Wang	Associate Prof., Department of Sustainable Resources Management, College of Environmental Science and Forestry,State University of New York (SUNY-ESF), USA
Dr. Jianxin Xu	Prof., Faculty of metallurgy and energy engineering, Kunming University of Science and Technology, China
Dr. Qingtai Xiao	Distinguished Associate Prof., Department of Energy and Power Engineering, Kunming University of Science and Technology, China
Abaubakry M' BAYE	Facilities, Utilities and Energy manager, Glaxo Smith & Kline, France
Dr. Omar Behar	Clean Combustion Research Center (CCRC), King Abdullah University of Science & Technology (KAUST), Saudi Arabia

Table of Contents

Volume 9, Issue 2, December 2023

Trends in Renewable Energy
OPEN ACCESS ISSN: 2376-2144
Peer-Reviewed Review Article futureenergysp.com/index.php/tre

A Review of Research on Emission Characteristics of Ethanol-Diesel Blends in Diesel Engines

Meng Chen*

School of Mechanical Engineering/Institute of Vehicles and New Energy Technology, North China University of Water Resources and Electric Power, Zhengzhou City, Henan, China

Received February 23, 2023; Accepted March 16, 2023; Published March 21, 2023

This paper reviews research on the emission characteristics of blended ethanol and other fuels. With the rapid development of modern industry, the extensive use of fuel engines has led to increasingly prominent contradictions between energy and the environment. In order to respond to sustainable development and reduce engine emissions in various countries, many scientific research institutions have conducted research on mixed fuels. The research of blended fuel mainly focuses on its sustainability, economy and environmental protection. Compared with gasoline engines, diesel engines have a lower fuel consumption rate and are widely used in heavy industry. But its fuel comes from refining crude oil, which is non-renewable and has poor cleanliness. As an emerging renewable fuel, ethanol is a fuel with good development prospects due to its good cleanliness, wide range of sources and renewable. If ethanol can be used as an alternative fuel for traditional internal combustion engines and diesel engines, it can save some traditional fuels and improve the emission problems of internal combustion engines to a certain extent. This paper introduces the research status of ethanol blended fuels, and the emission characteristics of engines (NO_x, HC and CO) under different ethanol ratios and different operating conditions. It can be seen that with the increase of ethanol blending ratio, NO_x content will increase, while CO and HC emissions will decrease.

Keywords: Ethanol; Diesel engine; Emission; Renewable

Introduction

With the rapid development of industrialization of human society, the consumption of traditional primary energy such as crude oil continues to increase. At present, the world's main primary energy sources are still oil, coal and natural gas, of which oil accounts for more than one-third of the total global energy consumption [1]. The current global energy structure is shown in Figure 1.

Countries around the world are facing the dual pressure of global warming and the depletion of oil resources caused by the greenhouse effect. Internal combustion engines are the main consumers of oil resources, consuming 60% of the world's oil. In addition, car ownership is growing rapidly year by year. China's oil consumption has increased year by year, and the dependence of oil on foreign countries has continued to increase [2]. China's limited oil reserves and heavy dependence on overseas imports have become important issues affecting China's energy security [3]. China's automobile growth and oil imports are shown in Figure 2. It can be predicted that with the further

*Corresponding author: 1281665160@qq.com

Tr Ren Energy, 2023, Vol.9, No.2, 107-119. doi: 10.17737/tre.2023.9.2.00155

improvement of China's economic level, China's fuel consumption will still maintain a growth trend in the future.

Fig. 1. Composition of the world's energy architecture

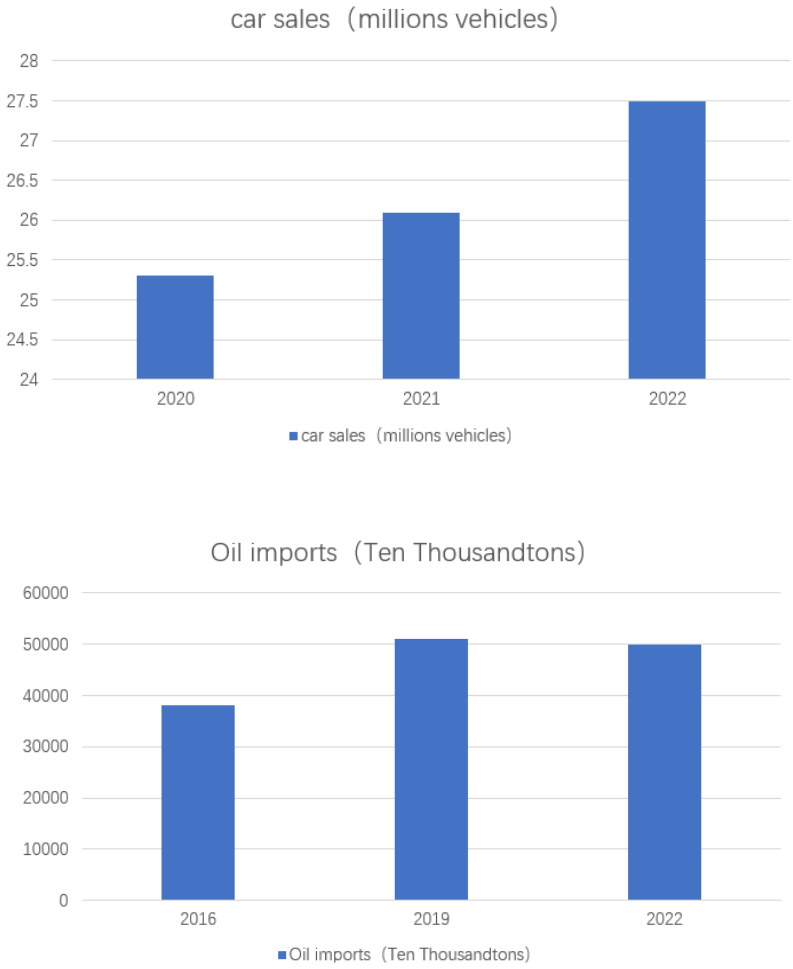

Fig. 2. China's automobile growth and oil imports

After more than 100 years of continuous development and progress, the internal combustion engine has been widely used in various fields with the advantages of high efficiency, low fuel consumption, strong environmental adaptability, simple structure and low failure rate [4]. Although new energy concepts are emerging in an endless stream, there is a tendency to overthrow the status of traditional internal combustion engines and replace them. However, the global internal combustion engine community and China's Ministry of Science and Technology still generally believe that the internal combustion engine will remain the most used engine in construction machinery, defense and military for a long time to come. In addition, the growing number of automobiles in addition have also increased the demand for primary energy such as oil. The huge production of vehicles also increases the burden on the environment, especially in commercial vehicles. Diesel engine has the characteristics of good thermal efficiency and economy, large torque and good durability, so it is widely used in large construction machinery and large passenger cars [5].

The combustion method of gasoline engine is mainly pre-mixed combustion, *i.e.,* the oil-gas mixture is formed outside the cylinder. The gas is sucked into the cylinder and then ignited by the spark plug. The gas burns to form a fire core, and then the surrounding mixed gas is sequentially ignited around the fire core. As the flame gradually expands, the temperature and pressure of the surrounding unburned mixed gas continue to rise, and the combustion gradually accelerates. The products produced after the combustion of gasoline are mainly CO, HC and NO_x.

The combustion method of diesel engine is mainly diffusion combustion. By compressing the air, the temperature of the air is higher than the ignition point of the fuel, thereby igniting the fuel. During the working process, diesel fuel will be sprayed into the combustion chamber in the form of a mist through the high-pressure oil pump, and the mist diesel fuel will continue to be mixed with the air in the cylinder after ignition by high-temperature gas. Due to the short formation time of the mixed gas, the concentration and temperature distribution of the mixed gas are uneven, and a part of the fuel oil cannot be completely burned under the condition of high temperature and lack of oxygen and is discharged with the exhaust gas, forming black smoke.

Generally speaking, diesel engines emit less CO and HC than gasoline engines, which are less than one-tenth of gasoline engine emissions. For NO_x, in the case of a large engine load, its emissions are not much different from the emission level of gasoline engines, while in the case of small loads, NO_x emissions will be lower than those of gasoline engines. In general, diesel engines emit CO, HC and NO_x below those of gasoline engine emission levels. However, the soot particles emitted by the diesel engine are much higher than the emissions of the gasoline engine, which is about 30~80 times the emission of the gasoline engine [6].

For the problem of motor vehicle exhaust pollution, most countries in the world have formulated relatively strict emission regulations. There are three mainstream motor vehicle emission standard systems in the world: Europe, the United States and Japan. At present, the European motor vehicle standard system is widely used because of its relatively loose testing requirements. Since 2000, China has formulated emission regulations suitable for China with reference to European automobile emission standards. China's Ministry of Environmental Protection has implemented "China VI-a" emission standards on July 1, 2020, while China VI-b Standard will be fully implemented by July 1, 2023. The China VI emission regulation has stricter restrictions on the regular emissions of vehicles than the China V emission regulation, which is also known as one

of the strictest emission regulations. Table 1 shows a comparison of China V and VI emission regulations. The limit values in China VI is about 40-50% stricter than those of China V. The strictness of China VI is not only reflected in the values of these emissions, but also in the following three main aspects: First, the test cycle is different, from the New European Driving Cycle of China V to the Worldwide Harmonized Light Vehicles Test Cycle; Second, the test procedure requirements are different, and the quality requirements and road load settings of the test vehicle directly affect the fuel consumption and emission performance of the vehicle; Third, emissions testing has been transferred from the laboratory to the actual road for the first time compared to the previous stage of the emission regulations [5].

Table 1. Comparison of China emission regulations

Emission regulations and standards	China V	China VI	China VI B
CO(mg/km)	1000	700	500
THC(mg/km)	1000	100	50
NMHC(mg/km)	68	68	35
NO_x(mg/km)	60	60	35
PM(mg/km)	4.5	4.5	3.0
PN(p/km)	6×10^{11}	6×10^{11}	6×10^{11}

As a clean alternative fuel, ethanol plays an important role in alternative energy, reducing environmental pollution, and promoting related agricultural development. Its production of raw materials is diverse and sustainable, which can reduce human dependence on fossil fuels. As a liquid fuel, ethanol is easy to transport and use, and can be mixed with gasoline and diesel without major changes to the original engine. At the same time, as an oxygenated fuel, ethanol can theoretically reduce the emission of engine particulate matter and some harmful gases. Based on the above advantages, ethanol has been widely studied. China began to carry out ethanol pilot work in 2002, because its nature is close to gasoline. The current technology of applying ethanol fuel on gasoline engines has been quite mature. However, due to the large difference between the characteristics of ethanol and diesel itself, ethanol will be stratified for a long time after mixed with diesel. Due to the low cetane number of ethanol, it is not easy to compress and ignite. So, the practical application of ethanol in diesel engines is relatively small. But it is still a major topic for many scholars in recent years. China's diesel engine car ownership is large, and the total annual diesel consumption is about twice that of gasoline. Diesel resources are tight, so the study of the applicability of ethanol in diesel engine is still of great practical significance. Ethanol production by country is shown in Figure 3.

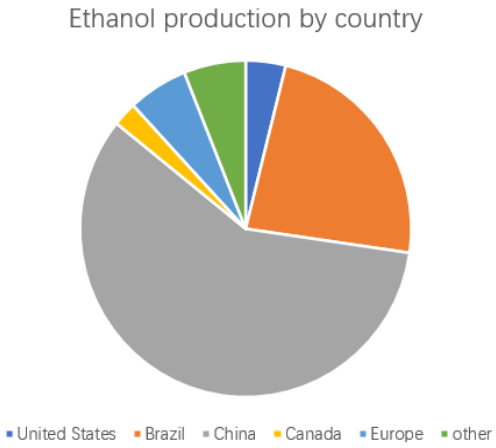

Fig. 3. Ethanol production by country

Ethanol Fuel Characteristics

Among the common biofuels, ethanol is the most widely used in combination with diesel fuel. Ethanol is a renewable fuel that can be made from residues from plants and crops and is also a typical oxygenated fuel. The comparison of the physical and chemical properties of ethanol, gasoline and diesel is shown in Table 2. It can be seen that the oxygen content of ethanol is as high as 34.8%. The high oxygen content can improve the area where the local mixture in the cylinder is too concentrated, and improve the quality of the mixture in the cylinder, thereby reducing the generation of soot. The latent heat of ethanol vaporization is 2.8 times that of gasoline and 3.2 times that of diesel, and the boiling point of ethanol is only 78℃. Compared with diesel and gasoline, it is easier to vaporize. The high latent heat of vaporization and low boiling point can not only improve the charge coefficient of the intake air and reduce the negative work of compression, but also reduce the maximum combustion temperature in the cylinder, achieve low-temperature combustion, and reduce the generation of NO_x. The activity of ethanol is relatively low compared with diesel and gasoline, and the research octane rating (RON) is as high as 108, and the low activity will inhibit the low-temperature exothermic process of diesel and delay the combustion process in the cylinder. The calorific value of ethanol is two-thirds that of gasoline or diesel. To get a fuel input of the same calorific value, ethanol has a third more mass than diesel.

Table 2. Comparison table of physical and chemical properties of three conventional fuels

Project	Ethanol	Diesel Fuel	Gasoline
Octane Number	108	20~30	70~90
Hexaoctane number	＜8	40~55	13~71
Auto-ignition temperature (℃)	426	≈250	420
boiling point (℃)	78	180~360	125.7
Latent heat of vaporization(KJ/kg)	826	250	297
Stoichiometric air-fuel ratio	9	14.3	14.8~15.1
Ignition limit (%)	4.3-19.0	1.4~7.6	1.0~6.0
Low calorific value (MJ/kg)	26.9	42.5~44.4	43.97
Density (g/mL)	0.725	0.86	0.679
Oxygen content (wt%)	34.8	0.2	0

As a renewable energy source, ethanol fuel comes from a wide range of sources. The general method of preparing ethanol is biological method. Ethanol fuel is obtained by fermentation using grain or crop straw as raw material. Another production method is synthesis, which produces ethanol by ethylene hydration reaction under certain conditions. So far, China's annual crop straw burning not only wastes energy but also pollutes the air. If these waste crops can be fully used for cellulosic ethanol production, both energy saving and environmental protection purposes can be achieved.

Emission Characteristics

NO_x Emissions

With the enhancement of environmental awareness, the national requirements for the emission of engine pollutants are getting stricter and stricter. High temperature, oxygen enrichment and combustion duration are the three main contributing factors to NO_x emissions. In order to study the effect of different ratios of ethanol-diesel blends on NO_x emissions, Luo [7] used YC6J180 diesel engine to measure NO_x emissions at different speeds and loads, and the results are shown in Table 3.

Table 3. NO_x emissions at different speeds and loads

Rotate speed (r/min)	Load (%)	NOx(ppm) E0	E10	E20
1200	25	498	691	680
1200	50	1095	1192	1290
1200	75	1481	1731	1814
1200	100	1792	2026	2273
1800	25	349	420	590
1800	50	765	855	959
1800	75	1087	1233	1339
1800	100	1324	1509	1699
2600	25	354	424	479
2600	50	621	727	819
2600	75	953	1064	1131
2600	100	1100	1285	1477

In order to more intuitively represent the emission comparison of NO_x under various conditions, the following comparison chart (Figures 4-6) is obtained based on the test data. The data shows that NO_x emissions from burning the same fuel increase with the load. It's believed that this is because NO_x emissions increase as the engine load increases, the maximum combustion temperature in the cylinder increases, and the combustion duration period becomes longer. At the same time, the NO_x emission concentration decreases with the increase of engine speed, because at high speed, the occupation time of each work cycle of the engine decreases, the fuel and gas mix poorly, and the combustion process deteriorates.

The water-cooled direct-injection diesel engine was used by Sun [8] to explore the impact of NO_x emissions from engines with different ethanol ratios. This study used a mixed fuel with mixed mass fractions of 10% and 20% ethanol, which were denoted as E10 and E20, respectively. The results are shown in Figure 7.

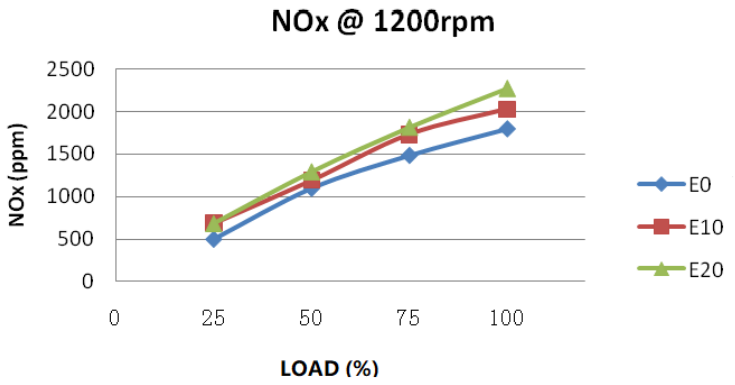

Fig. 3. Low engine NO_x emissions under different fuel mixing ratios

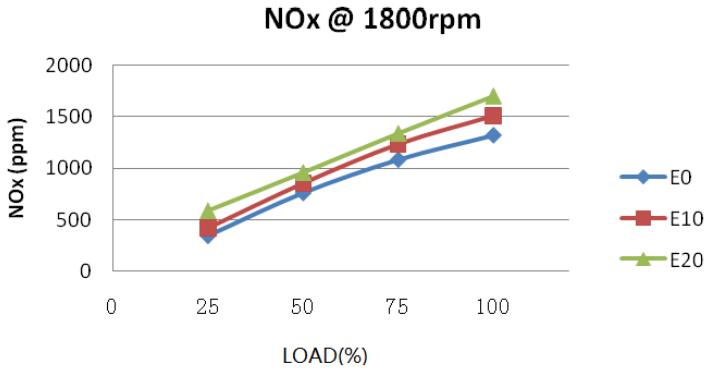

Fig. 4. Medium-speed NO_x emissions from engines at different fuel mixing ratios

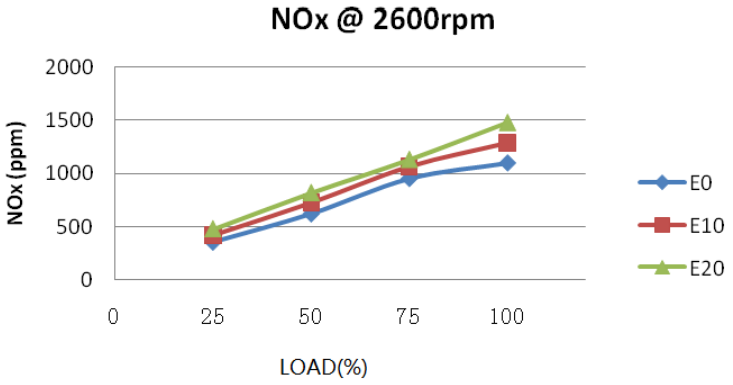

Fig. 5. High-speed NO_x emissions from engines under different fuel mixing ratios

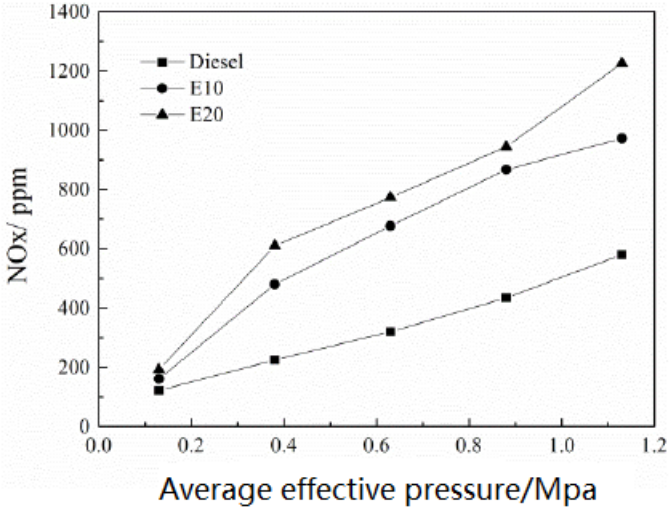

Fig. 6. Effect of ethanol addition ratio on NO_x emissions

The experimental results [8] show that NO_x emissions increase with the increase of ethanol addition. It can be seen from the figure that under low load, the addition of ethanol has little impact on the NO_x emissions of diesel engines. NO_x is mainly generated under high temperature, oxygen-rich conditions, under low load. Although the addition of ethanol will reduce the pressure and temperature in the cylinder, the amount of NO_x generation still increases slightly, which may be due to the addition of ethanol to make the fuel in the cylinder burn in an environment with a relatively high oxygen mass fraction compared with pure diesel, and eventually lead to a slight increase in NO_x production. Under medium and high load, the addition of ethanol increases the pressure and temperature in the cylinder, and the oxygenated ethanol provides oxygen-rich conditions for the combustion of the fuel, which finally increases the NO_x generation more obviously.

Yao *et al.* [9] found that under different working conditions, the fuel began to burn after the hysteresis period in the cylinder to produce NO_x. During combustion, the concentration of NO_x in the cylinder rises sharply, and then the fuel reacts chemically with the air and burns out. The concentration of NO_x in the cylinder tends to be stable and no longer changes until it is discharged through the exhaust duct. In this study, by exploring the effect of ethanol substitution rate on emissions under different operating conditions, it is shown that the maximum emission of NO_x in the combustion process of ethanol engines increases with the increase of ethanol replacement rate. It's believed this is because when burning pure diesel, only air enters the cylinder and not the ethanol/air mixture. The lag period is short, the temperature and pressure in the cylinder rise earlier, and the high temperature in the cylinder lasts longer. So, the amount of NO_x produced is less. With the increase of ethanol replacement rate, the amount of ethanol in the cylinder gradually increases, while the amount of diesel injection in the cylinder gradually decreases. The combustion temperature and pressure in the cylinder increase, the air flow movement in the cylinder is enhanced, the combustion duration is longer, and the combustion speed is faster, resulting in increased NO_x emissions. At the same time, the engine burns pure diesel with a shorter lag period than when adding ethanol combustion mode, so the NO_x generation time is earlier.

CO Emissions

CO is mainly produced by incomplete combustion of fuel. In order to study the effect of burning different proportions of ethanol diesel fuel blends on CO gas emissions. Luo [7] discussed the CO emissions of engines under different working conditions under different fuel mixing ratios. Finding that CO emissions are the least at medium speed and at medium load. The team believes that CO emissions rise sharply due to hypoxia caused by insufficient mixing of some fuel and air near full load, and that gas movement in the combustion chamber is too weak when diesel engine speeds are low. The mixture is unevenly formed, and there is more CO in the incomplete combustion product. At the same time, CO emissions decrease as the amount of ethanol in the fuel increases. Because ethanol is used as an oxygen-containing additive, it increases the oxygen content in the cylinder and also improves the uniformity of oxygen to a certain extent. This contributes to the reduction of CO emissions. In general, when the oxygen in the cylinder is sufficient and the gas is mixed evenly, it is conducive to reducing the emission concentration of CO.

Zhao [10] discussed the effect of ethanol ratio on CO emissions of dual-fuel dual-injection system under different working conditions. The results showed that with the increase of methanol, CO emissions of 0.2 MPa, 0.6 MPa and 1 MPa decreased first and then increased. The turning point for $R_{ethanol}$ was 80%. 40% and 60%, respectively. CO emissions decrease first with the increase of $R_{ethanol}$, because ethanol's higher laminar flame velocity, higher oxygen content and lower carbon content can accelerate the combustion process and make combustion more sufficient. Although further increasing $R_{ethanol}$ after the turning point will increase the oxygen content in the mixture, it will also lead to the phenomenon of pool fire near the intake valve, and a large amount of fuel accumulates near the intake valve to form a local concentration area of fuel, which is not conducive to full combustion of fuel, resulting in increased CO emissions.

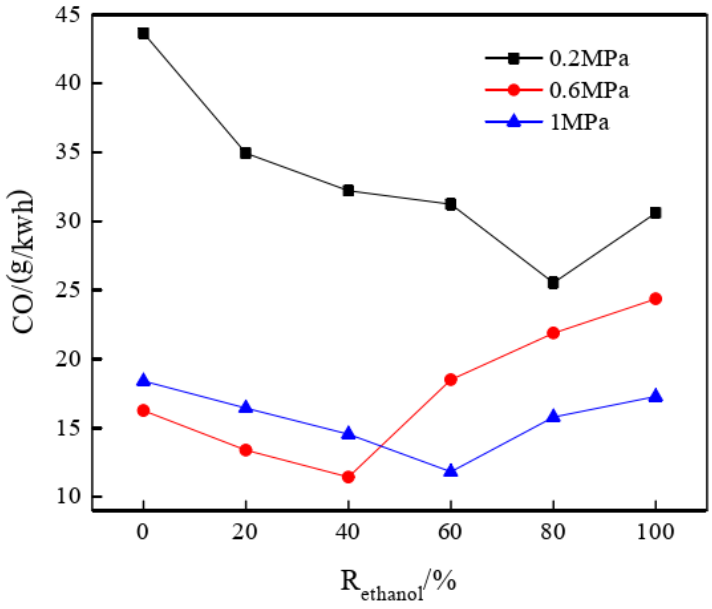

Fig. 7. CO emissions vary with $R_{ethanol}$ under each load

Li *et al.* [11] found through combustion tests that the blending of ethanol will reduce the power of diesel engines, increase the fuel consumption rate, and have lower CO emissions in a wide range of working conditions.

Wang and Tian [12] found that under the premise of maintaining the original parameters and structure of diesel engines, with the increase of the proportion of ethanol in the mixed fuel, the emission of soot and CO has improved significantly.

Britto and Martins [13] modified a single-cylinder diesel engine to achieve Reactivity Controlled Compression Ignition (RCCI) combustion of ethanol premix injection in the intake tract, and studied the impact of different ethanol replacement rates on diesel engine emissions. The results show that ethanol can achieve the best substitution rate when the injector flow rate is high and the vortex flow structure is high, and the NOx generation in the engine exhaust can be reduced under this working condition. But the generation of HC and CO exhaust pollutants is increased.

HC Emissions

HC gas emissions are produced due to incomplete combustion of fuel. Because the engine adopts the combustion method of injection fuel in the cylinder, it will lead to the fuel and air can not become completely uniform mixture. The mixture gas is locally too concentrated or too diluted, and the mixed gas near the cylinder wall will be affected by the cold shock effect. So, the fuel combustion is insufficient, resulting in HC emissions. In addition, fuel in the cylinder liner and piston clearance is less likely to participate in combustion, which is one of the reasons for the generation of HC emissions. Luo [7] separately explored the HC emissions of the engine under different working conditions and different fuel mixing ratio. It's found that with the increase of engine load, the temperature in the cylinder increased, which was conducive to fuel combustion. Compared with the HC emission concentrations of different fuels, HC emissions decreased with increasing ethanol content in fuels. Because ethanol is added to the fuel, the oxygen content increases, which promotes fuel combustion, thereby reducing HC emissions. The speed of the engine does not have much effect on HC emissions. Zou [14] explored the effects of ethanol replacement rates on engine emission characteristics under specific working conditions under an altitude of 1972 m and an ambient temperature of 20°C, when the ethanol replacement rate was selected as 0%, 10%, 20%, 30% and 40%, respectively. The results are shown in Figure 9.

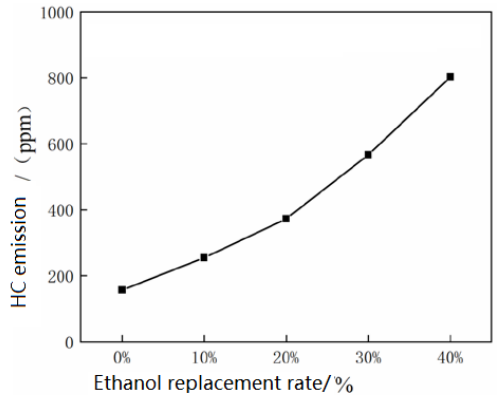

Fig. 8. Emission of HC

It can be seen from the figure that the HC emission generation after the introduction of ethanol combustion is higher than that of the original diesel engine, and the HC generation increases with the increase of ethanol replacement rate. After introducing ethanol combustion, when the intake valve is opened, the premixed homogeneous mixture quickly fills all corners of the combustion chamber. Examples include the gap between the top bank of the piston and the cylinder wall and the valve clearance that flame propagation cannot reach. Because the overall temperature in the cylinder is reduced and the quenching effect on the wall facing the flame is enhanced, the emission of HC is higher than that of pure diesel.

Morsy [15] used the fumigation method to carry out secondary injection with ethanol in the diesel engine, and the results showed that the emissions of NO, CO and HC were increased. Gnanamoorthi and Devaradjane [16] studied the effects of different ethanol blending ratios on diesel engines under different compression ratios. The results show that under the condition of testing the maximum compression ratio, the mixing of ethanol will increase the thermal efficiency of the diesel engine. At other compression ratios, the thermal efficiency decreases when ethanol is added beyond a certain range. The addition of ethanol delays ignition at different compression ratios, and the delay becomes more pronounced as the proportion of ethanol increases. At the same time, the addition of ethanol will significantly reduce HC, CO and soot.

CONCLUSIONS

Ethanol diesel is an alternative fuel to traditional diesel, and the production of diesel fuel by adding ethanol can effectively alleviate the shortage of petroleum resources caused by relying solely on traditional petroleum resources to produce diesel. At the same time, ethanol diesel can significantly reduce the emission of soot and particulate matter after combustion, and reduce the pollution to the environment.

In summary, several conclusions can be drawn as follows：

1. The increase of the proportion of ethanol in diesel fuel will increase the emission of NO_x, especially under large-load conditions. But in the case of low load, the emission growth of NO_x is less, and appropriately reducing the advance angle of fuel supply is conducive to improving engine thermal efficiency and reducing emissions.
2. The mixing of ethanol with diesel will reduce the power of the diesel engine. When the oxygen in the cylinder is sufficient and the gas is evenly mixed, the increase of ethanol content is beneficial to reduce the concentration of CO emission.
3. The emission of HC and CO from ethanol/diesel blends is related to the proportion of ethanol and engine conditions, and the proportion of ethanol in ethanol diesel fuel should not be too large from the comprehensive consideration of engine performance and emissions. Under the condition that the thermal efficiency of E20 is comparable to that of the original engine, the emission of HC, CO and NO may be reduced to a certain extent.
4. However, due to the difference in structure and properties, the compatibility of ethanol diesel is poor, and the addition of co-solvent to ethanol/diesel would increase the production cost of diesel. These factors hinder the promotion and application of ethylene/diesel blends to varying degrees, so the focus of

ethanol/diesel blends research in the future should be to develop efficient and economical co-solvents to reduce the cost of ethanol diesel. At the same time, when using ethanol diesel, technical measures to reduce NO_x should also be taken to reduce environmental pollution to a greater extent.

CONFLICTS OF INTEREST

The author declares that there is no conflict of interests regarding the publication of this paper.

REFERENCES

[1] Cheng Y., & Jiang J. (2019). Study on the combustion characteristics of ethanol fuel and its application. *Petrochemical Industry Application*, *38*(12):1-3.

[2] Kang, R. (2018). *Experimental Study on Combustion Characteristics of Ethanol/Gasoline in a Dual-fuel Dual-Direct injection Engine*. Tianjin University, Master thesis. doi: https://doi.org/10.27356/d.cnki.gtjdu.2018.000589

[3] Zhai, X. (2018). Visualization Test and Numerical Simulation of Low Temperature Premixed Combustion of Ethanol/Diesel Dual Fuel. Huazhong University of Science and Technology, Master thesis. doi: https://doi.org/10.27157/d.cnki.ghzku.2018.000016

[4] Zhao, Q. (2016). *An Experimental Study on the Gas and Soot Formation in Ethanol Pyrolysis*. Chongqing University, Master thesis.

[5] Zhang, Y. (2021). *Study on Electrostatic Spray of Ethanol-Biodiesel Blend Fuel.* Jiangsu University, Master thesis. doi: https://doi.org/10.27170/d.cnki.gjsuu.2021.000705

[6] Zhou, T. (2012). *An Experimental Study on Diesel Engine Combustion and Emissions with Butanol-Diesel Blend Fuels*. Hunan University, Master thesis.

[7] Luo, X. (2016). *Study on Diesel Engine Performance and Emission Characteristics Fueled with Ethanol Blends.* North China Electric Power University, Master thesis.

[8] Sun, Z. (2017). *Numerical and Experimental Study on the Combustion Process of Diesel/Ethanol Dual-Fuel Engine*. Wuhan University of Technology, Master thesis.

[9] Yao, C., Chen, X., Yang, J., Xu, Y., & Xia, Q. (2009). Investigations of Exhaust Emissions of Diesel/Ethanol Compound Combustion in a Turbocharged Inter-Cooled

Diesel Engine. *Transactions of CSICE, 27*(4):314-320. doi: https://doi.org/10.16236/j.cnki.nrjxb.2009.04.006

[10] Zhao, L. (2016). *Investigation on dual fuel dual injection system engine fuelled with ethanol and gasoline for fuel economy and emissions*. Tianjin University, Master Thesis.

[11] Li, H., Huang, J., Huang, H., & Chen, G. (2012). Contrast Experimental Study of a Diesel Engine Burning Rapeseed Oil-based Bio-diesel and Ethanol-diesel in Various Proportions. *Journal of Engineering for Thermal Energy and Power, 27*(4), 498-503+521-522.

[12] Wang, X., & Tian, G. (2013). Effect of ethanol-diesel hybrid fuel on emission characteristics of diesel engine. *Journal of Chinese Agricultural Mechanizatio*n, *34*(1), 95-97+106. doi: https://doi.org/10.3969/j.issn.2095-5553.2013.01.023

[13] Britto, R. F., & Martins, C. A. (2015). Emission analysis of a Diesel Engine Operating in Diesel–Ethanol Dual-Fuel mode. *Fuel, 148*, 191-201. doi: https://doi.org/10.1016/j.fuel.2015.01.008

[14] Zou, C. (2021). *Study on Injection Coordinated Control of Ethanol/Diesel Dual Fuel Engine*. Kunming University of Science and Technology, Master Thesis. doi: https://doi.org/10.27200/d.cnki.gkmlu.2021.000252.,2021

[15] Morsy, M. H. (2015). Assessment of a direct injection diesel engine fumigated with ethanol/water mixtures. *Energy Conversion and Management*, *94,* 406-414. doi: https://doi.org/10.1016/j.enconman.2015.01.086

[16] Gnanamoorthi, V., & Devaradjane, G. (2015). Effect of compression ratio on the performance, combustion and emission of DI diesel engine fueled with ethanol – Diesel blend. *Journal of the Energy Institute*, *88*(1), 19-26. doi: https://doi.org/10.1016/j.joei.2014.06.001

Trends in Renewable Energy
OPEN ACCESS ISSN: 2376-2144
Peer-Reviewed Article futureenergysp.com/index.php/tre

Assessing the Impact of Soiling, Tilt Angle, and Solar Radiation on the Performance of Solar PV Systems

Samuel Chukwujindu Nwokolo, [1,*] Anthony Umunnakwe Obiwulu,[2] Solomon Okechukwu Amadi,[3] Julie C. Ogbulezie[1]

[1]*Department of Physics, Faculty of Physical Sciences, University of Calabar, Nigeria*
[2]*Department of Physics, Faculty of Science, University of Lagos, Lagos, Nigeria*
[3]*Department of Physics, Faculty of Physical Sciences, Alex Ekwueme Federal University, Ndufu-Alike, Nigeria*

Received February 27, 2023; Accepted March 19, 2023; Published March 22, 2023

This research examined the observed datasets and a theoretically derived model for estimating yearly optimum tilt angle (β), maximum incident solar radiation (H_{max}), clean gain indicator (CGI), and soiling loss indicator (SLI) at Mumbwa, Zambia, the Mediterranean Region, and low latitude locations across the globe. The cleaned tilted collector emerged as the best performing collector due to H_{max} and much higher energy gains compared with the soiled collector. CGI showed an appreciable performance of 0.4737% over -0.4708% on the SLI, indicating that soiling on the surface of photovoltaic (PV) modules significantly depreciates the overall performance of PV modules. Two established empirical models obtained from the literature were compared with the established theoretical model (β=φ). The result revealed that the two models overestimated the observed annual optimum tilt angle in this paper, simply because the models were developed with high latitude location datasets from the Asia continent. However, the newly established monthly and yearly global radiation indicator (GRI) models by the authors in their previous paper performed excellently in the selected representative cities in the Mediterranean region.

Keywords: Global tilted irradiance; Global horizontal irradiance; Soiling; Optimum tilt angle; Maximum incident solar radiation

Introduction

Assessing the optimum tilt angle, maximum incident solar radiation, and soiling effect of solar PV module performance is of great importance in order to accurately evaluate the solar PV module's performance and its lifetime. During the life of a solar PV module, the tilt angle and orientation of the module can affect its efficiency due to changing seasonal variations and soiling effects caused by environmental factors such as dust, pollution, windblown debris, and moisture. It is therefore essential to consider the optimum tilt angle and orientation of a solar PV module in order to ensure maximum efficiency and performance during its lifetime. To accurately assess the optimum tilt angle and orientation of a solar PV module, several factors must be taken into account, such as the site location [1], local climate [2], seasonal changes in temperature [3] and

*Corresponding author: sam31628@gmail.com (S.C. Nwokolo)

Tr Ren Energy, 2023, Vol.9, No.2, 120-136. doi: 10.17737/tre.2023.9.2.00156

incident radiation [4], as well as soiling effects caused by dust [5] and other environmental factors [6].

As the tilt angle of a solar PV module increases, it will be exposed to more direct sunlight, which increases the maximum incident radiation on the module and therefore its performance and efficiency over the course of its lifetime [7]. During its lifetime, a solar PV module should be installed at an optimum tilt angle and orientation in order to maximize its efficiency and its return on investment [8,9,10]. The tilt angle and orientation of a solar PV module are thus important factors to consider when selecting a module for installation and should be taken into account when designing a solar PV system for a specific site location. In order to ensure that the installation of a solar PV module is optimized for maximum efficiency, these factors should be carefully considered and taken into account when selecting the tilt angle and orientation of the module.

This must be weighed against the additional costs associated with increasing the tilt angle of a solar PV module, such as additional costs for supporting structures, higher labour [11] and installation costs [12], and an increased risk of damage due to strong winds or snow loads [13]. Therefore, while it is important to consider the tilt angle and orientation of a solar PV module when selecting one for installation, this must be done in a balanced way to ensure that the costs are kept to a minimum [12] and that the efficiency of the module is maximized [11] while also ensuring that the risks of damage are minimized [14].

The selection of an optimal tilt angle and orientation for a solar PV module must be determined on a case-by-case basis [15], taking into account the local site conditions [16] and cost factors to ensure that the most effective and efficient selection is made for a given installation [17]. Generally, the selection of an optimal tilt angle and orientation for a solar PV module is an important consideration when installing one, as it can have a direct effect on the efficiency [18] and lifespan of the module [19]. Therefore, it is important to carefully weigh the potential costs associated with increasing the tilt angle of a solar PV module against the benefit of increased efficiency when making the decision [20].

Evaluating the optimum tilt angle, maximum incident solar radiation, and soiling effect of solar PV module performance in Mumbwa, Zambia, is an important part of understanding the potential of solar energy in this region in order to maximize its benefits in terms of cost efficiency [21], accessibility [22], and reliability of electricity production. By assessing these factors, researchers can determine the best time of year to install solar modules [23], the optimal tilt angle for maximum energy production [24], and gain insights into how frequently maintenance will be required due to soiling due to sand [25] and dust accumulation [26]. These assessments are key to determining the success of any solar energy initiatives in Mumbwa and ensuring that the citizens of Mumbwa are able to reap the full benefits of solar energy and have access to a reliable and cost-effective energy source.

The research conducted in Mumbwa is of paramount importance in helping to bring clean and reliable electricity to those who need it most. Furthermore, by studying the environmental and climatic conditions in Mumbwa, researchers can also determine what type of solar panels will be most appropriate for this region in order to maximize the efficiency of solar energy initiatives and ensure that these initiatives are cost-effective and capable of meeting the long-term energy needs of Mumbwa's citizens.

All of these findings can be used to inform policymakers on how best to use solar energy initiatives in Mumbwa, as well as which types of systems will provide the most reliable and cost-effective energy sources for the people living there. By properly assessing the environmental and climatic conditions in Mumbwa, as well as monitoring the successes of solar energy initiatives in the area, researchers can gain insight into how to best use solar energy to improve the lives of those living in Mumbwa and provide them with a sustainable source of electricity in a way that is both reliable and cost-effective. Ultimately, this research can have a huge impact on the quality of life for Mumbwa's citizens and provide them with a sustainable energy source that is reliable and cost-effective while also allowing them to benefit from the economic and social opportunities that come with having access to reliable electricity.

Numerous researchers have studied the effect of soiling and the optimum tilt angle on PV performance and found that soiling can reduce photovoltaic efficiency by up to 50% [11], while the optimum tilt angle can increase efficiency by up to 20% [12]. As such, maintaining clean solar panels and optimizing their tilt angle can have a significant positive impact on photovoltaic efficiency and should be taken into account when installing a solar PV system for maximum energy production. Indeed, these findings demonstrate that proper maintenance of solar modules can greatly improve the performance of photovoltaic systems and therefore should be a priority for those interested in maximizing their energy output.

This highlights the importance of having regular cleaning and maintenance routines for solar PV systems and making sure the solar modules are installed at an optimum tilt angle in order to capture the most energy from the sun and maximize the photovoltaic efficiency of the system over a given period of time. These findings suggest that careful attention must be paid to the cleanliness of PV modules and their tilt angle in order to maximize photovoltaic efficiency and energy production and to receive the most benefit from a solar photovoltaic system over the long run. Most studies revealed that soiling impacts negatively on the radiation and energy performance of PV systems and that it can be as high as 25% [18], which is substantial, and it could be argued that this underlines the importance of regular cleaning and maintenance of PV modules [25], whereas an optimal tilt angle enhances PV performance by increasing the amount of solar radiation absorbed and therefore increasing the efficiency of a PV system significantly [26].

The results of these studies clearly indicate the importance of ensuring regular cleaning and maintenance routines for solar PV systems, as well as making sure that the solar modules are installed at an optimum tilt angle in order to capture the most energy from the sun and maximize the photovoltaic efficiency of the system over a given period of time. These findings are further reinforced by other research studies conducted on the effects of tilt angle and soiling on photovoltaic efficiency and energy production, which have also revealed that soiling and the installation of the modules at an incorrect tilt angle can significantly reduce the efficiency of a PV system and could potentially lead to financial losses for the owners of the PV system due to lost energy production and increased operational costs. As such, it is important to note that regular maintenance of PV modules and their installation at an optimal tilt angle are both essential for maximizing photovoltaic efficiency and energy production over a given period of time.

In this paper, we have discussed the importance of ensuring proper maintenance routines and the installation angle of solar PV systems to ensure maximum photovoltaic efficiency and energy production over a given period of time. This is because soiling and

the installation of modules at incorrect tilt angles can have a severe impact on energy production, leading to financial losses for owners of the PV system due to the reduced efficiency of their system as well as increased operational costs due to the need to regularly clean their system and the increased cost of energy production. In order to determine the effects of soiling and the optimum tilt angle on PV performance capacity, the global tilted irradiance as well as the global horizontal irradiance were analyzed in this study. Additionally, novel cleaning datasets were used to determine the global radiation indicator and energy gain/loss on monthly and yearly timescales in Mumbwa, Zambia.

As a result, different mathematical expressions developed in our previous paper were used to evaluate the optimum tilt angle and global radiation indicator used for evaluating maximum incident solar radiation in Mumbwa, Zambia, the Mediterranean region, and low latitude locations across the globe. The authors also developed an energy loss indicator for evaluating radiation levels and energy loss due to soiling, as well as an energy gain indicator for evaluating energy gain as a result of routine cleaning of PV systems.

Materials and Methods

Data Acquisition

The measured datasets such as soiled and clean global tilted irradiance using silicon irradiance sensors and global horizontal irradiance (W/m^2) employing thermopile pyranometers 1 & 2 in this paper were obtained from the Energy Sector Management Assistance Program of the World Bank Group for ZM_Solar_Mumbwa_IFC, station, Zambia (Latitude 15.08^0E, Longitude 27.00^oE, Elevation 1103m (https://energydata.info/dataset/zambia-solar-radiation-measurement-data). The obtained raw data (1-minute summarization interval values) were post-processed in order to obtain monthly mean values of soiled and clean global tilted irradiance (W/m^2) and global horizontal irradiance (W/m^2) values, as shown in Table 1.

Theoretical Model for Estimating Yearly Optimum Tilt Angles

The theoretical models for evaluating optimum tilt angles for low latitude locations in both the Northern and Southern Hemispheres developed in our previous paper [27] were used in this study.

$$\beta = \tan^{-1}\left[\frac{2\tan\phi}{1-\tan^2\phi}\right] \quad (1)$$

Equation (1) is the theoretical model developed in this study for evaluating the yearly optimum tilt angle for low latitude locations ($5.14^o \leq \phi \leq 0.0025^o$) on the Earth using only latitude as an input parameter. Where β is the optimum tilt angle, φ is the latitude of the location, and δ is the solar declination angle. Two empirical models for estimating yearly optimum tilt angles for high latitude locations [28, 29] were used to compare with the theoretical model developed in this study as presented in Table 2.

Table 1. Monthly mean values of clean and soil global tilted irradiance from the silicon irradiance sensor over global horizontal irradiance from the thermopile pyranometer (pyr1 and pyr2)

Month	ghi_pyr_1	ghi_pyr_2	Mean ghi_pyr	gti_clean	gti_soil
Jan-2018	277.77	278.03	277.9024	252.47	250.93
Feb-2018	191.03	191.08	191.0525	186.69	185.27
Mar-2018	213.86	214.14	213.9999	216.27	214.77
Apr-2018	225.23	225.39	225.3068	241.43	239.4
May-2018	208.17	208.25	208.2096	235.77	234.34
Jun-2018	208.36	208.45	208.4035	242.38	241.7
Jul-2018	187.1	187.23	187.1657	208.93	209.15
Aug-2017	249.15	249.7	249.4255	266.91	266.2
Sep-2017	265.08	265.57	265.3234	269.56	268.93
Oct-2017	240.72	241.04	240.8798	232.35	231.48
Nov-2017	218.39	218.63	218.5139	203.76	202.78
Dec-2017	227.07	227.29	227.1813	208.9	207.66
Mean	**225.99**	**226.23**	**226.1137**	**230.45**	**229.38**

Table 2. Evaluation of yearly optimum tilt angles for low latitude locations across the globe using the theoretical model developed in this study and other models from the literature

Country	Capital	Latitude	Longitude	Present study (β=2φ)	Talebizadeh et al. [30]	Jamil et al. [31]
Nigeria	Port Harcourt	4.4	7.17	8.8	10.19676	12.0394
Nigeria	Uyo	5.05	7.97	10.1	10.63902	12.47555
Nigeria	Calabar	4.95	8.32	9.9	10.57098	12.40845
Nigeria	Yenegao	4.93	6.26	9.86	10.557372	12.39503
São Tomé und Príncipe	São Tomé (capital)	0.33	6.73	0.66	7.427532	9.30843
São Tomé und Príncipe	Santana	0.25	6.74	0.5	7.3731	9.25475
São Tomé und Príncipe	Trindade	0.29	6.81	0.58	7.400316	9.28159
Gabon	Libreville	0.42	9.47	0.84	7.488768	9.36882
Gabon	Oyem	1.59	11.57	3.18	8.284836	10.15389
Gabon	Moanda	1.53	13.24	3.06	8.244012	10.11363
Gabon	Mouila	1.87	11.05	3.74	8.475348	10.34177
Uganda	Kampala	0.34	32.58	0.68	7.434336	9.31514
Uganda	Nansana	0.36	32.52	0.72	7.447944	9.32856
Uganda	Kira	0.39	32.63	0.78	7.468356	9.34869
Lake Victoria	Kampala	0.34	32.58	0.68	7.434336	9.31514
Lake Victoria	Kira Town	0.39	32.63	0.78	7.468356	9.34869
Lake Victoria	Kisumu	0.09	34.76	0.18	7.264236	9.14739
Lake Victoria	Nkozi	0.0025	32.014	0.005	7.204701	9.0886775

Lake Victoria	Bukoba	1.33	31.8	2.66	8.107932	9.97943
Kenya	Nairobi	1.29	36.82	2.58	8.080716	9.95259
Kenya	Namanga	2.55	36.78	5.1	8.93802	10.79805
Kenya	Kibwezi	2.41	37.96	4.82	8.842764	10.70411
Somalia	Mogadishu	2.05	45.31	4.1	8.59782	10.46255
Somalia	Aadan Yabaa	3.78	46.25	7.56	9.774912	11.62338
Malaysia	Kuala Lumpur	3.13	101.68	6.26	9.332652	11.18723
Malaysia	Kuching	1.55	110.35	3.1	8.25762	10.12705
Malaysia	Johor Bahru	1.49	103.74	2.98	8.216796	10.08679
Singapore	Singapore	1.35	103.81	2.7	8.12154	9.99285
Singapore	Hougang	1.36	103.88	2.72	8.128344	9.99956
Singapore	Yishun	1.43	103.83	2.86	8.175972	10.04653
Indonesia	Batam	1.13	104.05	2.26	7.971852	9.84523
Indonesia	Medan	3.59	98.67	7.18	9.645636	11.49589
Indonesia	Makassar	5.14	119.43	10.28	10.700256	12.53594
Colombia	Bogota	4.71	74.07	9.42	10.407684	12.24741
Colombia	Cali	3.45	76.53	6.9	9.55038	11.40195

Mathematical Expressions for Computing Maximum Incident Solar Radiation under Clean and Soiled PV Modules

The following mathematical expressions were developed so as to evaluate the global radiation indicator (GRI) for clean and soiled global tilted irradiance in the Mediterranean region, as presented in Table 3.

$$GRI = \frac{Clean/Soiled \text{ global tilted irradiance (H clean/H soiled)}}{\text{global hoizontal irradiance (H pyr1/H pyr2/mean H pyr1 \& 2)}} \quad (2)$$

$$Clean\ global\ tilted\ irradiance\ (H\ clean) = 1.024 * H\ pyr1 \quad (3)$$

$$Clean\ global\ tilted\ irradiance\ (H\ clean) = 1.019 * H\ pyr2 \quad (4)$$

$$Clean\ global\ tilted\ irradiance\ (H\ clean) = 1.0235 * mean\ H\ pyr1\ \&\ pyr2 \quad (5)$$

$$Soiled\ global\ tilted\ irradiance\ (H\ Soiled) = 1.0193 * H\ pyr1 \quad (6)$$

$$Soiled\ global\ tilted\ irradiance\ (H\ Soiled) = 1.0183 * H\ pyr2 \quad (7)$$

$$Soiled\ global\ tilted\ irradiance\ (H\ Soiled) = 1.0188 * mean\ H\ pyr1\ \&\ pyr2 \quad (8)$$

Table 3. Maximum incident solar radiation under clean and soiled Silicon PV module

Country	city	Lat	Long	H	H tilted clean using pyr1	H tilted clean using pyr2	H tilted clean using mean pyr1 & pyr2	H tilted soiled using pyr1	H tilted soiled using pyr2	H tilted soiled using mean pyr1 & pyr2
Egypt	Luxor	25.69	32.64	261.93	268.21	266.90	268.08	266.98	266.72	266.85
Morocco	Smara	26.73	11.67	250.44	256.45	255.20	256.33	255.28	255.03	255.15
Egypt	Sharm Sheikkh	27.86	34.36	240.12	245.88	244.68	245.76	244.75	244.51	244.63
Morocco	Agadir	30.41	9.6	241.51	247.31	246.10	247.19	246.17	245.93	246.05
Libya	Sabha	30.63	18.35	239.66	245.41	244.21	245.29	244.28	244.04	244.16
Egypt	Alexandria	31.2	29.92	217.96	223.20	222.11	223.09	222.17	221.95	222.06

Palestine	Gaza	31.41	34.31	231.30	236.86	235.70	236.74	235.77	235.54	235.65
Libya	Tripoli	32.9	13.19	226.32	231.75	230.62	231.63	230.68	230.46	230.57
Syria	Damascus	33.51	36.28	226.20	231.63	230.50	231.52	230.57	230.34	230.45
Algeria	Mecheria	33.55	0.28	223.18	228.54	227.42	228.43	227.49	227.27	227.38
Lebanon	Beirut	33.88	35.5	212.86	217.97	216.90	217.86	216.97	216.76	216.86
Cyprus	Nicosia	35.16	33.38	204.97	209.89	208.87	209.79	208.93	208.72	208.83
Morocco	Larache	35.18	6.15	198.13	202.88	201.89	202.78	201.95	201.75	201.85
Greece	Heraklion	35.32	25.14	197.08	201.81	200.83	201.72	200.89	200.69	200.79
Syria	Latakia	35.52	35.8	200.68	205.50	204.49	205.40	204.55	204.35	204.45
Tunisia	Tunis	35.41	10.18	209.73	214.76	213.71	214.66	213.78	213.57	213.67
Malta	Vallella	35.89	14.51	199.06	203.83	202.84	203.73	202.90	202.70	202.80
Tunisia	Bizerte	37.27	9.86	185.83	190.29	189.36	190.20	189.42	189.23	189.33
Spain	Seville	37.38	5.98	183.16	187.56	186.64	187.47	186.70	186.52	186.61
Turkey	Isparta	37.76	30.55	195.34	200.03	199.06	199.93	199.11	198.92	199.02
Italy	Marsala	37.8	12.44	187.80	192.31	191.37	192.22	191.43	191.24	191.33
Greece	Anthen	37.97	23.73	189.08	193.62	192.67	193.52	192.73	192.54	192.63
Turkey	Bursa	40.18	29.06	169.82	173.90	173.05	173.81	173.10	172.93	173.02
Spain	Madrid	40.4	3.7	181.42	185.78	184.87	185.69	184.93	184.74	184.83
Albania	Vlore	40.46	19.49	176.78	181.03	180.14	180.94	180.20	180.02	180.11
Greece	Thessaloniki	40.63	22.94	174.23	178.41	177.54	178.33	177.59	177.42	177.51
Italy	Naples	40.83	14.27	175.74	179.96	179.08	179.87	179.13	178.96	179.04
Montenegro	Podgoria	42.47	19.26	157.41	161.19	160.40	161.11	160.45	160.29	160.37
Bosnia & Herzegovina	Sarajevo	43.51	18.41	150.10	153.71	152.96	153.63	153.00	152.85	152.93
Monaco	Monaco	43.73	7.42	163.33	167.25	166.43	167.17	166.48	166.32	166.40
Italy	Florence	43.77	11.26	158.34	162.14	161.35	162.06	161.40	161.24	161.32
Italy	Milan	45.46	9.19	157.06	160.83	160.05	160.76	160.10	159.94	160.02
France	Lyon	45.76	4.84	153.00	156.68	155.91	156.60	155.96	155.80	155.88
Croatia	Zagreb	45.81	15.98	140.13	143.49	142.79	143.42	142.83	142.69	142.76
Slovenia	Ljubljana	46.05	14.51	136.76	140.05	139.36	139.98	139.40	139.27	139.34

Energy Gain/Loss for Clean and Soiled Global Tilted Irradiance (MJm^2day^{-1})

Mathematically, the percentage gain or loss is the availability of global tilted irradiance of solar PV over global horizontal irradiance PV modules as presented in Table 4 and Fig. 1. This is evaluated using the following equations:

$$\text{Percentage gain (\%)} = \left(\frac{H_T\langle \beta = tited \rangle}{H\langle \beta = 0 \rangle} - 1 \right) \times 100 \quad (9)$$

$$\text{Percentage loss (\%)} = \left(1 - \frac{H_T\langle \beta = tited \rangle}{H\langle \beta = 0 \rangle} \right) \times 100 \quad (10)$$

Table 4. Monthly mean values of energy gain or loss under clean and soil global tilted irradiance from the silicon irradiance sensor over global horizontal irradiance from the thermopile pyranometer (pyr1 and pyr2)

Month	Clean tilted H vs H pyr1	Clean tilted H vs H pyr2	Soil tilted H vs H pyr1	Soil tilted H vs H pyr2	Clean tilted H vs /mean H pyr	Soil tilted H vs /mean H pyr	Clean Gain Index	Soiling loss Index
Jan-2018	-9.109	-9.195393	-9.66237	-9.7478	-9.1525	-9.7051	0.6120	-0.6083
Feb-2018	-2.268	-2.294056	-3.01528	-3.0411	-2.2811	-3.0282	0.77045	-0.7646
Mar-2018	1.1283	0.997946	0.424425	0.29496	1.06309	0.35965	0.7009	-0.6960
Apr-2018	7.1942	7.117796	6.293023	6.21725	7.15599	6.25512	0.8478	-0.8407
May-2018	13.256	13.21311	12.57008	12.5275	13.2345	12.5488	0.6093	-0.6056
Jun-2018	16.33	16.27633	16.00354	15.9501	16.3031	15.9768	0.2814	-0.2806
Jul-2018	11.668	11.59292	11.78406	11.7086	11.6306	11.7463	-0.1035	0.1036
Aug-2017	7.1291	6.894265	6.841287	6.60705	7.01157	6.72404	0.2694	-0.2687
Sep-2017	1.6896	1.500913	1.452322	1.26405	1.59518	1.3581	0.2339	-0.2334
Oct-2017	-3.475	-3.604361	-3.83891	-3.9674	-3.5399	-3.9032	0.3781	-0.3766
Nov-2017	-6.698	-6.801507	-7.14813	-7.251	-6.7499	-7.1996	0.4846	-0.4823
Dec-2017	-8.001	-8.091241	-8.54972	-8.6397	-8.046	-8.5947	0.6003	-0.5967
Mean	**2.4036**	**2.300561**	**1.929528**	**1.82688**	**2.35207**	**1.87817**	**0.4737**	**-0.4708**

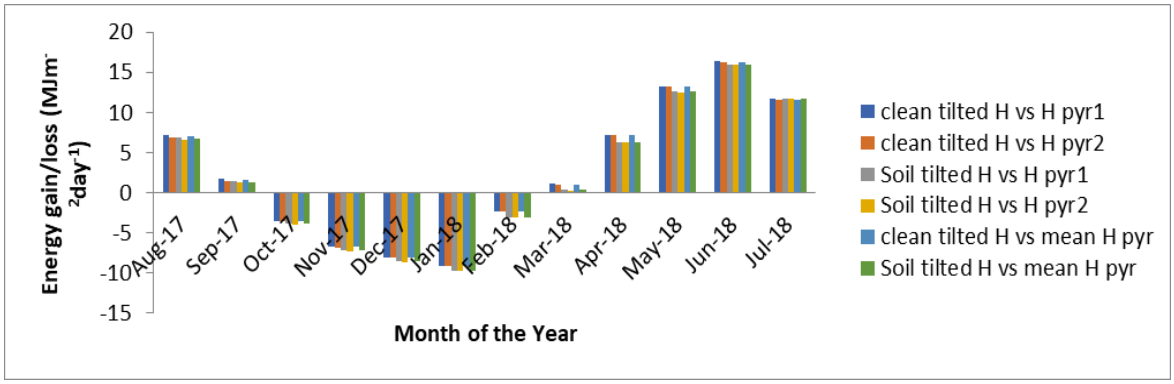

Fig. 1. Energy Gain/Loss versus months of the year under clean and soil global tilted irradiance from the silicon irradiance sensor over global horizontal irradiance from the thermopile pyranometer (pyr1 and pyr2)

Clean Gain Indicator (CGI) and Soiling Loss Indicator (SLI)

Mathematically, the clean gain indicator (CGI) and soiling loss indicator (SLI) for the silicon irradiance sensor in Mumbwe, Zambia, as presented in Table 4 and Fig. 2, are evaluated using the following:

$$Clean\ gain\ indicator = \frac{Soiled\ H - clean\ H}{clean\ H} * \frac{100}{1} \quad (11)$$

$$Soiled\ gain\ indicator = \frac{Clean\ H - Soiled\ H}{Soiled\ H} * \frac{100}{1} \quad (12)$$

where soiled H represents soiled global tilted irradiance, clean H represents clean global tilted irradiance.

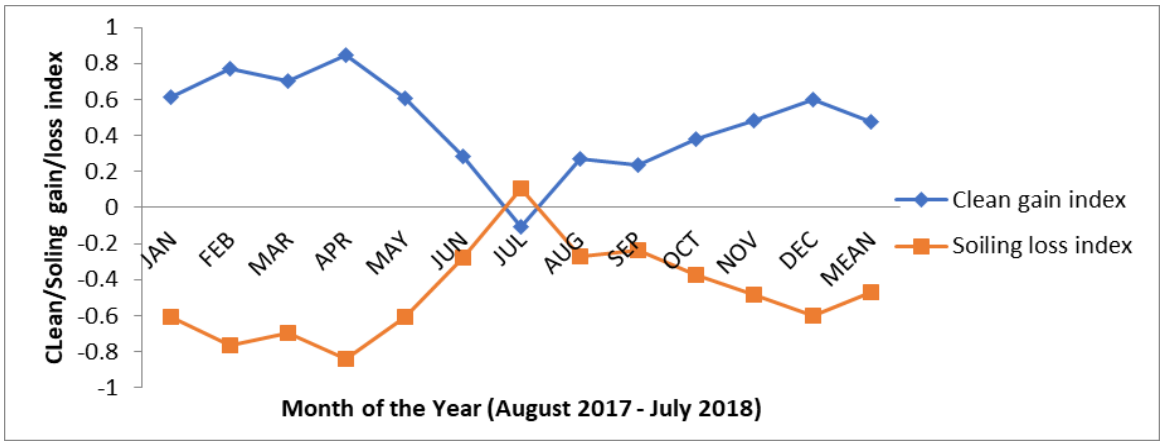

Fig. 2. Clean/Soiling gain/loss index for Mumbwa, Zambia

Results and Discussion

Table 1 presents the monthly and yearly global horizontal irradiance for pyr1 and pyr2, clean and soiled global tilted irradiance, for Mumbwe, Zambia. The data in Table 1 showed that the monthly and yearly global horizontal irradiance was higher in Pyr2 than in Pyr1, but both clean and soiled global tilted irradiance were generally lower than the global horizontal irradiance values. Furthermore, the data indicated that there was a decrease in both clean and soiled global tilted irradiance from Pyr1 to Pyr2 for all months, though the difference was more pronounced for the soiled global tilted irradiance than for clean global tilted irradiance. This suggests that the orientation and tilt of Pyr1 were better suited to capture sunlight than those of Pyr2, as the latter experienced reduced irradiance levels across both clean and soiled conditions.

As a result, the data presented in Table 1 indicates that the orientation and tilt of Pyr1 were better suited to capture sunlight than those of Pyr2, providing an insight into how the tilt and orientation of PV modules can affect their performance in terms of capturing solar irradiance and thus their potential to produce electricity. This understanding of the importance of tilt and orientation when installing PV modules is an important aspect to consider, as it can directly affect their performance and thus energy output. This finding is especially important for the installation and design of PV systems in different regions, as it highlights the importance of accounting for orientation and tilt when considering which PV modules to install in order to maximize energy output from PV systems in different environments.

It could be seen clearly that clean global tilted irradiance yielded higher radiation compared to soiled global tilted irradiance and global horizontal irradiance for both Pyr1 and Pyr2 which implies that the orientation and tilt of PV panels have a direct impact on the amount of solar irradiance they are able to capture, resulting in an increased electrical energy output This is further evidenced by the fact that Pyr1 generated more electrical energy in clean global tilted irradiance than Pyr2, suggesting that not only tilt but also orientation have an effect on the performance of PV panels when capturing solar irradiance and producing electricity. This validates the report found in the literature that an optimum tilt angle and a clean PV system perform better than horizontally mounted PV and soiled PV systems [32]. This finding is especially significant in terms of PV

system installation and design, as it indicates that orientation and tilt are critical when determining which PV modules to install in order to maximize energy output.

From Table 2, it can be seen that the yearly optimum tilt angle obtained from literature [33] overestimates optimum tilt angles compared to the latitude of the observed values developed from $\beta=2\varphi$ in the study location. This suggests that the optimum tilt angle for an inclined surface should be adjusted according to geographic latitude [34] and the orientation of a module to achieve maximum performance [35]. Furthermore, the findings of this research highlight the need for clean PV modules in order to obtain maximum energy output since the angle of incidence of light is directly related to the energy output from a PV module. As such, the findings of this research provide useful information that can be used by PV system installers and designers to determine the optimum tilt and orientation for a given installation in order to optimize the energy yield and increase overall efficiency [36]. Furthermore, the optimal tilt angle should be re-evaluated periodically as factors such as seasonal weather patterns, soiling, and dust accumulation can lead to a reduction in the energy output of the PV system if they are not taken into account in order to maximize the performance of the system. Additionally, it is important to consider other factors that may affect the performance of the PV module, such as cloud cover and snow accumulation, as these can significantly reduce the energy output from a system if they are not taken into consideration when deciding on the optimal tilt angle and orientation for a PV system. Thus, this research indicates that there are a number of factors to consider when determining the optimal tilt angle and orientation for a PV system in order to maximize its energy output, maximize its overall efficiency, and ensure that it continues to yield the maximum possible energy output over time. In general, this research highlights the importance of considering a variety of factors when deciding on the optimal tilt angle and orientation for a PV system in order to maximize its efficiency.

From Table 3, it can be seen that the global horizontal irradiance and maximum incident solar radiation estimated using equations 2–8 vary considerably from one site to another, even for locations with equivalent latitude angles, which further emphases the importance of taking all relevant factors into consideration when determining the optimal tilt angle and the orientation of a PV system. These results demonstrate the importance of taking location-specific characteristics [37], such as local climate [38] and cloud cover [39], into account when deciding on the optimal tilt angle and orientation for a PV system in order to maximize its efficiency and ensure that it continues to yield the maximum possible energy output over time. The results of this research indicate that the optimal tilt angle and orientation of a PV system should be determined based on the combination of multiple factors such as global horizontal irradiance [40], latitude [41], maximum incident solar radiation [42], and cloud cover [43].

In addition to latitude, orientation, and tilt angle, the intensity of cloud cover [44] and snow accumulation [45] should also be taken into consideration when deciding on the optimal tilt angle and orientation for a PV system in order to maximize its efficiency and ensure that it continues to yield the maximum possible energy output over time. Furthermore, the results of this research provide a valuable insight into the importance of accurately assessing the local climate conditions and taking all relevant factors into consideration when deciding on the optimal tilt angle and orientation for a PV system in order to maximize its efficiency and ensure that it continues to yield the maximum possible energy output over time.

For instance, although Bujumbura and Yaounde reported equivalent latitudes (3.61 ^{o}N and 3.84 oN, respectively), their yearly global solar radiation registered 194.4 W/m^2 and 184.3 W/m2, respectively indicating that Bujumbura receives significantly more solar radiation than Yaounde due to the different cloud cover [45], and snow accumulation factors [46] demonstrating that these are important elements to consider when making decisions regarding PV systems in different locations. The study further showed that even in locations with similar latitudes, other local climate factors such as cloud cover and snow accumulation could significantly affect the performance of a PV system and, therefore, should be taken into consideration in order to ensure that the PV system continues to yield the maximum possible energy output over its lifetime. Similarly, Monaco and Sarajevo recorded equivalent latitudes (43.73 ^{o}N and 43.51 oN, respectively), and their yearly global solar radiation recorded 163.33 W/m^2 and 150.1 W/m2, respectively demonstrating that even though the two locations share the same latitude, Monaco still receives significantly more solar radiation due to a combination of different local factors [47] , showing again how important it is to consider other climate factors in addition to latitude when deciding on the optimal tilt angle and orientation for a PV system in order to maximize its efficiency and ensure that it continues to yield the maximum possible energy output over time.

These results indicate that while latitude is an important factor to consider when determining the optimal tilt angle and orientation for a PV system, other local climate factors such as cloud cover and snow accumulation must also be taken into account in order to ensure that the system continues to perform at peak capacity and yield the maximum possible energy output over its lifetime. These findings are further evidence that latitude alone is not enough to accurately predict the energy output of a PV system and that an analysis of all local climate factors is necessary in order to accurately determine the optimal tilt angle and orientation for a given PV system in order to ensure that the system continues to yield the maximum possible energy output over its lifetime. Other relevant climate factors must also be taken into consideration when designing and installing a PV system in order to accurately predict the energy output and determine the optimal tilt angle and orientation of a PV system.

Higher annual energy gains were reported for clean global tilted irradiance using pyr1 (2.403%), pyr2 (2.3006%), and 2.35207% for mean pyr1 and pyr2 compared to 1.929528%, 1.82688%, and 1.87817% recorded for soiled global tilted irradiance using pyr1, pyr2, and mean pyr1 and pyr2 respectively, as presented in Table 4 and Fig. 1. These findings show that the optimal tilt angle and orientation of a PV system should not be based solely on latitude, but also on other climate factors such as cloud cover, snow accumulation, and global tilted irradiance. These findings demonstrate the importance of accurately determining the optimal tilt angle and orientation of a PV system in order to ensure that the system is able to yield the maximum possible energy output over its lifetime. In addition to latitude, it is also important to consider other local climate factors when designing and installing a PV system, as they can greatly affect the amount of energy the system is able to generate.

These results are lower than the annual energy for an annual timescale of 65% reported by Jamil et al. [31] and 4.39% for a temperate climate for an annual optimum tilt in comparison with a horizontal surface Jamil et al. [48]. These findings indicate that the determination of the optimal tilt angle and orientation of a PV system must take into account local climate conditions, such as cloud cover, snow accumulation, and global tilted irradiance, to ensure that the system is able to generate the maximum amount of

energy over its lifetime. In general, the optimal tilt angle and orientation of a PV system must be determined accurately in order to maximize its energy output over its lifetime. For example, a PV system in the northern hemisphere with a tilt angle of 15° and an azimuth angle of 180° will provide a higher energy yield than one with an azimuth angle of 135° due to seasonal differences in radiation. These differences can be attributed to the fact that the impact of soiling on PV in Jodhpur and Bangalore, India, is higher in Mumbwe, Zambia, located in Sub-Saharan Africa, because of its proximity to an arid environment.

The findings suggest that the determination of the optimal tilt angle and orientation for a PV system is essential to ensuring that it performs optimally over its lifetime and that, depending on the location of the system, soil and environmental conditions should be taken into consideration when calculating the optimal tilt angle and orientation. From Table 4, it can be seen that the clean energy indicator yielded appreciable values from January to December and annually (0.4737%) except the month of July, 2018 that reported a negative value of -0.1035%; whereas, the soiling loss indicator vehemently yielded excepted negative values throughout the months except the month of July, 2018 that recorded a positive value of 0.1036% as shown in Fig. 2.

This indicates that in Mumbwe, Zambia, the soiling loss has a more significant effect on the performance of PV systems than the impact of seasonal variations in radiation when compared to Jodhpur and Bangalore, India. The main reason for this difference can be attributed to the presence of an arid climate in Mumbwe, Zambia, which leads to a high level of soiling due to dust and other airborne particles, thus reducing the efficiency of the PV system significantly when compared to the other locations. Thus, confirming that soiling impacts negatively on PV performance as reported by numerous studies worldwide [49, 50, 51]. The findings of this study support the notion that regular cleaning of solar panels is a necessity in Mumbwe, Zambia, for optimal performance. This is in stark contrast to Jodhpur and Bangalore, India, where soiling did not appear to have a major effect on PV performance due to the lower levels of airborne particles present in their respective climates. As such, the data collected from Mumbwe, Zambia, serves as evidence that the environment can have a profound impact on PV performance and therefore should be taken into account when installing a solar system in any given region. The results from the study conducted in Mumbwe, Zambia, show that the environment can have a significant impact on PV performance and, as a result, regular cleaning of solar panels is essential in order to ensure optimal performance in the region and should be taken into consideration when planning a solar system installation. This research has revealed the importance of regular cleaning of solar panels, particularly in Mumbwe, Zambia, where airborne particles can have a significant effect on PV performance.

CONCLUSIONS

The orientation and tilt of PV modules can affect their performance in terms of capturing solar irradiance and thus their potential to produce electricity. This research validates the report that an optimum tilt angle and a clean PV system perform better than horizontally mounted PV and soiled PV systems. The optimal tilt angle and orientation for a PV system should be determined based on multiple factors such as global horizontal irradiance, latitude, maximum incident solar radiation, and cloud cover. This research

provides insight into the importance of accurately assessing local climate conditions and taking all relevant factors into consideration when deciding on the optimal tilt angle and orientation for a PV system. The following represents the major findings from this study:

1. The cleaned tilted collector emerged as the best performing collector due to higher H_{max} and energy gain, while CGI showed an appreciable performance of 0.4737% over SLI.
2. As a result of adjusting PV cleaning schedules for the greatest return on investment in Mumbwe, Zambia, CGI increases noticeably, by about 0.4737%.
3. Due to the fact that the models were generated using high latitude location datasets from the Asian continent, the results showed that the two models taken from the literature overestimated the observed yearly optimum tilt angle in this paper.
4. The maximum incident solar radiation values were significantly higher than the global horizontal irradiance (H) as expected in all locations investigated, demonstrating excellent performance of the newly established monthly and yearly global radiation indicator (GRI) coefficient models used for evaluating maximum incident solar radiation in the Mediterranean region and other low latitude locations around the world.

ACKNOWLEDGMENTS

The authors are grateful to the Energy Sector management Assistance Program power by the World Bank Group for providing the data used in this research.

CONFLICTS OF INTEREST

The authors declare that there is no conflict of interests regarding the publication of this paper.

REFERENCES

[1] Nwokolo, S. C., & Ogbulezie, J. C. (2018). A qualitative review of empirical models for estimating diffuse solar radiation from experimental data in Africa. *Renew Sustain Energy Rev*, *92,* 353-393. doi: https://doi.org/10.1016/j.rser.2018.04.118

[2] Nwokolo, S. C., & Ogbulezie, J. C. (2018). A quantitative review and classification of empirical models for predicting global solar radiation in West Africa. *Beni-Suef Univ J Basic Appl Sci*, *7*, 367–96. doi: https://doi.org/10.1016/j.bjbas.2017.05.001

[3] Obiwulu, A. U., Erusiafe, N., Olopade, M. A., & Nwokolo, S. C. (2020). Modeling and optimization of back temperature models of mono-crystalline silicon modules with special focus on the effect of meteorological and geographical parameters on PV performance. *Renew Energy*, *154*, 404-431. doi : https://doi.org/10.1016/j.renene.2020.02.103

[4] Obiwulu, A. U., Chendo, M. A. C., Erusiafe, N., & Nwokolo, S. C. (2020).

Implicit meteorological parameter-based empirical models for estimating back temperature solar modules under varying tilt-angles in Lagos, Nigeria. *Renew Energy, 145*, 442-457. doi: https://doi.org/10.1016/j.renene.2019.05.136

[5] Hassan, M. A., Bailek, N., Bouchouicha, K., & Nwokolo, S. C. (2021). Ultra-short-term exogenous forecasting of photovoltaic power production using genetically optimized non-linear auto-regressive recurrent neural networks. *Renew Energy*, *171*, 191–209. doi: https://doi.org/10.1016/j.renene.2021.02.103

[6] Hassan, M. A., Bailek, N., Bouchouicha, K., Ibrahim, A., Jamil, B., Kuriqi, A Nwokolo, S. C., & El-kenawy, E. M. (2022). Evaluation of energy extraction of PV systems affected by environmental factors under real outdoor conditions. *Theor Appl Climatol*, *150,* 715–729. doi: https://doi.org/10.1007/s00704-022-04166-6

[7] Nwokolo, S. C., Obiwulu, A. U., & Ogbulezie, J. C. (2023). Machine Learning and Analytical Model Hybridization to Assess the Impact of Climate. *Physics and Chemistry of the Earth*,*120*, 103389.

[8] Agbor, M. E., Udo, S. O., Ewona, I. O., Nwokolo, S. C., Ogbulezie, J. C., Amadi, S. O., & Billy, U. A. (2023). Effects of Angstrom-Prescott and Hargreaves-Samani Coefficients on Climate Forcing and Solar PV Technology Selection in West Africa. *Trends in Renewable Energy*, *9*, 78-106. doi: https://doi.org/10.17737/tre.2023.9.1.00150

[9] Agbor, M., Udo, S., Ewona, I., Nwokolo, S. C., & Ogbulezie, J. A. (2023). Potential impacts of climate change on global solar radiation and PV output using the CMIP6 model in West Africa. *Clean Eng Technol*, (In Press).

[10] Nwokolo, S. C., Julie, C., Ogbulezie, J. A., & Obiwulu, A. U. (2022). Impacts of Climate Change and Meteo-Solar Parameters on Photosynthetically Active Radiation Prediction Using Hybrid Machine Learning with Physics-Based Models. *Advances in Space Research*, *70*(11), 3614–37

[11] Martial, A., Akata, E. A., Njomo, D., Agrawal, B., Mackpayen, A., & Ali, A. M. (2022). Tilt Angle and Orientation Assessment of Photovoltaic Thermal (PVT) System for Sub-Saharan Tropical Regions: Case Study Douala, Cameroon. *Sustainability*, *14*(23), 15591. doi: https://doi.org/10.3390/su142315591

[12] Karahüseyin, T. S. A. (2022). Performance Loss Rates of a 1 MWp PV Plant with Various Tilt Angle , Orientation and Installed Environment in the Capital of Cyprus. *Sustainability*, *14*(15), 9084. doi: https://doi.org/10.3390/su14159084

[13] Dhimish, M., & Alrashidi, A. (2022). Photovoltaic degradation rate affected by different weather conditions: A case study based on pv systems in the uk and australia. *Electronics*, *9*(4), 650. doi: https://doi.org/10.3390/electronics9040650

[14] Jordan, D. C., Silverman, T. J., Wohlgemuth, J. H., Kurtz, S. R., & VanSant, K. T. (2017). Photovoltaic failure and degradation modes. *Prog Photovoltaics Res Appl*, *25*(4), 318-326. doi: https://doi.org/10.1002/pip.2866

[15] Frick, A., Makrides, G., Schubert, M., Schlecht, M., & Georghiou, G. E. (2020). Degradation rate location dependency of photovoltaic systems. *Energies*, *13*(24), 6751. doi: https://doi.org/10.3390/en1324675

[16] Khan, F., & Kim, J. H. (2019). Performance Degradation Analysis of c-Si PV Modules Mounted on a Concrete Slab under Hot-Humid Conditions Using Electroluminescence Scanning Technique for Potential Utilization in Future Solar Roadways. *Materials*, *12*(24), 4047. doi: https://doi.org/10.3390/ma12244047

[17] Kyranaki, N., Smith, A., Yendall, K., Hutt, D. A., Whalley, D. C., Gottschalg, R.,

& Betts, T. R. (2022). Damp-heat induced degradation in photovoltaic modules manufactured with passivated emitter and rear contact solar cells. *Prog Photovoltaics Res Appl*, *30*(9), 1061-1071. doi: https://doi.org/10.1002/pip.3556

[18] Quansah, D. A., Adaramola, M. S., & Takyi, G. (2020). Degradation and longevity of solar photovoltaic modules—An analysis of recent field studies in Ghana. *Energy Sci Eng*, *8*(6), 2116-2128. doi: https://doi.org/10.1002/ese3.651

[19] Gopi, A., Sudhakar, K., Keng, N. W., & Krishnan, A. R. (2021). Comparison of normal and weather corrected performance ratio of photovoltaic solar plants in hot and cold climates. *Energy for Sustainable Development, 65,* 53-62. doi: https://doi.org/10.1016/j.esd.2021.09.005

[20] Ameur, A., Berrada, A., Bouaichi, A., & Loudiyi, K. (2022). Long-term performance and degradation analysis of different PV modules under temperate climate. *Renewable Energy*, *188*, 37-51. doi: https://doi.org/10.1016/j.renene.2022.02.025

[21] Silvestre, S., Tahri, A., Tahri, F., Benlebna, S., & Chouder, A. (2018). Evaluation of the performance and degradation of crystalline silicon-based photovoltaic modules in the Saharan environment. *Energy*, *152*, 57-63. doi: https://doi.org/10.1016/j.energy.2018.03.135

[22] Malvoni, M., Kumar, N. M., Chopra, S. S., and Hatziargyriou, N. (2020). Performance and degradation assessment of large-scale grid-connected solar photovoltaic power plant in tropical semi-arid environment of India. *Solar Energy*, *203*, 101-113. doi: https://doi.org/10.1016/j.solener.2020.04.011

[23] Hassan Daher, D., Gaillard, L., & Ménézo, C. (2022). Experimental assessment of long-term performance degradation for a PV power plant operating in a desert maritime climate. *Renewable Energy*, *187*, 44-55. doi: https://doi.org/10.1016/j.renene.2022.01.056

[24] Lu, H., Lu, L., & Wang, Y. (2016). Numerical investigation of dust pollution on a solar photovoltaic (PV) system mounted on an isolated building. *Applied Energy*, *180*, 27-36. doi: https://doi.org/10.1016/j.apenergy.2016.07.030

[25] Ekoe A Akata, A. M., Njomo, D., & Agrawal, B. (2017). Assessment of Building Integrated Photovoltaic (BIPV) for sustainable energy performance in tropical regions of Cameroon. *Renewable and Sustainable Energy Reviews, 80*, 1138-1152. doi: https://doi.org/10.1016/j.rser.2017.05.155

[26] Gholampour, M., & Ameri, M. (2016). Energy and exergy analyses of Photovoltaic/Thermal flat transpired collectors: Experimental and theoretical study. *Applied Energy*, *164*, 837-856. doi: https://doi.org/10.1016/j.apenergy.2015.12.042

[27] Obiwulu, A. U., Erusiafe, N., Olopade, M .A., & Nwokolo, S. C. (2022). Modeling and estimation of the optimal tilt angle, maximum incident solar radiation, and global radiation index of the photovoltaic system. *Heliyon*, *8*(6). doi: https://doi.org/10.1016/j.heliyon.2022.e09598

[28] Maghami, M. R., Hizam, H., Gomes, C., Radzi, M. A., Rezadad, M. I., & Hajighorbani, S. (2016). Power loss due to soiling on solar panel: A review. *Renewable and Sustainable Energy Reviews*, *59,* 1307-1316. doi: https://doi.org/10.1016/j.rser.2016.01.044

[29] Jacobson, M. Z., & Jadhav, V. (2018). World estimates of PV optimal tilt angles and ratios of sunlight incident upon tilted and tracked PV panels relative to horizontal panels. *Solar Energy*, *169*, 55-66. doi:

https://doi.org/10.1016/j.solener.2018.04.030
[30] Talebizadeh, P., Mehrabian, M. A., & Abdolzadeh, M. (2011). Determination of Optimum Slope Angles of Solar Collectors Based on New Correlations. *Energy Sources, Part A: Recovery, Utilization, and Environmental Effects*, *33*(17), 1567-1580. doi: https://doi.org/10.1080/15567036.2010.551253
[31] Jamil, B., Siddiqui, A. T., & Denkenberger, D. C. (2019). Solar radiation on south-facing inclined surfaces under different climatic zones in India. *Environ Prog Sustain Energy*, *38*(3), e13050. doi: https://doi.org/10.1002/ep.13050
[32] Mulcué-Nieto, L. F., & Mora-López, L. (2015). Methodology to establish the permitted maximum losses due to shading and orientation in photovoltaic applications in buildings. *Applied Energy*, 137, 37-45. doi: https://doi.org/10.1016/j.apenergy.2014.09.088
[33] N'Tsoukpoe, K. E. (2022). Effect of orientation and tilt angles of solar collectors on their performance: Analysis of the relevance of general recommendations in the West and Central African context. *Scientific African*, *15*, e01069. doi: https://doi.org/10.1016/j.sciaf.2021.e01069
[34] Haghdadi, N., Copper, J., Bruce, A., & MacGill, I. (2017). A method to estimate the location and orientation of distributed photovoltaic systems from their generation output data. *Renewable Energy*, *108*, 390-400. doi: https://doi.org/10.1016/j.renene.2017.02.080
[35] Hartner, M., Ortner, A., Hiesl, A., & Haas, R. (2015). East to west – The optimal tilt angle and orientation of photovoltaic panels from an electricity system perspective. *Applied Energy*, *160*, 94-107. doi: https://doi.org/10.1016/j.apenergy.2015.08.097
[36] Mukisa, N., & Zamora, R. (2022). Optimal tilt angle for solar photovoltaic modules on pitched rooftops: A case of low latitude equatorial region. *Sustainable Energy Technologies and Assessments, 50,* 101821. doi: https://doi.org/10.1016/j.seta.2021.101821
[37] Nwokolo, S. C., Amadi, S. O., Obiwulu, A. U., Ogbulezie, J. C., & Eyibio, E. E. (2022). Prediction of global solar radiation potential for sustainable and cleaner energy generation using improved Angstrom-Prescott and Gumbel probabilistic models. *Cleaner Engineering and Technology, 6,* 100416. doi: https://doi.org/10.1016/j.clet.2022.100416
[38] Nwokolo, S. C., Obiwulu, A. U., Ogbulezie, J. C., & Amadi, S. O. (2022). Hybridization of Statistical Machine Learning and Numerical Models for Improving Beam, Diffuse and Global Solar Radiation Prediction. *Cleaner Engineering and Technology*, *9*, 100529. doi: https://doi.org/10.1016/j.clet.2022.100529
[39] Nwokolo, S. C., & Otse C. (2019). Impact of Sunshine Duration and Clearness Index on Diffuse Solar Radiation Estimation in Mountainous Climate. *Trends Renew Energy, 5,* 307–32. doi: https://doi.org/10.17737/tre.2019.5.3.00107
[40] Ituen, E. E., Esen, N. U., Nwokolo, S. C., & Udo, E. G. (2012). Prediction of global solar radiation using relative humidity, maximum temperature and sunshine hours in Uyo, in the Niger Delta Region, Nigeria. *Adv Appl Sci Res*, *3,* 1923–37.
[41] Nwokolo, S. C., & Ogbulezie, J. C. (2017). A single hybrid parameter-based model for calibrating hargreaves-samani coefficient in Nigeria. *Int J Phys Res*, *5*, 49. doi: https://doi.org/10.14419/ijpr.v5i2.8042
[42] Nwokolo, S. C., & Ogbulezie, J. C. (2017). A critical review of theoretical models

for estimating global solar radiation between 2012-2016 in Nigeria. *Int J Phys Res, 5,* 60. doi: https://doi.org/10.14419/ijpr.v5i2.8160

[43] Nwokolo, S. C., & Ogbulezie, J. C. (2017). Performance evaluation of existing sunshine-based computing models for estimating global solar radiation at Lagos, Nigeria. *Int J Adv Astron, 5,* 106. doi: https://doi.org/10.14419/ijaa.v5i2.8308

[44] Nwokolo, S. C., & Ogbulezie, J. C. (2017). Estimation of direct normal irradiance under various sky condi-tions in data sparse tropical ecological zones in Nigeria. *Int J Adv Astron*, *5,* 90. doi: https://doi.org/10.14419/ijaa.v5i2.8329

[45] Ogbulezie, J. C., James, O. J., & Nwokolo, S. C. (2017). A review of regression models employed for predicting diffuse solar radiation in North-Western Africa. *Trends Renew Energy, 3*(2), 160-206. doi: https://doi.org/10.17737/tre.2017.3.2.0042

[46] Nwokolo, S. C. (2017). A comprehensive review of empirical models for estimating global solar radiation in Africa. *Renew Sustain Energy Rev*, *78*, 955–95. doi: https://doi.org/10.1016/j.rser.2017.04.101

[47] Amadi, S., Dike, T., Nwokolo, S. C. & Amadi, S. (2020). Global Solar Radiation Characteristics at Calabar and Port Harcourt Cities in Nigeria. *Trends in Renewable Energy, 6,* 101-120. doi: 10.17737/tre.2020.6.2.00114

[48] Jamil, B., Siddiqui, A. T., & Akhtar, N. (2016). Estimation of solar radiation and optimum tilt angles for south-facing surfaces in Humid Subtropical Climatic Region of India. *Engineering Science and Technology, an International Journal*, *19*(4), 1826-1835. doi: https://doi.org/10.1016/j.jestch.2016.10.004

[49] Ghazi, S., Sayigh, A., & Ip, K. (2014). Dust effect on flat surfaces – A review paper. *Renewable and Sustainable Energy Reviews, 33,* 742-751. doi: https://doi.org/10.1016/j.rser.2014.02.016

[50] Darwish, Z. A., Kazem, H. A., Sopian, K., Al-Goul, M. A., & Alawadhi, H. (2015). Effect of dust pollutant type on photovoltaic performance. *Renewable and Sustainable Energy Reviews, 41,* 735-744. doi: https://doi.org/10.1016/j.rser.2014.08.068

[51] Mani, M., & Pillai, R. (2010). Impact of dust on solar photovoltaic (PV) performance: Research status, challenges and recommendations. *Renewable and Sustainable Energy Reviews*, *14*(9), 3124-3131. doi: https://doi.org/10.1016/j.rser.2010.07.065

Trends in Renewable Energy
OPEN ACCESS ISSN: 2376-2144
Peer-Reviewed Review Article futureenergysp.com/index.php/tre

Research Progress of Nanofluid Heat Pipes in Automotive Lithium-ion Battery Heat Management Technology

Xinyu Wang,* Yanan Zhao, Yezhu Jin

School of Mechanical Engineering, North China University of Water Resources and Electric Power, Zhengzhou, Henan 450045, China

Received March 11, 2023; Accepted March 21, 2023; Published March 22, 2023

Power batteries are a crucial component of electric vehicles and other electric equipment. Their long-term high-rate discharge generates a lot of heat, which can lead to battery failure, shortened battery life, and even safety accidents if not managed properly. Due to its high thermal conductivity, the heat pipe can quickly conduct heat away from the battery and separate the heat source from the heat sink. In addition, due to its excellent isothermal performance, the heat pipe can also achieve the characteristics of low-temperature preheating and high-temperature cooling of the power battery by reducing the inhomogeneity of the battery temperature field to reduce the temperature difference. In this paper, we review the current state of the art in thermal management of automotive lithium-ion battery, and highlight the current state of thermal management of batteries based on the combination of nanofluids and heat pipes. Finally, the development of nanofluidic heat pipes in lithium-ion battery heat management systems is prospected.

Key Words: Battery heat management; Heat pipe; Nanofluid heat pipe; Lithium-ion battery

Introduction

As one of the pillars of development, energy plays a decisive role in social and economic development. But with the overuse of traditional fossil energy, global warming, and frequent haze, people pay more and more attention to environmental problems in recent years. Countries have recognized the need for energy transition, and electric vehicles have become a strategic choice [1]. Because of its high energy density and long service life, the lithium-ion battery has become the mainstream of electric vehicle power cells and has a great development prospect in the automotive industry [2]. With the development of lithium-ion battery technology and the support of national policies, the sales of electric vehicles are increasing, so the demand for lithium-ion batteries is also increasing [3]. According to the 2022 Green Battery Annual Conference and the 1,000 people conference on lithium-ion new energy in China, global power lithium-ion battery shipments will be 685.3GWh in 2022. It is expected to reach about 1.7 TWh in 2025, this is 1.5 times more than in 2022 (Figure 1).

*Corresponding author: 1278792329@qq.com

Tr Ren Energy, 2023, Vol.9, No.2, 137-156. doi: 10.17737/tre.2023.9.2.00157

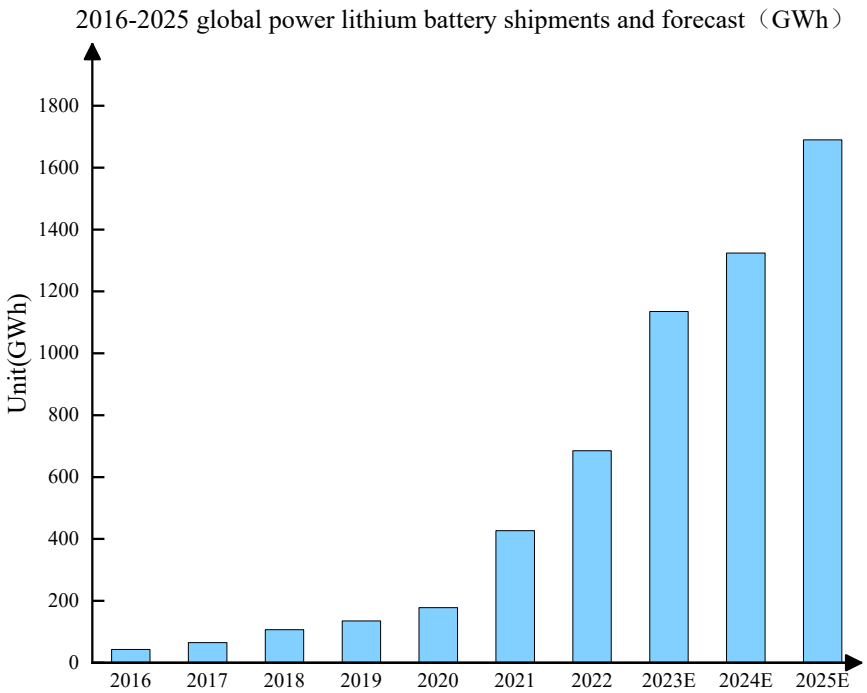

Figure 1. Global shipments of lithium batteries

However, behind the high sales volume is also hidden a huge security risk. In recent years, with the gradual maturity of lithium-ion battery technology, the increasing energy density of lithium-ion batteries and the increasing number of batteries used, electric vehicles have experienced frequent spontaneous combustion accidents [4]. According to statistics, in the first quarter of 2022 alone, there were 640 spontaneous combustion accidents of electric vehicles, an increase of 31% year-on-year, including many well-known brands such as Jády, Tesla, and Xiaopeng. Some safety incidents are shown in Table 1. Most of these spontaneous combustion accidents are caused by the overheating of the battery pack and the out-of-control heating of the battery, which leads to the rupture of the battery case. These accidents seriously threaten the safety of drivers and passengers and draw people's attention to the safety of lithium batteries.

Table 1. Statistics on domestic electric vehicle spontaneous combustion accidents in the first half of 2022

Date of accident	Brand	Type of battery	Event
7.22	Tesla	Ternary lithium battery	The car caught fire after the crash
7.14	Weimar	Ternary lithium battery	Fire during charging
7.5	Roc	Ternary lithium battery	The car caught fire after the crash
7.3	Roewe	Ternary lithium battery	A fire broke out while driving
6.14	Byd	Lithium iron phosphate battery	Stationary parking (caused by car owner modification)
6.6	Byd	Lithium iron phosphate battery	A fire broke out while driving

The lithium-ion battery is mainly composed of five parts: positive pole, negative pole, electrolyte, diaphragm, and shell [5] (as shown in Figure 2). At the same time, the heat generation of lithium batteries mainly comes from the electrochemical reaction heat during charging and the ohmic internal resistance joule heat during discharge [6]. According to research, the temperature of lithium-ion batteries has a great impact on their life. At 20~40 ℃, the battery life will be shortened by 60 days for each degree of temperature increase [7]. When the temperature is too high, the solid electrolyte facial mask (SEI film) in the lithium-ion battery will accelerate the decomposition and generate gas in the battery, thus causing the battery to break or even fire [8]. If the lithium battery catches fire, it will not only damage the car but also cause unnecessary casualties. Therefore, the selection of an appropriate thermal management system and the research on lithium-ion battery cooling systems are of great significance in improving the performance and economy of electric vehicles [9].

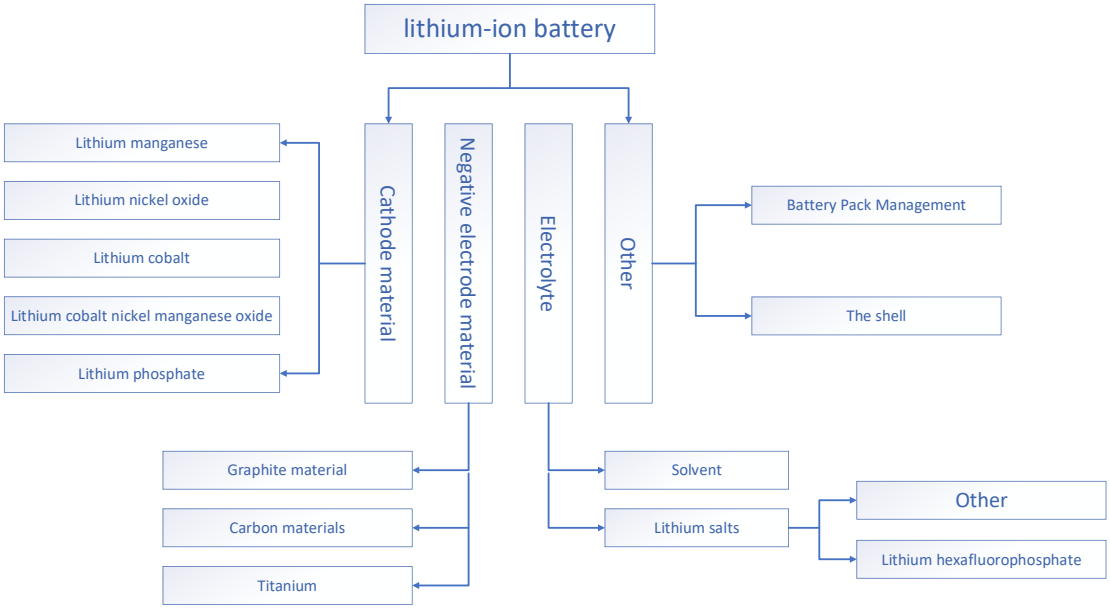

Figure 2. Structure diagram of lithium battery.

Common Battery Cooling Technology

There are five common battery cooling technologies: air cooling, liquid cooling, refrigerant direct cooling, phase change material cooling, and heat pipe cooling [10]. Among them, the cooling mode of air, liquid, and refrigerant is active cooling, and the phase change materials and heat pipes are passive cooling (as shown in Figure 3). This article will describe four methods of cooling: air cooling, liquid cooling, phase change material cooling, and heat pipe cooling, with emphasis on the research status of nanofluid heat pipe cooling technology in lithium ion vehicle batteries.

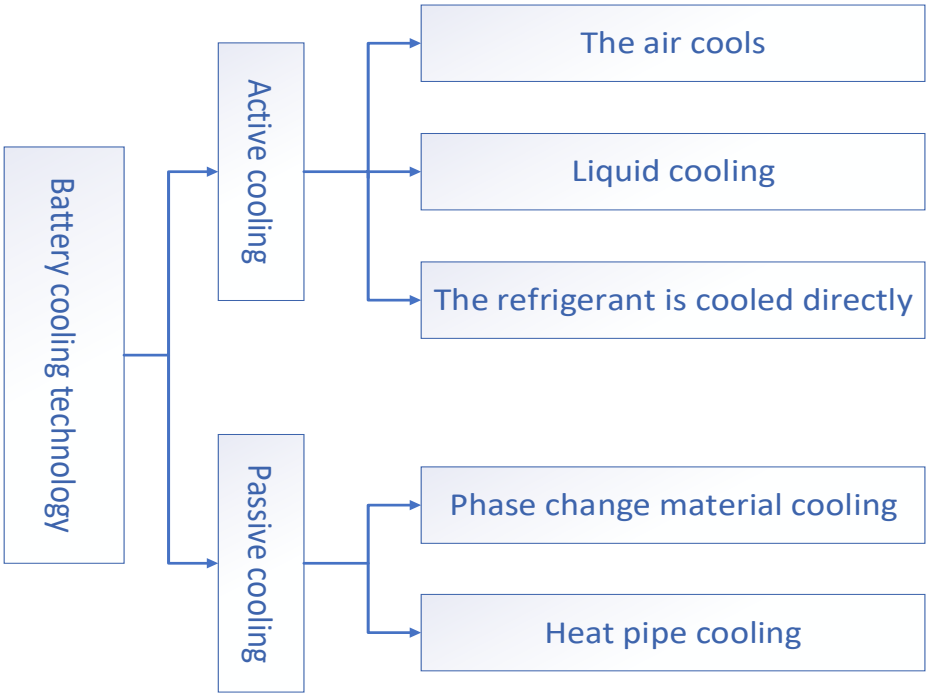

Figure 3. Classification of battery cooling technology.

Air Cooling

Air cooling includes natural convection and forced convection. Natural convection is to use the natural flow of external air to make the airflow through each surface of the battery, thus achieving the cooling effect. Forced convection generally uses fans to extract external air and control wind speed to achieve the effect of battery cooling. Compared with natural air convection, forced convection is more controllable for battery cooling. Because air cooling has the characteristics of low cost, easy maintenance, small use space and simple design, air cooling has always been a common cooling method in battery thermal management systems.

There are two ways to dissipate heat in the air duct: series and parallel [11] (as shown in Figure 4). It is easy to know from Figure 4 (a) that the heat dissipation of the series air duct will lead to the phenomenon of low inlet temperature and high outlet temperature, and the whole temperature field is uneven. Compared with the series air duct, the airflow of each part is the same, and the temperature distribution is relatively uniform. For example, Honda Insight and Toyota RAV-4 adopt the parallel air duct design.

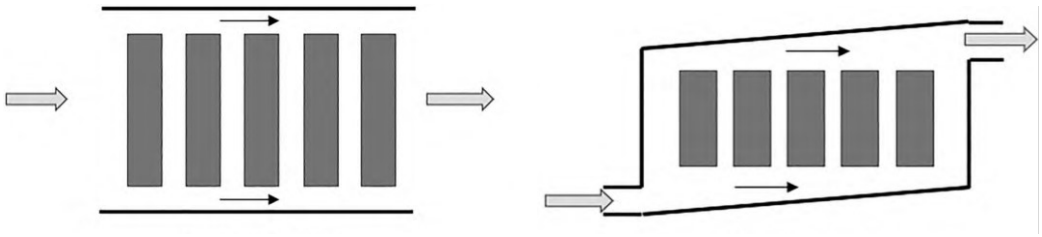

Figure 4. a) Series air duct b) Parallel air duct

The key to the quality of air cooling technology is the size of the air inlet and the quality of the air channel. Therefore, the improvement and optimization of air ducts and

the arrangement of batteries are the main research directions of air cooling. However, in essence, although air cooling has a simple structure and saves space, it has a low thermal conductivity and absorbs less heat than the same volume of liquid. Therefore, air cooling is currently mainly used for the cooling requirements of low-power and small-volume battery packs. With the continuous development of lithium-ion batteries, air cooling is gradually difficult to meet the required technical requirements [12].

Liquid Cooling

The heat transfer coefficient of liquid is greater than that of gas. Under high load, the cooling effect of liquid is better than that of gas. When liquid cooling is used at the same time, the volume is smaller and the space is saved [13]. There are two types of liquid cooling: direct cooling and indirect cooling [14]. Direct cooling is to directly contact the coolant with the object to be cooled, or even completely soak the object to achieve the purpose of cooling. The advantage of direct cooling is that it can maintain the constant temperature of the object to be cooled, and the overall temperature difference is small. The disadvantage is that it has high requirements for the type of cooling liquid. The more commonly used cooling liquid is mineral oil and glycol. Indirect cooling is generally achieved by winding an infusion pipe with coolant inside the object to be cooled, or by using a cooling plate without direct contact with the object. Indirect cooling has fewer restrictions on the type of coolant, but it needs a series of supporting equipment, which is not conducive to the lightweight design of vehicles [15].

Due to the risk of liquid leakage from direct cooling and the high requirements for cooling medium insulation. Currently, the indirect cooling method is mostly used, as shown in Figure 5, the bottom plate cooling system is the mainstream of current liquid cooling research. In the research of liquid plate cooling, Jiaqiang *et at.* [16] designed a rectangular channel coolant plate, and the study showed that the average temperature of the power cell was the lowest when the width of the rectangular channel was 45 mm, the height was 5 mm, the number of channels was 4, and the coolant flow rate was 0.07 m/s. Among these four influencing parameters, the number of channels has the greatest effect on the cell temperature, and the size of the rectangular channels has the least effect on the cell temperature. In addition, the heat transfer performance of the coolant, *i.e.,* the thermal conductivity of the coolant, is also an important factor affecting the cooling effect. Maxwell [17] was the first to propose increasing the percentage of solid particles in the liquid to enhance the thermal conductivity of the coolant. However, solid particles tended to accumulate in coolants with low flow rates and cause blockages. Therefore, the use of smaller particles (*i.e.*, nanoparticles) may improve this problem. For example, Deng *et al.* [18] added nanoparticles to water, which led to improved cooling. Eastman *et al.* [19] added Cu nanoparticles with a volume fraction of 0.3% to a glycol solution, and the resulting nanofluid thermal conductivity was improved by 40%. According to the experimental data, the cooling effect of the coolant is better than that of water using nanofluids at low flow rates. At fast flow rates, water cooling is better than nanofluid.

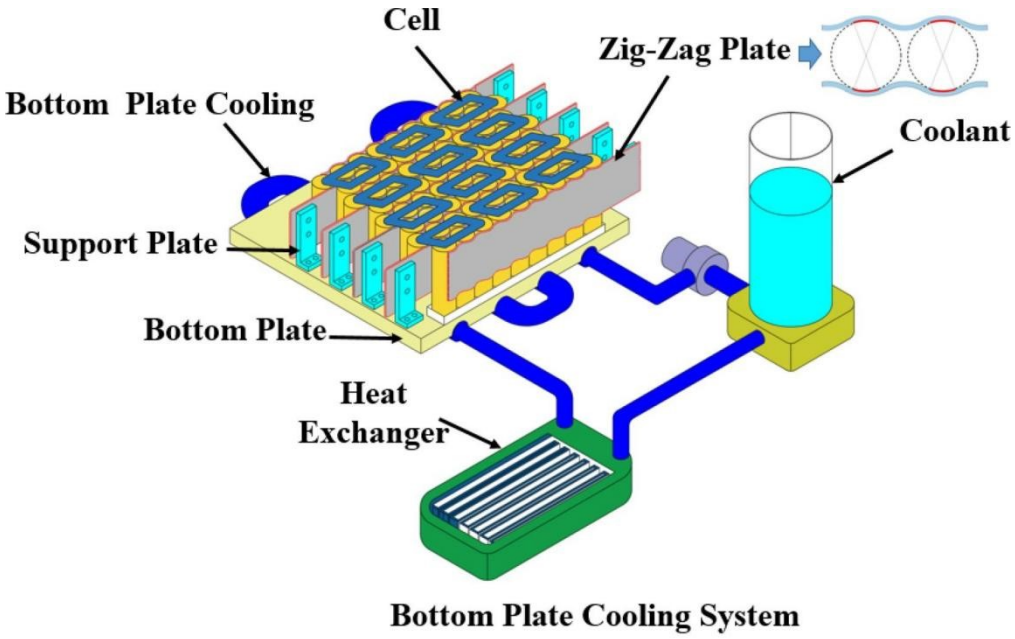

Figure 5. Bottom plate liquid cooling system [20].

Phase Change Material Cooling

With the change of temperature, the material whose state also changes is called phase change materials (PCM). Phase-change materials can absorb or release a large amount of heat under a small temperature change. Therefore, the cooling technology of phase-change materials absorbs the heat generated by battery charging and discharging during phase change through this characteristic of phase-change materials [21]. Phase change materials can be divided into solid-solid, solid-liquid, solid-gas and liquid-gas phase change materials according to the form and process of phase change, and can be divided into organic phase change materials and inorganic phase change materials according to the composition of the materials. Phase change materials, which are clean, pollution-free and heat storage capacity, are widely used in construction, clothing, refrigeration, aerospace, military, communications, power and other industries. In the cooling of lithium-ion batteries, paraffin is a phase change material that has been studied extensively. Schematic diagram of phase change material cooling in the battery is shown in Figure 6.

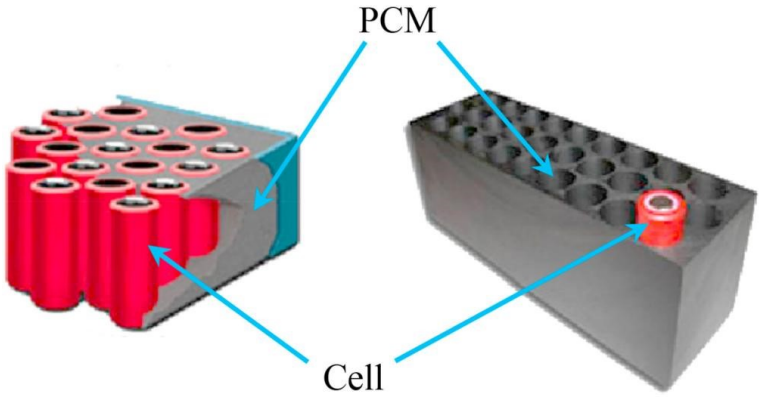

Figure 6. Phase-change material cooling system [22].

According to the research, under the condition of high temperatures and high discharge rates, the use of phase change material cooling is better than the use of air cooling. At the same time, phase change material cooling does not need a fan, which reduces the power compared with air cooling. Zou *et al*. [23] have prepared multi-walled carbon nanotubes (MWCNT), graphene-based, and MWCNT/graphene-based composite phase change materials (PCM) and carried out experimental studies. The results showed that the thermal conductivity of PCM was increased by 31.8%, 55.4%, and 124%, respectively, Compared with that of graphene-based PCM, MWCNT-based PCM, and pure PCM. The composite PCM shows great potential in thermal management of li-ion power batteries. Due to the low thermal conductivity of paraffin, Jiang *et al*. [24] combined graphene with paraffin to make graphene-paraffin composite phase change material (CPCM). The results showed that the composite material of graphene and paraffin can significantly reduce the temperature rise of lithium-ion batteries, and has an excellent performance in controlling the temperature uniformity of the battery pack. In addition, there are also studies on the structure of PCM, phase change materials, and other materials. Weng *et al*. [25] studied the thickness of phase change cooling and found that when the thickness of the PCM module is 10 mm, the cooling effect is the best. Choudhai *et al*. [26] combined phase change materials with fins, which reduced the battery temperature by 9.28%.

Phase change material cooling has simple structure, easy to manufacture and low cost, but there are a series of technical problems. Phase change material cooling belongs to passive cooling. When working in a long time and high temperature environment, timely heat dissipation is required, otherwise there is a risk of complete melting, leading to failure of the cooling system. At the same time, PCM melting will lead to volume increase and risk of leakage. In the research of phase change materials, the practicability of single phase change material is not high. It is necessary to focus on the research of composite phase change materials to obtain a safer and more effective phase change cooling system.

Heat Pipe Cooling

The heat pipe is efficient heat transfer equipment, developed by NASA in the early 1960s, used for heat pipe cooling systems in spacecraft. It is heat transfer equipment that can efficiently transfer heat under high-temperature and low-temperature environments. It has the advantages of fast heat transfer speed, high heat transfer efficiency and small thermal resistance, and is widely used in various heat management fields.

Heat pipe (HP) is a kind of passive cooling equipment. In most cases, it does not need to consume any external energy [27]. As shown in the cross-section of the conventional heat pipe in Figure 7, the heat pipe is composed of three parts: evaporation section, thermal insulation section, and condensation section. The working medium is usually liquid, forming a two-phase flow state of steam and liquid in the pipe. According to the thermodynamic principle, when a heat source heats one end of a heat pipe, the working medium inside the pipe vaporizes, carrying the absorbed heat to the other end, where it condenses into liquid, transferring the heat to the surrounding environment.

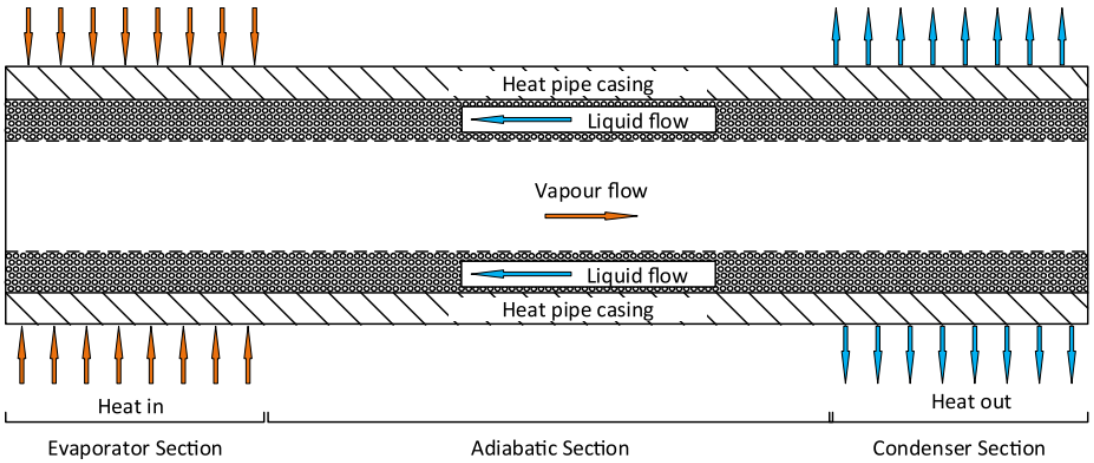

Figure. 7. Cross-section of a conventional heat pipe[28].

The heat pipe has been widely used in aerospace, electronics, machinery, and other fields due to its simple structure, reliable operation, and high heat transfer efficiency. For example, in spacecraft, a heat pipe can effectively control the temperature of spacecraft and prevent electronic components from overheating, thus improving the reliability and life of spacecraft. In electronic equipment, a heat pipe can effectively dissipate heat and protect electronic components from high temperature, thus improving the performance and life of electronic equipment. It has broad application prospects and huge development potential. For example, Mbulu *et al.* [29] developed a battery thermal management system (BTMS) based on heat pipes, as shown in Figure 8. The system uses L-shaped and I-shaped heat pipes instead of traditional battery clamps. The evaporator part absorbs heat from the aluminum plate surface, while the condenser part transfers heat to the copper bracket. With water as the cooling medium, the heat pipe is tested at 30, 40, 50, and 60W input power, and the condenser is cooled with 0.0167, 0.0333, and 0.05kg/s mass flow. The results show that the designed BTMS based on heat pipe can keep the maximum temperature (T_{max}) below 55℃ and the temperature difference at both ends of the battery even at the maximum input power(Δ T) Keep below 5℃.

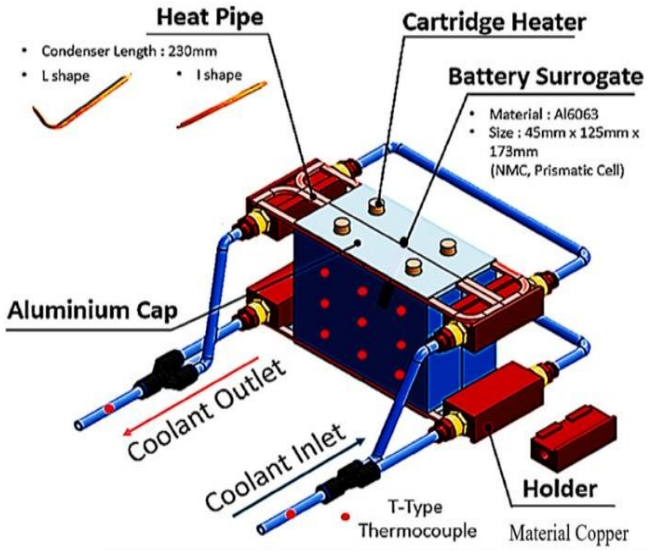

Figure 8. Battery BTMS based on L-shaped/I-shaped heat pipe [40].

Zhang and Wei [30] studied a heat pipe cooling system for square cells, which uses flat heat pipes to cool the battery pack. The results are shown in Figure 9. Compared with natural convection cooling and aluminum plate cooling, the maximum temperature difference is reduced by 73.7% and 50.1%, respectively. The use of a flat heat pipe can effectively reduce the maximum temperature and temperature difference of the battery while reducing energy consumption.

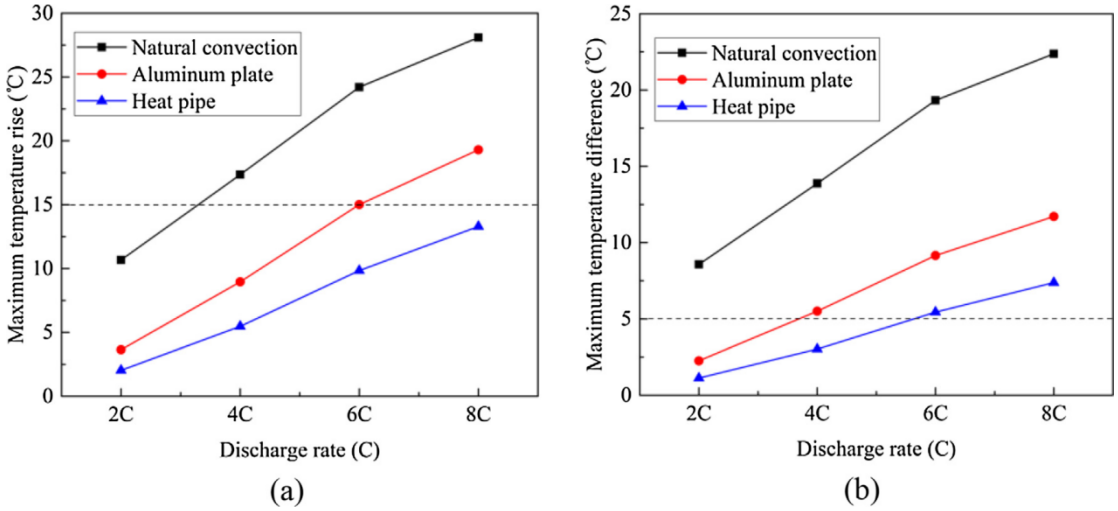

Figure 9. The maximum temperature rise and difference of the battery pack using different heat dissipation methods: (a) max temperature rise and (b) max temperature difference [30].

Battery Thermal Management System Based on Nano-fluid Heat Pipe

Nanofluid is a mixture of nanoparticles, molecules, and liquids with special physical and chemical properties [31]. As shown in Figure 10, nanofluids are widely used in various fields, such as biomedicine, material science, environmental science, energy engineering, etc. [32]. Compared with traditional fluids, nanofluids have a larger specific surface area and higher surface activity because their particle size is at the nanometer level. These characteristics make nanofluids show different properties from traditional fluids in terms of heat conduction, friction resistance, viscosity, etc. In addition, nanofluids also have good thermal stability and chemical stability, enabling them to operate stably under high temperatures, high pressure, and chemical corrosion environment. At the same time, nanofluids show outstanding characteristics in improving boiling heat transfer performance. Therefore, the method of applying nanofluids to heat pipes to improve the heat transfer efficiency of heat pipes came into being.

Baheta *et al.* [33] studied the effect of copper nanofluid with an average particle size of 20 nm and particle concentration of 0-4% on the heat transfer performance of cylindrical heat pipes. The results show that the thermal resistance of the heat pipe is reduced by 17.5% and the performance of the heat pipe is improved when the concentration of water-based copper nanofluid is 4% and the heat input is 100W. Reji *et al.* [34] used deionized water and aluminum (Al) nanofluids as heat transfer media in the heat pipe and conducted research in the range of heat input values from 40W to 200W. The results are shown in Figure 11. Compared with deionized water, the performance of siphon heat pipe using Al nanofluid is improved by 41%, and the maximum efficiency can reach 88% when the dip angle of the heat pipe is 60°.

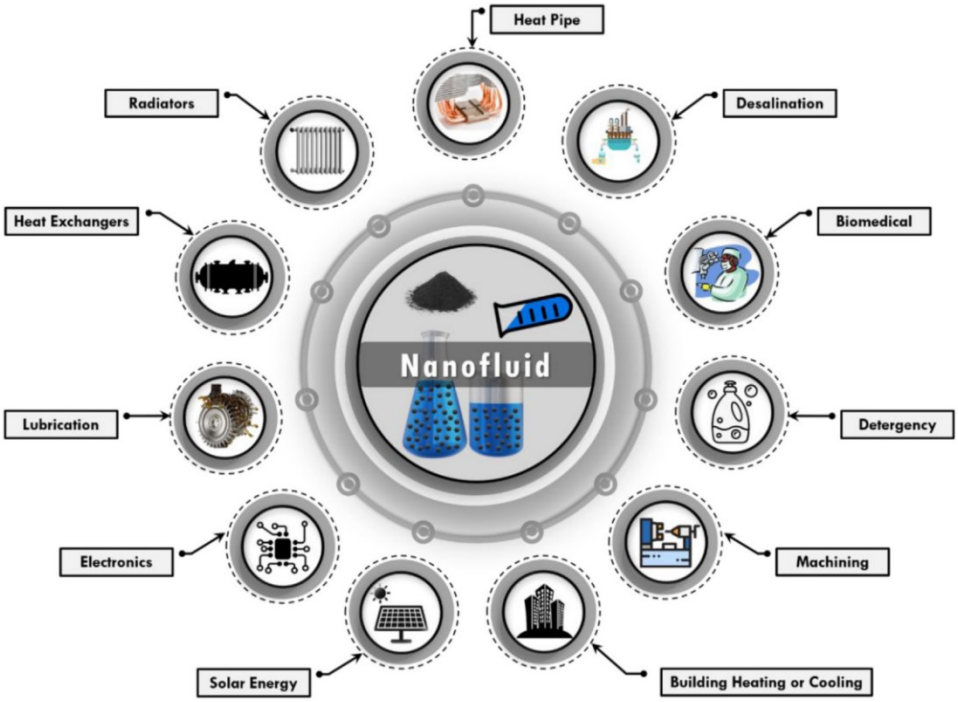

Figure 10. Nanofluid applications in different areas [32].

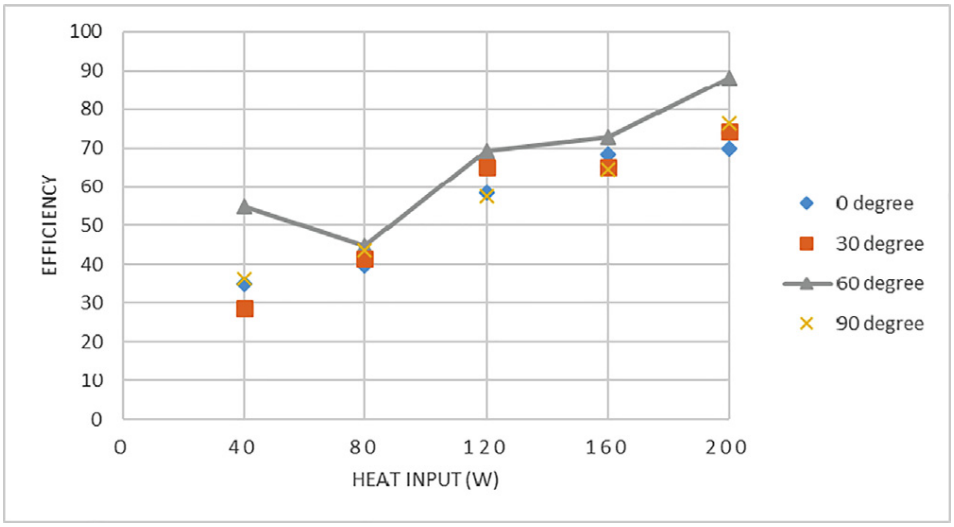

Figure 11. Effificiency of Heat Pipe with Nano Fluid [34].

Riehl *et al.* [35] studied and analyzed the loop heat pipe (LHP) using nickel oxide (NiO)-water (H_2O) nanofluid and the pulsating heat pipe using copper oxide (CuO)-water (H_2O) nanofluid, and compared the performance of the two with that of the loop heat pipe and pulsating heat pipe using deionized water. The results showed that LHP and OHP using nanofluid have higher heat transfer performance than the base fluid, The performance has been improved to different degrees. Zhang *et al.* [36] used the experimental device as shown in Figure 12 to carry out visualization experiments on SiO_2-H_2O nanofluid pulsating heat pipes with concentrations of 0.5 wt%, 1.0 wt%, 1.5 wt%, and 2.0 wt%, respectively using high-speed cameras. The results show that the addition of nanoparticles increases the instantaneous driving force of the working fluid, promotes the phase change of the working fluid of the pulsating heat pipe, is conducive to

the reflux of the condensate, and improves the performance of the heat pipe. When the heating power is 50W and the concentration is 1.0 wt%, the maximum heat transfer efficiency of the heat pipe can be increased by 40.1%.

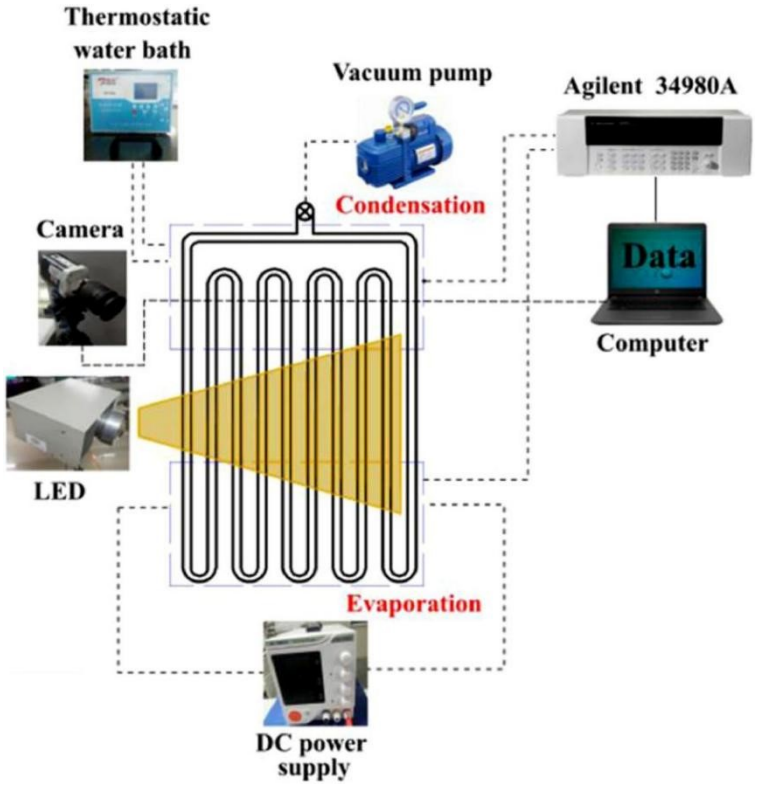

Figure. 12. Schematics of experimental apparatus[36].

To sum up, as a new type of working medium, nanofluid can greatly improve the heat transfer efficiency of heat pipe by selecting the appropriate nanofluid combined with heat pipe. The nanofluid heat pipe combines the advantages of the two and has a broader application prospect in the field of heat transfer. For example, it is of great significance to apply the nanofluid heat pipe to the thermal cooling of batteries [37].

Nasir *et al.* [38] conducted an experimental and numerical study on the application of alumina (Al_2O_3) nanofluid heat pipes in a lithium-ion battery thermal management system (HPTMS). The results showed that the battery temperature was reduced by 7.28°C (1.5%), when using 4.44 vol% alumina nanofluid heat pipe at a thermal load of 30 W, as shown in Figure 13a. In addition, at 30 W, 1.5 vol% alumina nanofluid was able to reduce the thermal resistance of the heat pipe from 0.4677 °C/W to 0.394 °C/W (15% reduction), as shown in Figure 13b.

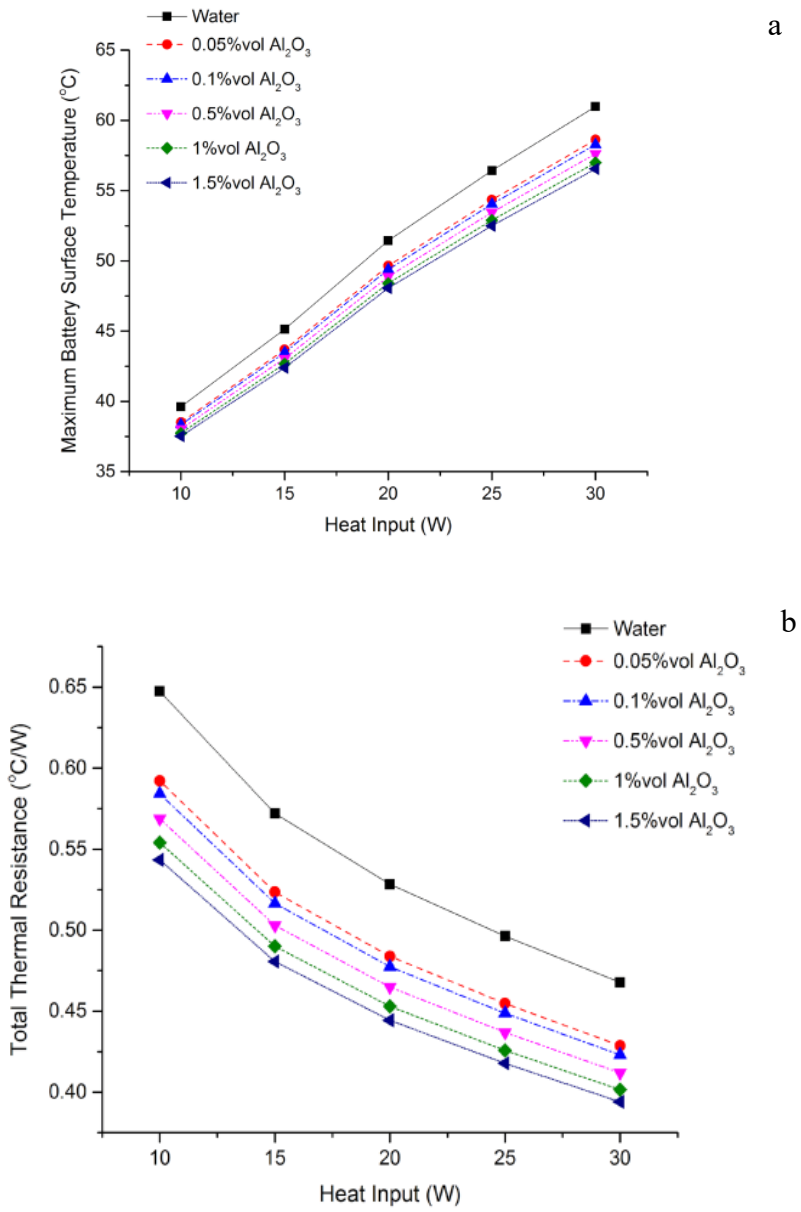

Figure 13. a) Maximum battery surface temperature at different heat inputs, b) Thermal resistance of HPTMS at different heat inputs [38]

Zhou *et al.* [39] proposed a mixed cooling system, which is an oscillating heat pipe (OHP) composed of a copper plate evaporator with six parallel circular channels and a capillary copper tube condenser. They used the ethanol solution of carbon nanotubes (CNTs) as the working fluid of the oscillating heat pipe, with the mass concentration ranging from 0.05 wt% to 0.5 wt%. The experimental results show that the cooling system with a concentration of 0.2 wt% maintains a thermal resistance of 0.066 °C/W and an average evaporator temperature of 43.1°C. Figure 14 shows the average temperature change of the power input analog battery pack from 8 to 56 W under different CNT concentrations. Obviously, the use of carbon nanotube nanofluids has greatly reduced the average temperature of the battery pack.

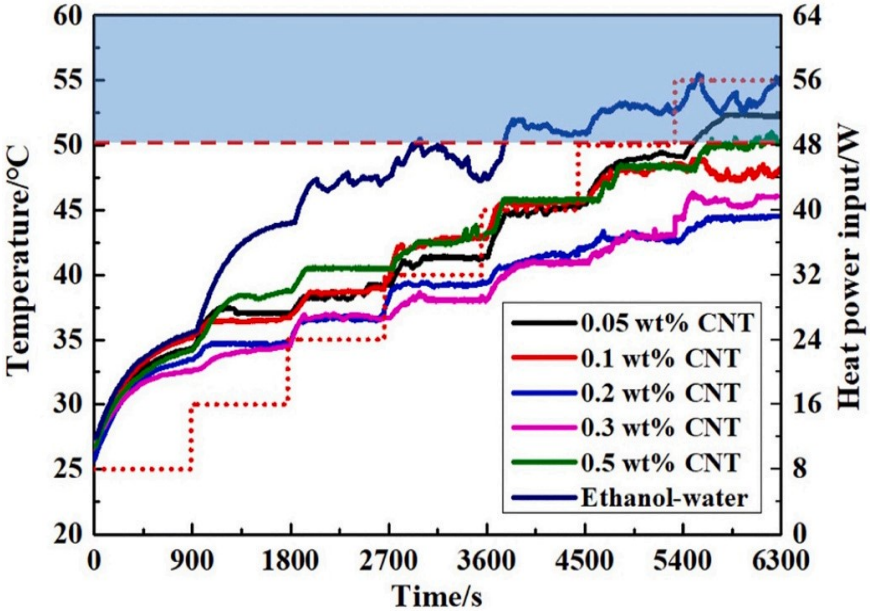

Figure 14. Average temperature variation for hybrid cooling system with at different mass concentrations [39].

Chen *et al.* [40] applied TiO_2 nanofluid as the working fluid in the thermal management system of lithium-ion batteries in vehicles with pulsating heat pipe (PHP) and compared three thermal management modes (no PHP, H_2O-PHP, and TiO_2 PHP) at 25℃ ambient temperature and 1C. The results are shown in Figure 15. When there is no PHP, H_2O-PHP, and TiO_2-PHP are used, the maximum temperature T_{max} of the battery surface is 40.31℃, 38.78℃, and 35.86 ℃ respectively. During continuous discharge, the maximum temperature gradient ΔTmax is 4.67℃, 2.03 ℃ and 1.15℃, respectively. Therefore, the pulse heat pipe battery thermal management system using TiO_2 nanofluid can effectively reduce the temperature of the battery pack and improve the uniformity of the surface temperature.

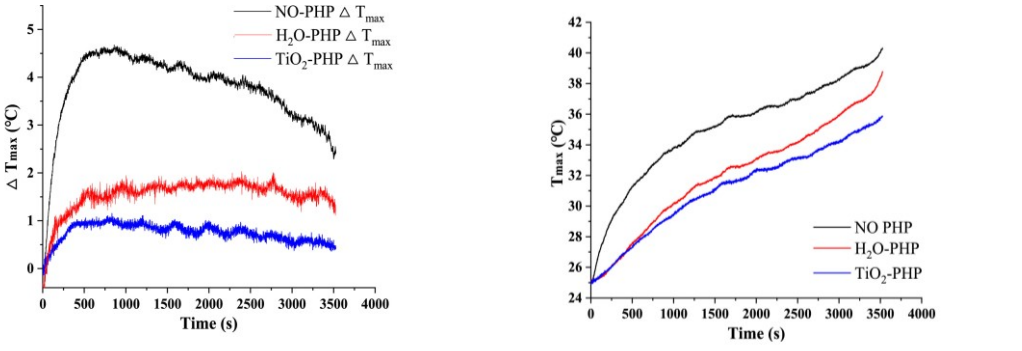

(a) Variation curve of maximum temperature difference ΔT_{max} over time. (b) Variation curve of the maximum temperature of the battery T_{max} over time

Figure 15. Variation curves of battery temperature over time under diffffferent modes of heat dissipation [40]

Patel *et al.* [41] applied the hybrid nanofluid loop heat pipe (LHP) of 5% alumina (Al_2O_3)-water (H_2O) nanofluid and 1% titanium dioxide (TiO_2) in the battery thermal management system. The results show that compared with the other two working fluids, the loop heat pipe mixed with nanofluids has better thermal management performance,

and can reduce the heat of the battery simulator to 47 ℃ under the operating limit of the lithium-ion battery. As shown in Figure 16, when heating at 40 W, compared with nanofluid and base fluid, the mixed nanofluid can provide a temperature drop of about 15.8 ℃, and the performance of the heat pipe is improved by 12%.

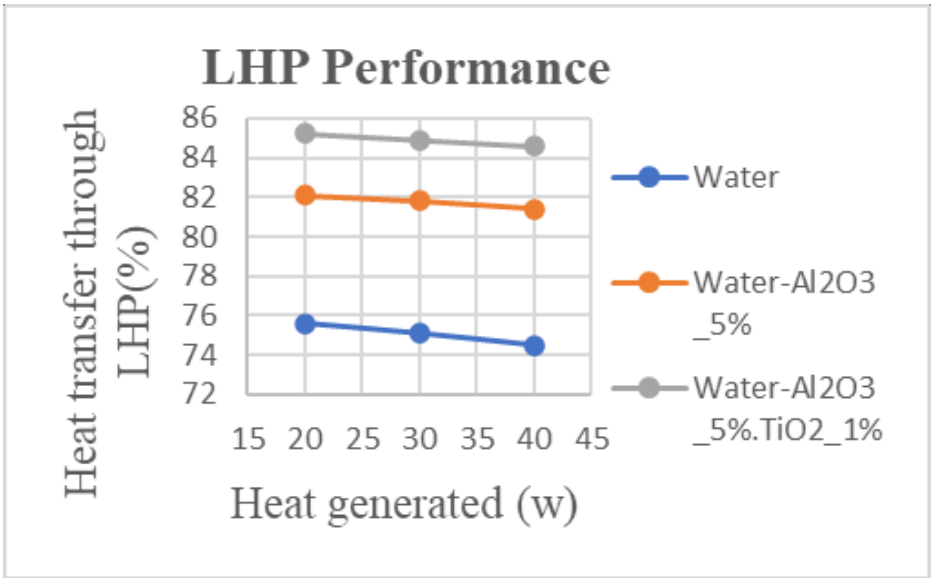

Figure 16. Loop heat pipe performance [41]

Smaisim *et al.* [42] applied the nanofluid loop heat pipe with the working fluid of graphene oxide (GO)-water to the thermal management system of lithium-ion batteries in automobiles, and carried out experimental research and simulation analysis. The results show that the maximum temperature is 49°C, 52°C, 52°C and 52.5°C at the filling ratio of 20%, 35%, 50% and 65%, which is basically consistent with the experimental results of 52.5°C, 52°C, 49.8°C and 46°C, effectively reducing the temperature of the battery pack.

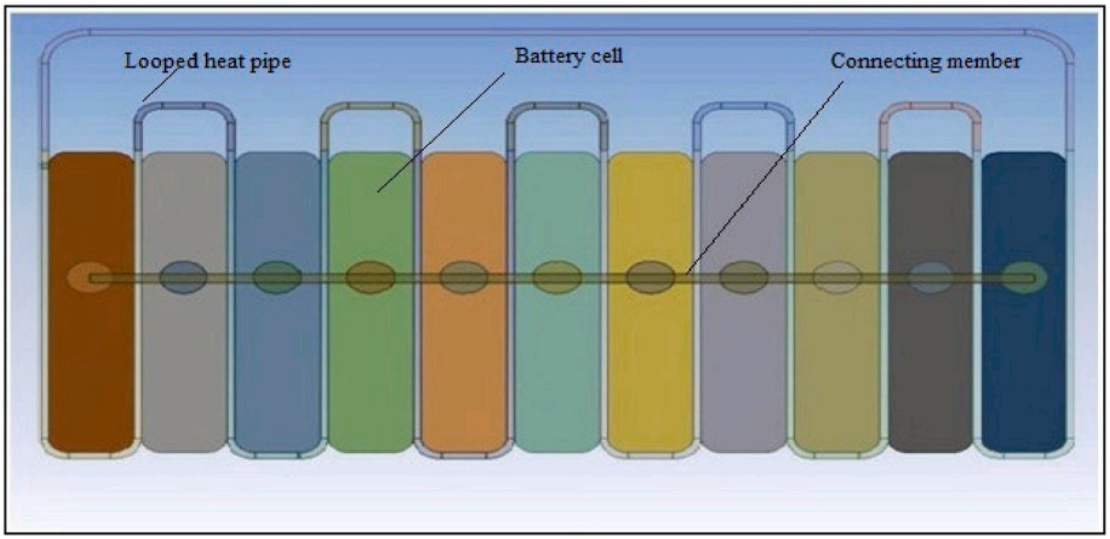

Figure. 17. Arrangement of Li-ion battery cells with heat pipe[42].

Figure 18 shows the line diagram of the micro-heat pipe with the experimental device. Narayanasamy *et al.* [43] applied the annular micro-heat pipe with acetone, deionized water, and graphene oxide nanofluid as the working fluid to the lithium-ion battery thermal management system. Their research results show that compared with acetone and deionized water, the thermal conductivity of tetrahydrofuran-graphene nanofluid is increased by 61%, thus speeding up the heat transfer rate and reducing the thermal resistance range by 0.09-0.64 °C/W.

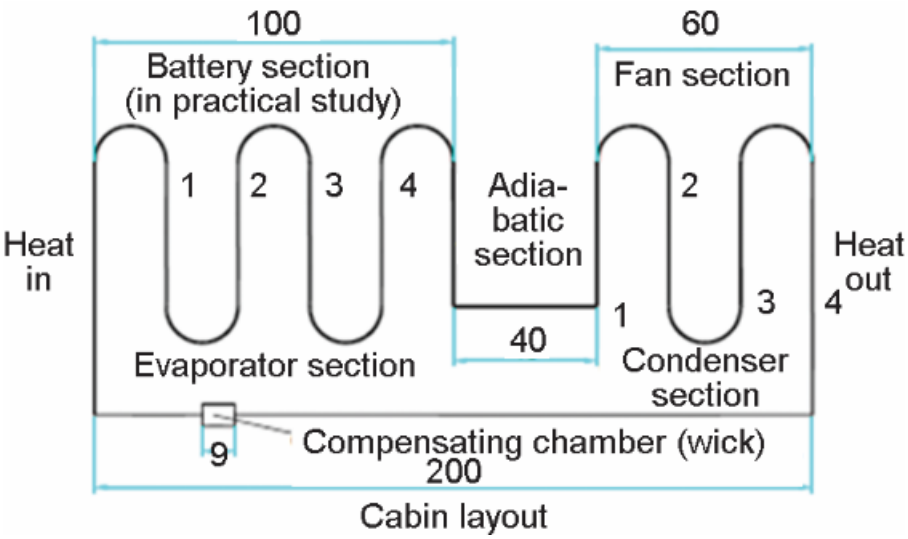

Figure 18. Line diagram of micro-heat pipe [43].

CONCLUSIONS

This paper reviews the research on the application of nanofluid heat pipe in lithium battery thermal management system in recent years, and it is known through the literature that using nanofluid as the workpiece of heat pipe can improve the thermal efficiency, reduce the thermal resistance and improve the heat transfer performance of heat pipe. The application of nanofluid heat pipe in the battery thermal management system can largely improve the uniformity of battery temperature distribution and effectively control the maximum temperature of the battery, which has great application prospects.

According to the literature, the following suggestions are put forward for the future research on the thermal management system of nanofluid heat pipe batteries:

1. Because the working principle and structure of nanofluid heat pipe are similar to that of the heat pipe, and it is easy to use with other cooling methods, domestic and foreign scholars should strengthen the research on the coupling of nanofluid heat pipe with air cooling, liquid cooling, and other battery thermal management technologies.
2. Domestic and foreign scholars mainly focus on the heat transfer performance of nanofluid heat pipe battery heat management technology using nanofluid heat pipe, but little on the time-dependent characteristics of nanofluid heat pipe battery heat pipe systems. Therefore, it is necessary to conduct in-depth research on the service life of nanofluid heat pipes in the battery heat management system and the stability of nanofluid.

3. Compared with the battery thermal management system using a single nanofluid heat pipe, the hybrid nanofluid loop heat pipe (LHP) battery thermal management system studied by Patel *et al.* [41] in the literature shows that the hybrid nanofluid heat pipe battery thermal management system performs better than the single nanofluid heat pipe battery thermal management system. Therefore, the battery thermal management system of hybrid nanofluid heat pipe will be an important research direction for future scholars.

CONFLICTS OF INTEREST

The authors declare that there is no conflict of interests regarding the publication of this paper.

REFERENCES

[1] Subramanian, M., Hoang, A. T., B, K., Nižetić, S., Solomon, J. M., Balasubramanian, D., C, S., G, T., Metghalchi, H., & Nguyen, X. P. (2021). A technical review on composite phase change material based secondary assisted battery thermal management system for electric vehicles. *Journal of Cleaner Production, 322*, 129079. doi: https://doi.org/10.1016/j.jclepro.2021.129079

[2] Zhang, D., He, Z., Guan, J., Tang, S., & Shen, C. (2022). Heat transfer and flow visualization of pulsating heat pipe with silica nanofluid: An experimental study. *International Journal of Heat and Mass Transfer, 183*, 122100. doi: https://doi.org/10.1016/j.ijheatmasstransfer.2021.122100

[3] Cen, J., & Jiang, F. (2020). Li-ion power battery temperature control by a battery thermal management and vehicle cabin air conditioning integrated system. *Energy for Sustainable Development, 57*, 141-148. doi: https://doi.org/10.1016/j.esd.2020.06.004

[4] Shahid, S., & Agelin-Chaab, M. (2022). A review of thermal runaway prevention and mitigation strategies for lithium-ion batteries. *Energy Conversion and Management: X, 16*, 100310. doi: https://doi.org/10.1016/j.ecmx.2022.100310

[5] Zhang, T., Gao, Q., Gu, Y., & li, Y. (2021). Studies on thermal management of lithium-ion battery using non-metallic heat exchanger. *Applied Thermal Engineering, 182*, 116095. doi: https://doi.org/10.1016/j.applthermaleng.2020.116095

[6] Behi, H., Karimi, D., Behi, M., Jaguemont, J., Ghanbarpour, M., Behnia, M., Berecibar, M., & Van Mierlo, J. (2020). Thermal management analysis using heat pipe in the high current discharging of lithium-ion battery in electric vehicles. *Journal of Energy Storage, 32*, 101893. doi: https://doi.org/10.1016/j.est.2020.101893.

[7] Wu, W., Wang, S., Wu, W., Chen, K., Hong, S., & Lai, Y. (2019). A critical review of battery thermal performance and liquid based battery thermal management. *Energy Conversion and Management, 182*, 262-281. doi: https://doi.org/10.1016/j.enconman.2018.12.051

[8] Jouhara, H., Delpech, B., Bennett, R., Chauhan, A., Khordehgah, N., Serey, N., & Lester, S. P. (2021). Heat pipe based battery thermal management: Evaluating the

potential of two novel battery pack integrations. *International Journal of Thermofluids, 12*, 100115. doi: https://doi.org/10.1016/j.ijft.2021.100115

[9] Luo, J., Zou, D., Wang, Y., Wang, S., & Huang, L. (2022). Battery thermal management systems (BTMs) based on phase change material (PCM): A comprehensive review. *Chemical Engineering Journal, 430*, 132741. doi: https://doi.org/10.1016/j.cej.2021.132741

[10] Hamed, M. M., El-Tayeb, A., Moukhtar, I., El Dein, A. Z., & Abdelhameed, E. H. (2022). A review on recent key technologies of lithium-ion battery thermal management: External cooling systems. *Results in Engineering, 16*, 100703. doi: https://doi.org/10.1016/j.rineng.2022.100703

[11] Shen, X., Cai, T., He, C., Yang, Y., & Chen, M. (2023). Thermal analysis of modified Z-shaped air-cooled battery thermal management system for electric vehicles. *Journal of Energy Storage, 58*, 106356. doi: https://doi.org/10.1016/j.est.2022.106356

[12] Liu, H., Wei, Z., He, W., & Zhao, J. (2017). Thermal issues about Li-ion batteries and recent progress in battery thermal management systems: A review. *Energy Conversion and Management, 150*, 304-330. doi: https://doi.org/10.1016/j.enconman.2017.08.016

[13] Madani, S. S., Swierczynski, M. J., & Kær, S. K. (2017). *A review of thermal management and safety for lithium ion batteries.* Paper presented at the 2017 Twelfth International Conference on Ecological Vehicles and Renewable Energies (EVER). Monte Carlo, Monaco, pp. 1-20, doi: https://doi.org/10.1109/EVER.2017.7935914.

[14] Li, Y., Zhou, Z., Hu, L., Bai, M., Gao, L., Li, Y., Liu, X., Li, Y., & Song, Y. (2022). Experimental studies of liquid immersion cooling for 18650 lithium-ion battery under different discharging conditions. *Case Studies in Thermal Engineering, 34*, 102034. doi: https://doi.org/10.1016/j.csite.2022.102034

[15] Kalaf, O., Solyali, D., Asmael, M., Zeeshan, Q., Safaei, B., & Askir, A. (2021). Experimental and simulation study of liquid coolant battery thermal management system for electric vehicles: A review. *International Journal of Energy Research*, *45*(5), 6495-6517. doi: https://doi.org/10.1002/er.6268

[16] Jiaqiang, E., Han, D., Qiu, A., Zhu, H., Deng, Y., Chen, J., Zhao, X., Zuo, W., Wang, H., Chen, J., & Peng, Q. (2018). Orthogonal experimental design of liquid-cooling structure on the cooling effect of a liquid-cooled battery thermal management system. *Applied Thermal Engineering, 132*, 508-520. doi: https://doi.org/10.1016/j.applthermaleng.2017.12.115

[17] Maxwell, J. C. (1873). *A treatise on electricity and magnetism* (Vol. 1). Oxford: Clarendon Press.

[18] Deng, Y., Feng, C., E, J., Zhu, H., Chen, J., Wen, M., & Yin, H. (2018). Effects of different coolants and cooling strategies on the cooling performance of the power lithium ion battery system: A review. *Applied Thermal Engineering, 142*, 10-29. doi: https://doi.org/10.1016/j.applthermaleng.2018.06.043

[19] Eastman, J. A., Choi, S. U. S., Li, S., Yu, W., & Thompson, L. J. (2001). Anomalously increased effective thermal conductivities of ethylene glycol-based nanofluids containing copper nanoparticles. *Applied physics letters*, *78*(6), 718-720. doi: https://doi.org/10.1063/1.1341218

[20] Angani, A., Kim, H.-W., Hwang, M.-H., Kim, E., Kim, K.-M., & Cha, H.-R. (2023). A comparison between Zig-Zag plated hybrid parallel pipe and liquid cooling battery thermal management systems for Lithium-ion battery module. *Applied Thermal*

Engineering, 219, 119599. doi: https://doi.org/10.1016/j.applthermaleng.2022.119599

[21] Wang, S., Zhang, D., Li, C., Wang, J., Zhang, J., Cheng, Y., Mei, W., Cheng, S., Qin, P., Duan, Q., Sun, J., & Wang, Q. (2023). Numerical optimization for a phase change material based lithium-ion battery thermal management system. *Applied Thermal Engineering, 222*, 119839. doi: https://doi.org/10.1016/j.applthermaleng.2022.119839

[22] Bashirpour-Bonab, H. (2020). Thermal behavior of lithium batteries used in electric vehicles using phase change materials. *International Journal of Energy Research, 44*(15), 12583-12591. doi: https://doi.org/10.1002/er.5425

[23] Zou, D., Ma, X., Liu, X., Zheng, P., & Hu, Y. (2018). Thermal performance enhancement of composite phase change materials (PCM) using graphene and carbon nanotubes as additives for the potential application in lithium-ion power battery. *International Journal of Heat and Mass Transfer, 120*, 33-41. doi: https://doi.org/10.1016/j.ijheatmasstransfer.2017.12.024

[24] Jiang, G., Huang, J., Fu, Y., Cao, M., & Liu, M. (2016). Thermal optimization of composite phase change material/expanded graphite for Li-ion battery thermal management. *Applied Thermal Engineering, 108*, 1119-1125. doi: https://doi.org/10.1016/j.applthermaleng.2016.07.197

[25] Weng, J., Yang, X., Zhang, G., Ouyang, D., Chen, M., & Wang, J. (2019). Optimization of the detailed factors in a phase-change-material module for battery thermal management. *International Journal of Heat and Mass Transfer, 138*, 126-134. doi: https://doi.org/10.1016/j.ijheatmasstransfer.2019.04.050

[26] Choudhari, V. G., Dhoble, A. S., & Panchal, S. (2020). Numerical analysis of different fin structures in phase change material module for battery thermal management system and its optimization. *International Journal of Heat and Mass Transfer, 163*, 120434. doi: https://doi.org/10.1016/j.ijheatmasstransfer.2020.120434

[27] Li, Z., Sarafraz, M. M., Mazinani, A., Moria, H., Tlili, I., Alkanhal, T. A., Goodarzi, M., & Safaei, M. R. (2020). Operation analysis, response and performance evaluation of a pulsating heat pipe for low temperature heat recovery. *Energy Conversion and Management, 222*, 113230. doi: https://doi.org/10.1016/j.enconman.2020.113230

[28] Weragoda, D. M., Tian, G., Burkitbayev, A., Lo, K.-H., & Zhang, T. (2023). A comprehensive review on heat pipe based battery thermal management systems. *Applied Thermal Engineering, 224*, 120070. doi: https://doi.org/10.1016/j.applthermaleng.2023.120070

[29] Mbulu, H., Laoonual, Y., & Wongwises, S. (2021). Experimental study on the thermal performance of a battery thermal management system using heat pipes. *Case Studies in Thermal Engineering, 26*, 101029. doi: https://doi.org/10.1016/j.csite.2021.101029

[30] Zhang, Z., & Wei, K. (2020). Experimental and numerical study of a passive thermal management system using flat heat pipes for lithium-ion batteries. *Applied Thermal Engineering, 166*, 114660. doi: https://doi.org/10.1016/j.applthermaleng.2019.114660

[31] Mehta, B., Subhedar, D., Panchal, H., & Said, Z. (2022). Synthesis, stability, thermophysical properties and heat transfer applications of nanofluid – A review. *Journal of Molecular Liquids, 364*, 120034. doi: https://doi.org/10.1016/j.molliq.2022.120034

[32] Said, Z., Sundar, L. S., Tiwari, A. K., Ali, H. M., Sheikholeslami, M., Bellos, E., & Babar, H. (2022). Recent advances on the fundamental physical phenomena behind stability, dynamic motion, thermophysical properties, heat transport, applications, and challenges of nanofluids. *Physics Reports, 946*, 1-94. doi: https://doi.org/10.1016/j.physrep.2021.07.002
[33] Baheta, A. T., Oumer, A. N., & Hailegiorgis, S. M. (2018). Analysing the thermal performance of heat pipe using copper nanofluids. *Journal of Advanced Research in Fluid Mechanics and Thermal Sciences*, *45*(1), 149-155.
[34] Reji, A. K., Kumaresan, G., Sarathi, A., Saiganesh, A. G. P., Suriya Kumar, R., & Shelton, M. M. (2021). Performance analysis of thermosyphon heat pipe using aluminum oxide nanofluid under various angles of inclination. *Materials Today: Proceedings, 45*, 1211-1216. doi: https://doi.org/10.1016/j.matpr.2020.04.247
[35] Riehl, R. R., & Murshed, S. M. S. (2022). Performance evaluation of nanofluids in loop heat pipes and oscillating heat pipes. *International Journal of Thermofluids, 14*, 100147. doi: https://doi.org/10.1016/j.ijft.2022.100147
[36] Zhang, D., He, Z., Guan, J., Tang, S., & Shen, C. (2022). Heat transfer and flow visualization of pulsating heat pipe with silica nanofluid: An experimental study. *International Journal of Heat and Mass Transfer, 183*, 122100. doi: https://doi.org/10.1016/j.ijheatmasstransfer.2021.122100
[37] Ghorabaee, H., Emami, M. R. S., Moosakazemi, F., Karimi, N., Cheraghian, G., & Afrand, M. (2021). The use of nanofluids in thermosyphon heat pipe: A comprehensive review. *Powder Technology, 394*, 250-269. doi: https://doi.org/10.1016/j.powtec.2021.08.045
[38] Nasir, F. M., Abdullah, M. Z., Majid, M. F. M. A., & Ismail, M. A. (2019). Nanofluid-filled heat pipes in managing the temperature of EV lithium-ion batteries. *Journal of Physics: Conference Series, 1349*(1), 012123. doi: https://doi.org/10.1088/1742-6596/1349/1/012123
[39] Zhou, Z., Lv, Y., Qu, J., Sun, Q., & Grachev, D. (2021). Performance evaluation of hybrid oscillating heat pipe with carbon nanotube nanofluids for electric vehicle battery cooling. *Applied Thermal Engineering, 196*, 117300. doi: https://doi.org/10.1016/j.applthermaleng.2021.117300
[40] Chen, M., & Li, J. (2020). Nanofluid-based pulsating heat pipe for thermal management of lithium-ion batteries for electric vehicles. *Journal of Energy Storage, 32*, 101715. doi: https://doi.org/10.1016/j.est.2020.101715
[41] Patel, A. K., Patel, T. V., Patel, P. D., & Patel, J. J. (2021). Experimental analysis of temperature control of lithium-ion battery by utilize heat pipe[J]. *Vidyabharati International Interdisciplinary Research Journal, 13*(1), 302-309.
[42] Smaisim, G. F., Al-Madhhachi, H., & Abed, A. M. (2022). Study the thermal management of Li-ion batteries using looped heat pipes with different nanofluids. *Case Studies in Thermal Engineering, 37*, 102227. doi: https://doi.org/10.1016/j.csite.2022.102227
[43] Narayanasamy, M. P., Gurusamy, S., Sivan, S., & Senthilkumar, A. P. (2021). Heat transfer analysis of looped micro heat pipes with graphene oxide nanofluid for Li-ion battery. *Thermal Science*, *25*(1 Part A), 395-405.

Trends in Renewable Energy
OPEN ACCESS ISSN: 2376-2144
Peer-Reviewed Article futureenergysp.com/index.php/tre

Optimized Lightweight Frame for Intelligent New-energy Vehicles

Peipei Wu*

Department of First, North China University of Water Resources and Electric Power, Zhengzhou, China, 450000

Received April 19, 2023; Accepted May 19, 2023; Published June 2, 2023

In this paper, a joint optimization method based on multi-objective response surface approximation model and finite element simulation program is proposed to realize the lightweight optimization of new-energy vehicle frames. Under the premise of satisfying the constraints of strength, frequency and vibration, the thickness of different important parts is optimized to achieve the goal of minimizing the quality of intelligent vehicles. In order to obtain the stress distribution of each part and the vibration frequency of the frame, various finite element analyses of the intelligent vehicle frame are analyzed. In order to achieve optimization, this paper adopts the response surface method for multi-objective optimization. Sample data was generated by the central composite design, and the response surface optimization method was used to filter out 5 design variables that had a large impact on the frame. As a result, the weight of the frame was reduced from 25.05 kg to 19.86 kg, a weight reduction of 20.7%, achieving a significant weight reduction effect. This method provides important reference value and guiding significance for the optimization of frame and its lightweight. In this way, the design of the frame can be better optimized to make it lighter, thereby improving the performance of the smart car. At the same time, this method can also be applied to optimization problems in other fields to achieve more efficient and accurate optimization goals.

Keywords: Intelligent new-energy vehicle, Vehicle frame; Finite element analysis; Lightweight; Optimization

Introduction

With the continuous development of intelligent new-energy vehicle technology, the importance of intelligent new-energy vehicle frames has been paid more and more attention. The lightweight design of the frame of the intelligent new-energy vehicle can not only improve the performance of the whole vehicle, but also reduce energy consumption and reduce environmental pollution. Therefore, it is of great theoretical and practical value to study the lightweight design of intelligent new-energy vehicle frames. The lightweight design of the frame of intelligent new-energy vehicles can be realized by various methods, such as material optimization, structural design optimization and process optimization. In this paper, a joint optimization method based on multi-objective response surface approximation model and finite element simulation program is proposed to realize the lightweight optimization of intelligent new-energy vehicle frames. This method can achieve the lightweight goal of intelligent new-energy vehicle frame by

Corresponding author: wupiepei0211@163.com

Tr Ren Energy, 2023, Vol.9, No.2, 157-166. doi: 10.17737/tre.2023.9.2.00159

optimizing the thickness of different important parts under the premise of meeting the constraints of strength, frequency and vibration. These methods and tools provide useful references and guidance for the lightweight design of intelligent new-energy vehicle frames. The lightweight design of intelligent new-energy vehicle frame is an important research direction in the field of intelligent vehicles, which is of great significance for improving the performance of new-energy vehicles, reducing energy consumption and reducing environmental pollution.

Aiming at the lightweight research of the frame structure, Tang and Xia [1] improved the structural structure of the subframe, increased the safety factor of the frame, and verified the rationality of the side frame design. Zhang and Ran [2] proposed a lightweight optimization idea based on ant colony algorithm for frame structure design made of TC4 titanium alloy. Yu *et al.* [3] established a full-size finite element model of pure electric vehicles (PEV) and used the finite element method to realize the lightweight design of the frame. Feng *et al.* [4] has designed a lightweight fire truck frame based on Ansys software to reduce the mass of the frame, while meeting the strength requirements. Yang *et al.* [5] integrated four driving conditions (including full load bending conditions, torsional conditions, emergency braking and emergency steering) and used finite element analysis to optimize the lightweight design of the electric bus frame.

In this paper, the static analysis of the frame of intelligent new-energy vehicles is first carried out to understand its static mechanical properties. Then, the vibration characteristics of the intelligent vehicle frame at natural frequency were analyzed by modal analysis. Finally, this paper uses the method of random vibration analysis to study the vibration characteristics of intelligent vehicle frame in complex environment. In short, by studying the mechanical characteristics and lightweight analysis of intelligent vehicle frames, this paper successfully proposes a lightweight design scheme based on the multi-objective response surface method, which provides important reference value and guiding significance for the lightweight design of intelligent new-energy vehicle frames.

Establishment of Frame Model

Creation of 3D Model

For numerical simulation, a simplified analysis of the frame is carried out and a simple frame model is built. Due to the simplicity and versatility, a simple frame model was established using Solidworks software, as shown in Figure 1. The model contains only important parts of the frame (such as stringers and beams) as well as other necessary details like wheels and tires.

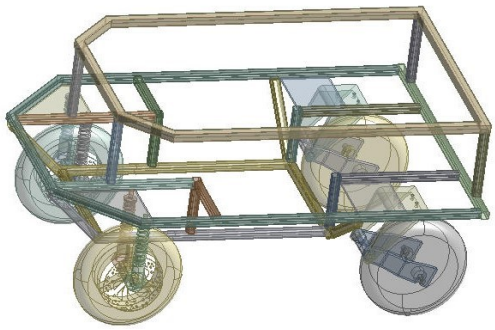

Figure 1. Full vehicle model

Establishment of Finite Element Model

Table 1 lists some parameters of material attributes. Due to the complex structure of the frame, in order to reduce its mass, five representative parts were selected for local analysis. These parts are: the middle front steel pipe 1, the front right steel pipe 2, the front right steel pipe 3, the rear side cross steel pipe 4, and the upper whole circle steel pipe 5, as shown in Figure 2.

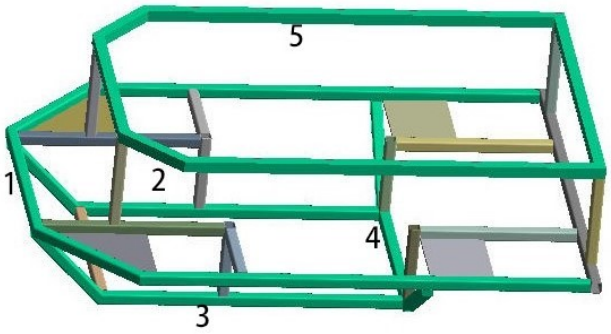

Figure1. Simplified frame

Table 1. Material attributes

Material	Structural steel
Poisson's ratio	0.3
Elastic modulus/Pa	2E+11
density/(kg·m^{-3})	7850
Yield strength/MPa	250

Finite Element Analysis of the Frame

Static Analysis of the Frame

The static analysis of frames is an important research field, which has a wide range of applications in the field of intelligent vehicles. Static analysis refers to a method of analyzing and calculating the force situation of an object at rest or in uniform motion. It is necessary to divide the frame into several small units, and then analyze the force of the unit to obtain the force of the entire frame. It is also possible to perform calculations using traditional matrix methods, which are less efficient and are usually only used for preliminary design and estimation. In order to study the strength and deformation characteristics of the frame under load, the finite element method was used to analyze the statics of the frame, and the static characteristics of the frame under multiple working conditions such as bending and torsional conditions were considered.

Bending Conditions

The frame is mainly statically loaded in bending conditions, and reasonable constraints are set to ensure that the model reflects the real situation well. Since the speed of the intelligent car is not too fast, the safety factor is selected as 1.5, and the allowable stress of the intelligent car frame can be obtained at this time as 120MPa. The constraints are shown in Table 2. The results of the finite element analysis are shown in Figure 3.

Table 2. Constraints under bending conditions

Constraint points	Degrees of freedom restrictions
Left front wheel	X , Z
Left rear wheel	Z
Right front wheel	X ,Y , Z
Right rear wheel	Y , Z

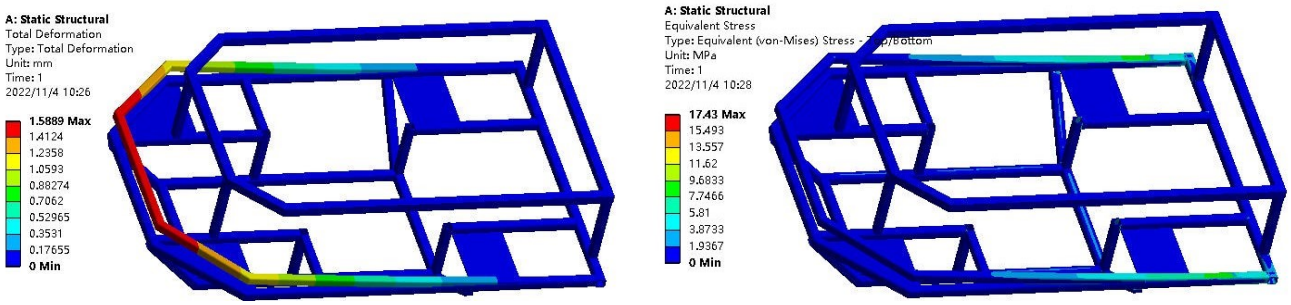

a Total deformation of bending b Bending and other effects

Figure2 Static properties under bending conditions

After calculation, the initial result is that under the bending moment condition of fully loaded intelligent car, the maximum frame equivalent force is 100.2 MPa, and the maximum frame total deformation displacement is 0.555 mm.

Twist the Operating Conditions

When the low-speed fully loaded intelligent vehicle is driving on a rough road, the four wheels will be in different planes, and the structural condition of the intelligent vehicle frame can be analyzed. The frame is mainly affected by torsional loads. In view of the occurrence of various situations, this paper selects a typical special case, that is, the right front wheel is raised 15 mm upwards and the left rear wheel is concave 15mm downward. The safety factor is selected as 1.2, and the allowable stress of the intelligent car frame can be obtained as 100 MPa. Table 3 lists the constraints, while the results are shown in Figure 4.

Table 3. Constraints under torsional conditions

Constraint points	Degrees of freedom restrictions
Left front wheel	X, Y, Z
Left rear wheel	Z and Y 15 mm downwards
Right front wheel	X and Y upwards 15mm
Right rear wheel	Y

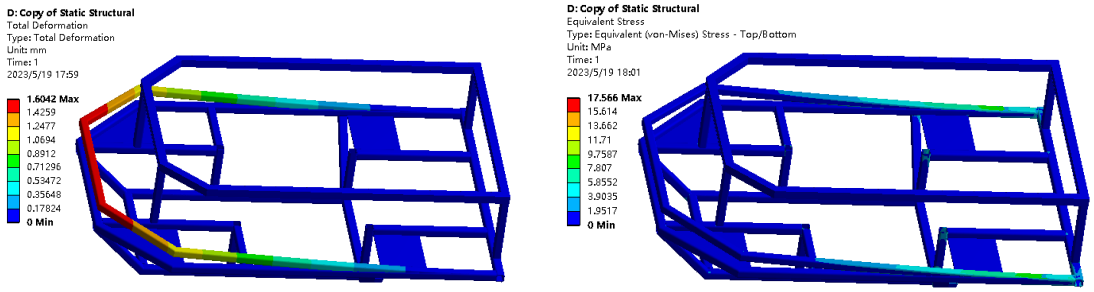

a Total deformation b Equivalent forces

Figure 4. Static properties under torsional conditions

After calculation, the initial result is that under the torsional condition of fully loaded intelligent vehicle, the maximum frame equivalent force is 58.249 MPa, and the maximum frame total deformation displacement is 0.263 mm.

Random Vibration Analysis of the Frame

The frame refers to the frame structure of the intelligent car, whose main role is to support the overall structure of the carrier, and must have sufficient strength and rigidity. The random vibration analysis of the frame is because the intelligent car will be randomly excited by different road surface conditions during driving, in this case, the frame will produce random vibration. When the excitation force is large or the long-term acceptance of some kind of excitation, it may promote the failure of the frame structure, so it is necessary for the frame to do random vibration analysis [6-9].

Modal Analysis

The frame is a multi-degree-of-freedom vibration structure, so the modal analysis of the frame structure can be established through finite element analysis, and the vibration system of the frame can be further understood.

The natural frequencies of the first 6 stages of the frame are shown in Table 4, and the natural frequencies of the first order of the frame belong to the low frequency range, which is in line with the range of avoiding resonance frequencies [10-13]. The modal mode diagram of the frame is shown in Figure 5.

Table 4. Frame modal analysis results

Order	Natural frequency/Hz	Order	Natural frequency/Hz
1	14.062	4	62.386
2	25.581	5	71.960
3	36.417	6	82.357

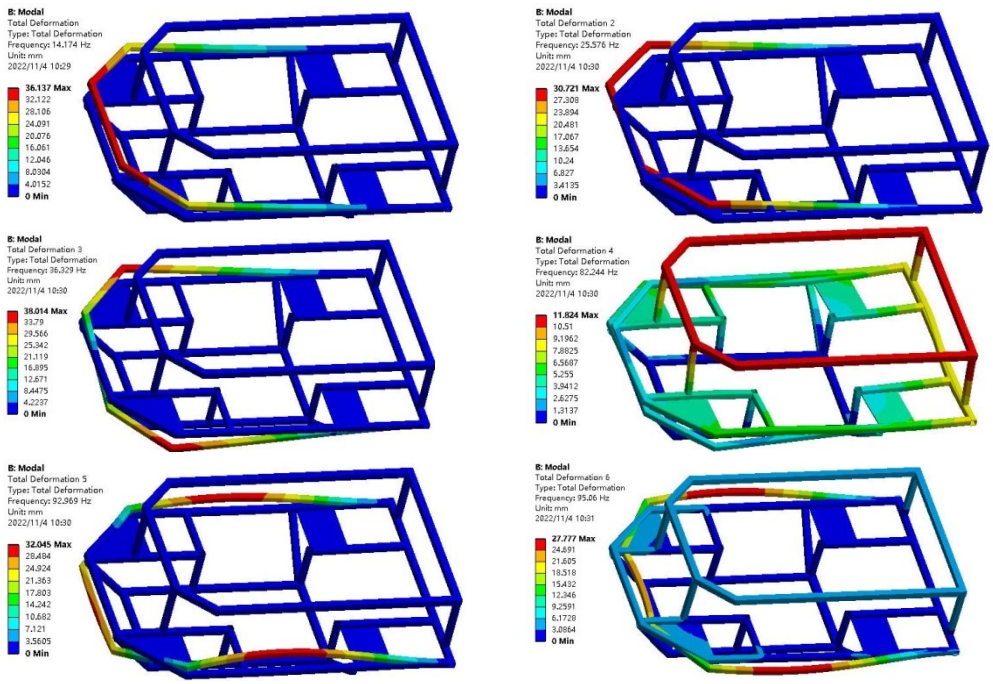

Figure3 Displacement modes of steps 1-6

Stochastic Vibration Analysis

Random vibration is one of the important challenges faced by smart cars while driving. Therefore, the random vibration analysis of intelligent vehicles not only helps to improve the driving safety of intelligent vehicles, but also provides an important theoretical basis for future intelligent vehicle research.

Random vibration will affect the suspension system, control system and other aspects of intelligent vehicles, thereby affecting the driving stability and safety of intelligent vehicles. Therefore, random vibration analysis of intelligent vehicles can help to study the dynamic characteristics of automotive systems, identify vibration sources in systems, and evaluate the adaptability of vehicles to vibration environments. Finally, the results are evaluated and optimized to improve the adaptability of intelligent vehicles to random vibrations and improve the driving safety and comfort of intelligent vehicles [14]. Below are selected typical displacement power spectral densities that enable random vibration analysis. The four typical mode shapes of the smart car frame are shown in Figure 6.

Table 4. Class D pavement with displacement power spectral density (20 km/h)

f(Hz)	$G_q(f)$ (mm^2/Hz)	f(Hz)	$G_q(f)$ (mm^2/Hz)
1	163.810	11	1.354
3	18.201	22	0.338
5	6.552	44	0.085
8	2.560	66	0.038

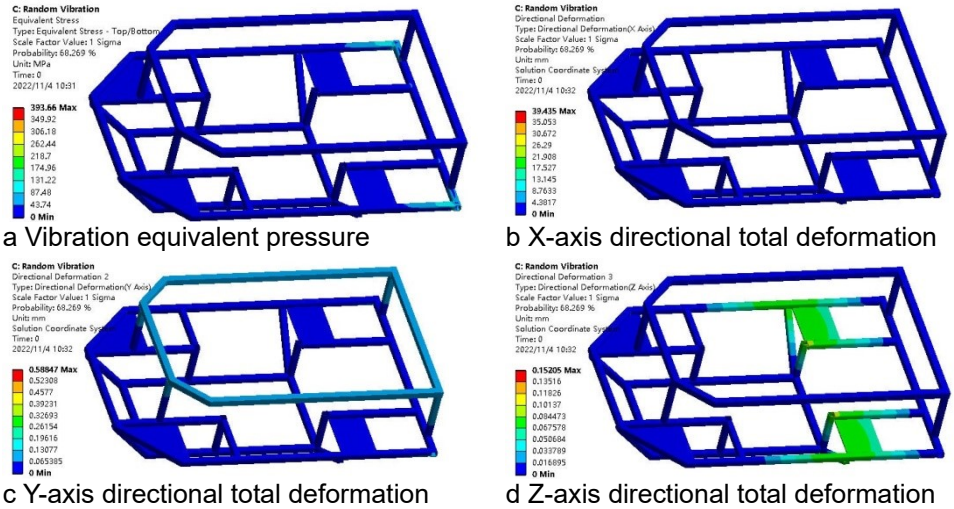

a Vibration equivalent pressure b X-axis directional total deformation

c Y-axis directional total deformation d Z-axis directional total deformation

Figure4. Four typical mode shape diagrams

In short, the random vibration analysis of intelligent vehicles is of great significance to improve the driving safety and stability of intelligent vehicles. Scientists should attach importance to the research of random vibration analysis of intelligent vehicles, continuously improve the technical level and application scenarios, and explore intelligent vehicles as an important research direction in the field of modern transportation.

Frame Lightweight Optimization Design

Frame lightweighting improves the fuel efficiency and performance of automobiles. We can use topology optimization to determine the optimal shape and finite element analysis to calculate the stress distribution of the frame. We can also use another optimization technique, which is parameter optimization. Parameter optimization can adjust parameters such as material selection, wall thickness and support structure. According to different design requirements to minimize the weight of the frame, aluminum alloy and carbon fiber also have high specific strength and specific stiffness, which can effectively improve the strength and stiffness of the frame.

In terms of structural design, a simplified structure should be adopted as much as possible to avoid excessive complexity. For example, unnecessary connections and traditional vertical pipe connection structures should be avoided in frame design. In addition, the use of hollow structure and multi-layer structure is also a common scheme in frame lightweight design.

Response Surface Optimization Analysis

Through the central composite test design of each part of the frame, and the screening of the parameters by the F test method, the response surface equation of the thickness of each part and the parameters (such as stress, deformation and self-vibration frequency) was finally constructed. The equation of some parameters is shown in the following equation, and the response surface diagram is shown in Figure 7. Among them, d1, d2, d3, d4, and d5 in formulas (1) and (2) represented the middle front steel pipe 1, the right front steel pipe 2, the right front copper pipe 3, the rear horizontal steel pipe 4, and the upper full circle steel pipe 5, respectively (as shown in Figure 2).

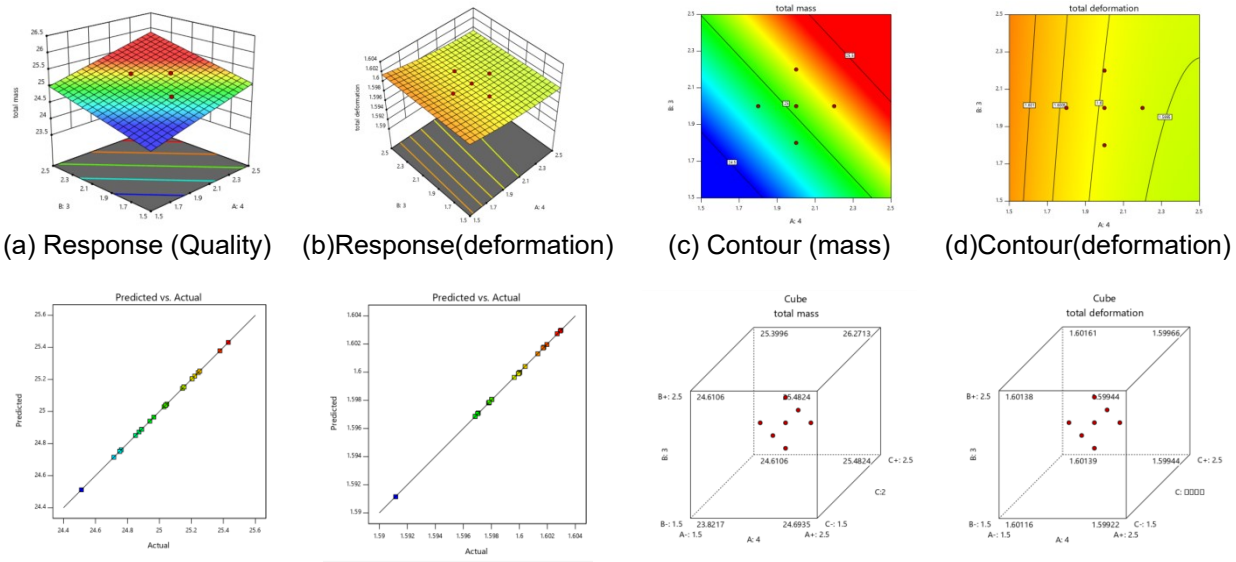

(a) Response (Quality) (b)Response(deformation) (c) Contour (mass) (d)Contour(deformation)

(e)Forecast vs. Actual Chart (Quality) (f)Forecast vs. Actual Chart (Deformation) (g)Cube diagram (mass) (h)Cube diagram (deformation)

Figure 7. Response Surface Optimization Diagram

$$Total\ deformation = +1.48784 - 0.009484 * d4 + 0.000220 * d3 + 0.000228 * d2 + 0.059409 * d1 + 0.028771 * d5 + 0.001886 * d4^2 - 0.004064 * d1^2 - 0.009368 * d5^2 \quad (1)$$

$$Total\ mass = 11.48305 + 0.871769 * d4 + 0.788938 * d3 + 0.788938 * d2 + 2.67332 * d1 + 1.65877 * d5 \quad (2)$$

From Figures 7e~f, it can be seen that the response surface method is reasonable instead of finite element simulation, and has high accuracy.

Results and Validation

Using the constructed response surface model instead of the finite element model for optimization iterations, the multi-objectives such as stress, deformation and total mass were taken into account for lightweighting analysis, and the multi-objective optimization solution was carried out using the optimization method to obtain the best solution for the thickness of the frame of the intelligent new-energy vehicle (as shown in Table 5). It can be seen that the mass of the steel tube 2, 3, 4 and 5 parts are all reduced by about 50%. The overall mass of the frame was reduced by 5.187 kg, a 20.71% reduction in mass. At the same time, the equivalent force before and after optimization was reduced by 4.13% and the first 6th order frequency was increased, reducing the possibility of frame resonance and indicating that the optimized frame is safer.

It can be seen that the optimized frame of the intelligent new-energy vehicle is obviously lighter and the thickness of the five components is more reasonable, which meets the requirements of strength, stiffness, modal and random vibration of each part while making full use of the material, reflecting the rationality of the proposed method.

Table 5. Comparison values before and after optimization

Initial value		Optimize the value			Optimize before and after comparison /%
		Rsd value	Fem value	error/%	
steel tube1/mm	2	1.596	1.596	-	20.2
steel tube2/mm	2	1.015	1.015	-	50
steel tube3/mm	2	1.003	1.003	-	50
steel tube4/mm	2	1.000	1.000	-	49.9
steel tube5/mm	2	1.000	1.000	-	50
quality/kg	25.047	19.872	19.86	-0.06	-20.71
Static total deformation/mm	1.553	1.585	1.589	0.25	2.32
Static stress/MPa	18.181	17.391	17.43	0.22	-4.13
First-order frequency	14.062	14.152	14.174	0.16	0.80
Second-order frequency	25.581	25.589	25.576	-0.05	-0.02
Third-order frequency	36.417	36.441	36.429	-0.03	0.03
Fourth-order frequency	62.386	84.836	82.244	-3.06	31.83
Fifth order frequency	71.96	92.571	92.969	0.43	29.2
Sixth-order frequency	82.357	93.299	95.06	1.89	15.42
Vibration stress/MPa	24.992	12.585	13.200	4.89	-47.18
X-axis directional deformation/mm	37.951	39.243	39.435	0.49	3.91
Y-axis directional deformation/mm	0.549	0.526	0.529	-0.57	7.29

CONCLUSIONS

(1) The central composite experimental design method and response surface optimization method are applied to the optimization and lightweight design of intelligent new-energy vehicle frame, effectively achieving the goal of structural lightweight.

(2) In order to improve the calculation efficiency, the central composite experimental design analysis is carried out by using finite element software before the response surface optimization, and the design variables that have a great influence on the total mass results of the frame are selected to participate in the subsequent optimization. Finally, the optimized frame achieves a reduction of 20.47% in the total mass of the intelligent frame, while ensuring the static and dynamic characteristics.

(3) The structural strength of the improved intelligent new-energy vehicle frame has been significantly improved, indicating that the structural optimization of the frame has good practical engineering application prospects and good reliability.

CONFLICTS OF INTEREST

The author declares that there is no conflict of interests regarding the publication of this paper.

REFERENCES

[1] Tang, P., & Xia, J. S. (2014). Finite element analysis of car's sub-frame. In *Applied Mechanics and Materials* (Vol. 651, pp. 733-737). Trans Tech Publications Ltd.

[2] Zhang, J., & Ran, W. (2021, May). Lightweight optimization design of a light electric commercial vehicle frame. In *Journal of Physics: Conference Series* (Vol. 1939, No. 1, p. 012038). IOP Publishing.

[3] Yu, L., Gu, X., Qian, L., Jiang, P., Wang, W., & Yu, M. (2021). Application of tailor rolled blanks in optimum design of pure electric vehicle crashworthiness and lightweight. *Thin-Walled Structures, 161*, 107410. doi: https://doi.org/10.1016/j.tws.2020.107410

[4] Feng, Q., Yu, S., Luo, J., & Chu, J. (2010, November). Research on lightweight design of vice-frame structure of fire-engine on basis of ANSYS. In *2010 IEEE 11th International Conference on Computer-Aided Industrial Design & Conceptual Design 1* (Vol. 2, pp. 1347-1350). IEEE.

[5] Yang, Z., Deng, B., Deng, M., & Sun, G. (2018). A study on finite element analysis of electric bus frame for lightweight design. In *MATEC Web of Conferences* (Vol. 175, p. 03049). EDP Sciences.

[6] Wang, S., Zheng, S., Feng, J., & Liu, X. (2013). Lightweight design for front sub-frame of a fuel cell vehicle. *Journal of Machine* Design, 30(2), 41-44.

[7] Luo, W., Zheng, Z., Liu, F., Han, D., & Zhang, Y. (2020, October). Lightweight design of truck frame. In *Journal of Physics: Conference Series* (Vol. 1653, No. 1, p. 012063). IOP Publishing.

[8] Yun, S. W., Go, S. H., Kim, H. G., & Yi-goo, K. (2018). Numerical Analysis of Deck Frame for Lightweight Trucks. *Journal of the Korean Society of Manufacturing Process Engineers, 17(3),* 127-133.
[9] Chen, Z., Wang, T., Zhao, Z., Shen, J., Zhen, D., & Gu, F. (2012, September). The lightweight design of a dump truck frame based on dynamic responses. In *18th International Conference on Automation and Computing (ICAC)* (pp. 1-5). IEEE.
[10] Wang, L., Yang, X., Lu, C., & Sun, X. (2012). Lightweight Design and Simulation of Vehicle Frame Based on FEM. *Modern Machinery, 2012(5),* 12-14.
[11] Sun, L., Tan, J., Jiang, C., & Chu, Z. (2010). Lightweight Study for Coach Body Frame under Multiple Loading Conditions. *Auto Mobile Science & Technology, 3*, 20-24.
[12] Han, K., Qu, X., & Fang, H. (2015). Lightweight Study of Frame Based on Sensitivity Analysis and Calculation of Dynamic Stiffness. *Journal of Hubei University of Automotive Technology, 29(4),* 21-25.
[13] Zheng, W., Lan, F., & Chen, J. (2016). Research on Topology Optimization and Lightweight Design for Frame Structure of FSAE Racing Car. *Chinese Journal of Automotive Engineering, 6(1),* 35-42.
[14] Chen, X., Lou, W., Jiang, Y., Yu, H., & Huang, Y. (2015). Static and Dynamic Performance Analysis and Lightweight Design of ATV Frame. *Journal of Chongqing University of Technology (Natural Science), 29(2),* 1-6.

Trends in Renewable Energy
OPEN ACCESS ISSN: 2376-2144
Peer-Reviewed Article futureenergysp.com/index.php/tre

Temperature Forecasting as a Means of Mitigating Climate Change and Its Effects: A Case Study of Mali

Utibe Akpan Billy,[1,*] Sunday O. Udo,[1] Igwe O. Ewona,[2] Mfon D. Umoh,[3] and Agbor Mfongang[1]

1: Department of Physics, University of Calabar, Calabar
2: Department of Physics, Cross River State University of Science and Technology
3: Department of research, strategy and development, Maritime Academy of Nigeria

Received March 23, 2023; Accepted June 5, 2023; Published June 15, 2023

Temperature forecasts and trend analyzes were carried out for several locations in Mali as an important tool for warning of potentially threatening weather events such as severe heat waves, storms, droughts and floods, which could pose a great risk to humans and their environment. Five locations (Segou, Sikasso, Kayes, Gao and Taoudenni) across Mali (170 00'N – 40 00'W) were chosen for this research work. Satellite data of annual temperature obtained from the European Centre for Medium-Range Weather Forecast (ECMWF) database for 35 years (1985-2019) was used for this work. The Mann-Kendall trend test was carried out for various locations to observe and study the trend. Four Models including Auto Regressive and Integrated Moving Average (ARIMA), Exponential smoothening (ETS), TBATS (Trigonometric seasonality, Box-Cox transformation, ARMA errors, Trend and Seasonal components) and the linear model were employed to forecast average temperature for 10 years for all the locations. The model that produces the best forecast at the 95% confidence level is expected to have the lowest Root Mean Square Error (RMSE) value. The results showed that no significant trends were recorded at the considered locations. The linear model produced the best forecast for Segou, Kayes and Taoudenni, while the TBATS model produced the best forecast for Gao and the ARIMA model produced the best forecast for Sikasso.

Keywords: Trend Analysis; Forecast; Temperature; Mali; Mann-Kendall; Models

Introduction

Temperature is a physical quantity that expresses quantitatively the perceptions of hotness and coldness of a body or a place [1]. Increase in temperature are strongly associated with the changes in the earth's climate and tends to have negative effects on live and livelihood [2]. This has made it very important to study the trends and forecast the parameter thereby providing a clear picture of the climate of a location. Temperature forecasts are crucial because Mali's economy, which is heavily reliant on mining and agriculture, would expand if favorable climate circumstances were to occur [3]. Long-term variations in temperature and precipitation are important in defining the current and future changes seen in nature [4]. Monthly precipitation distortions may be desirable or undesirable in various months of the year, as crop growth period can be disrupted by

*Corresponding author: utbilly2001@yahoo.com

Tr Ren Energy, 2023, Vol.9, No.2, 167-179. doi: 10.17737/tre.2023.9.2.00158

heating from high temperatures [5]. Crop production and water-use efficiency are expected to be very inefficient due to reduced precipitation during this period, leading to increased demand for water at high temperatures [6].

Changes in surface temperature also tend to increase due to rapid land use conversions and modifications, which may present greater potential for climate-related hazards such as flooding, erosion, and any other relevant environmental hazards [7]. These harsh conditions are expected to double in the future due to increased levels of migration due to favorable socioeconomic, agricultural, political and natural factors, which pose a major threat to water resources, agricultural activities and ecosystem services [8]. These temperature variations are a strong indicator that the future of any place depends on it, and weather forecasting is in high demand for a variety of applications in areas such as agriculture, air traffic services, flooding, energy and environmental control [9].

The changes in the trends of temperature contribute greatly to the increase in global warming of any location. According to the Intergovernmental Panel on Climate Change (IPCC), emitted greenhouse gases are the main contributor to the increase in temperature, making global warming longer than expected unless the release of greenhouse gases is strictly controlled [10]. Daramola *et al.* [11] in their analysis of temperature over the climatic zones across Nigeria used data from ten Global Circulation Models (GCM) re-grided to a 1° x 1° spatial resolution. His analysis showed the standardized temperature forecast and anomaly over the different climatic zones in Nigeria from 2011-2100. From the summary statistics of the temperature anomaly for the zones, he concluded that positive anomaly exceeds the negative anomaly across all the zones, indicating more warm years than colder years.

Yusuf *et al.* [12] investigated the temperature trend in Nigeria using a network of ground based Automatic Weather Stations (AWS) installed at different locations in Nigeria. The results reveal a continuous variability that is seasonally dependent in each of the years. It was also seen that the results showed a steady increase in temperature recorded in the locations under study. This temperature increase is connected to the climate change observed in the locations under study as a result of increase in the concentration of greenhouse gases.

Short term predictions of temperature have failed to give a clear picture on future climate conditions, thereby creating the need to engage multiple models to forecast temperature [13]. The ideal model will be the one that forecasts temperature for that location with the lowest root mean square error [14]

Materials and Methods

For the purpose of this research work, the atmospheric data were satellite remote sensing data obtained from the archives of the European Centre for Medium-Range Weather Forecasts (ECMWF) Website. This dataset represents one of the best systematic estimates of the average annual temperature anomalies of the Earth's surface, taking all land and sea surfaces together, based on historical observations. The dataset is regularly updated and is freely available.

The meteorological data which was in degree Celsius were obtained using the geographical coordinates of each of the locations for the period of 35 years (1985 – 2019) covering 5 different locations across Mali. The locations are Segou, Sikasso, Kayes, Gao

and Taoudenni. Using the Anaconda software created and maintained by Anaconda, Inc. Austin, Texas, USA, which was established by Peter Wang and Travis Oliphant in 2012, the data that were initially griddled in NetCDF format were converted to readable format. The hourly data were further averaged to daily, monthly and yearly data using the same software to reduce the data, to obtain smoother profiles for easy analysis.

Data Analysis

Mann-Kendall trend analysis was carried out using the R programming language in all the locations to understudy and observe the trend of the parameter so as to compare with the forecasted values. Four different models were employed to run a decadal forecast of the parameter using the already obtained set of data for each of the locations. These models are Auto regressive integrated moving average (ARIMA), Exponential smoothing (ETS), TBATS (Trigonometric seasonality, Box-Cox transformation, ARMA errors, Trend, Seasonal components) and the linear regression models. The best model was selected using the root mean squared error (RMSE). The root mean square error is commonly used to evaluate quality predictions, because it measures the differences between predicted values and the observed or recorded values. Root mean square error can be expressed as:

$$RMSE = \sqrt{\frac{\sum_{i=1}^{n}(p_i - o_i)^2}{n}} \quad (1)$$

where P = predicted values, O = Observed values, n = sample size or number of data points, and Pi – Oi = the residual.

In machine learning, it is extremely helpful to have a single number to judge a model's performance, whether it be during training, cross-validation, or monitoring after deployment. Root mean square error is one of the most widely used measures for this. It is a proper scoring rule that is intuitive to understand and compatible with some of the most common statistical assumptions. The RMSE indicates the absolute fit of the model to the data by telling us how close the observed data points are to the models forecasted values. RMSE is a perfect measure of how accurately a model predicts the response, and it is the most important fit criterion if the primary purpose of the model is prediction. The lower values of RMSE portrays a better fit [15].

Results and Discussion

From the Mann-Kendall trend analysis, the parameters obtained include the Z-value, the Mann-Kendall statistic (S), the probability value (p-value) and the tau (τ). These parameters were computed for the period of study which covers all locations in the scope. The Mann-Kendall parameters for all the locations in Mali are presented below in Table 1.

Table 1 shows the Mann-Kendall trend analysis parameters for Segou, Sikasso, Kayes, Gao and Taoudenni. Results shows there are no significant Mann-Kendall trends recorded in the considered locations. This is because the p-values obtained in all the locations are greater than the set alpha value of 0.05. The positive z-value as well as the positive tau value becomes insignificant since there is no trend.

Table 1. Mann-Kendall trend test parameters for locations in Mali

MALI	Z-value	Sens's slope	p-value	tau(τ)	Trend Status
Segou	1.050906	0.012757	0.29330178	0.12605	No Trend
Sikasso	0.454446	0.005117	0.649507976	0.055462	No Trend
Kayes	1.704172	0.019308	0.08834899	0.203361	No Trend
Gao	-0.02865	-0.00025	0.97734084	-0.00504	No Trend
Taoudenni	-1.29666	-0.01854	0.20120399	-0.15294	No Trend

SEGOU

From Figure 1, average annual temperature was observed to vary over the years in Segou with the highest value at 24.073℃ in 2006 and the lowest value of 20.632℃ in 1989.

For the Arima Model, temperature was forecasted at the 95% confidence level and the forecast can go as high 22.67℃ as and as low as 20.98℃.

For the ETS model, temperature was forecasted at the 95% confidence level and the forecast could go as high 22.75℃ as and as low as 21.05℃.

For the linear regression model, temperature was forecasted at the 95% confidence level and the forecast could go as high 22.24℃ as and as low as 21.21℃.

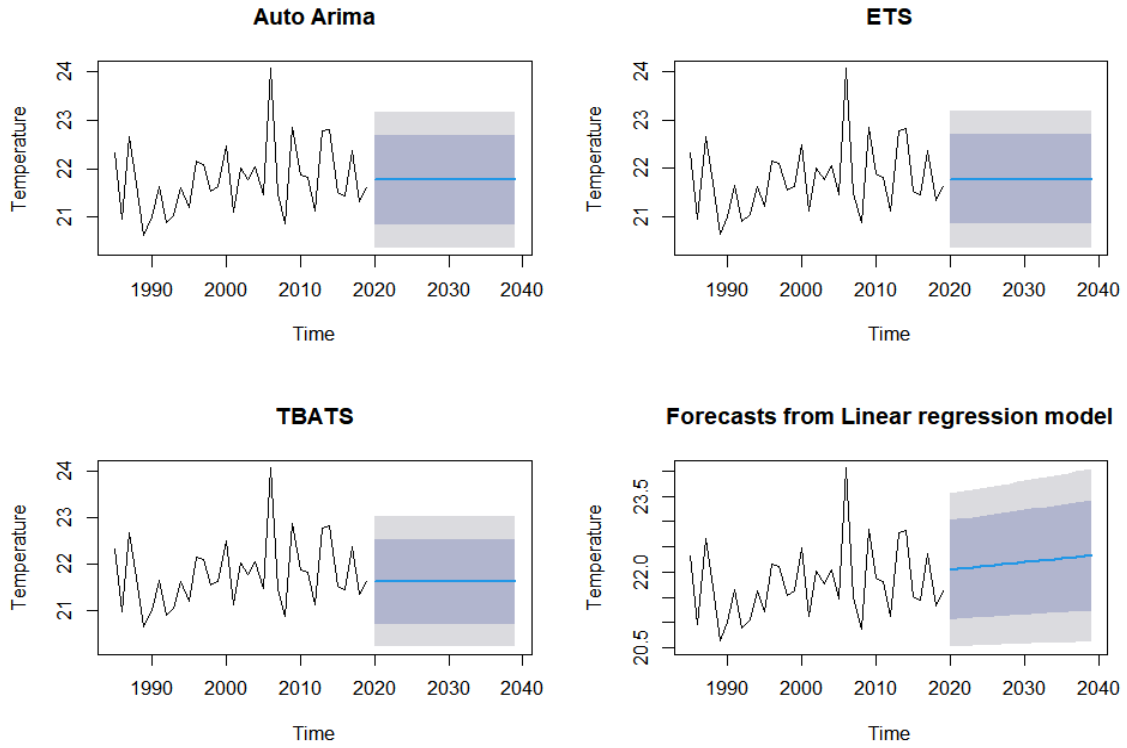

Fig. 1. Graphs showing temperature variations between 1985 and 2019 and forecast between 2020 and 2030 for Segou using the different models.

For the TBATS model, temperature was forecasted at the 95% confidence level and the forecast could go as high 22.65℃ as and as low as 20.82℃.

From Table 7, the model that made the best forecast was the linear model since it recorded the lowest Root Mean Square Error value of 0.690 for the location with a forecast range of 21.21℃ – 22.24℃. The average observed value was 22.35℃ and the forecast value is 21.73℃ with a percentage anomaly of -2.7%.

Below is a table showing the forecast coefficients for Segou.

Table 2: Forecast coefficients for Segou.

SEGOU	AIC	AICC	BIC	MEAN	R^2	SE	P value	INTERCEPT	ACF
ARIMA	79.04	79.41	82.15	21.7719	-	0.1195	-	-	-0.134
ETS	106.1503	106.9245	110.8163	-	-	-	-	-	-0.134
LINEAR	-	-	-	-	0.01734	0.24556	0.2148	21.50101	-0.204
TBATS	105.0908	-	-	-	-	-	-	-	-0.126

SIKASSO

From Figure 2, average annual temperature was observed to vary over the years in Sikasso with the highest value at 22.50℃ in 2006 and the lowest value of 20.04℃ in 1989.

For the Arima Model, temperature was forecasted at the 95% confidence level and the forecast can go as high 21.75℃ as and as low as 20.44℃.

For the ETS model, temperature was forecasted at the 95% confidence level and the forecast could go as high 21.65℃ as and as low as 20.31℃.

For the Linear regression model, temperature was forecasted at the 95% confidence level and the forecast could go as high 22.29℃ as and as low as 20.53℃.

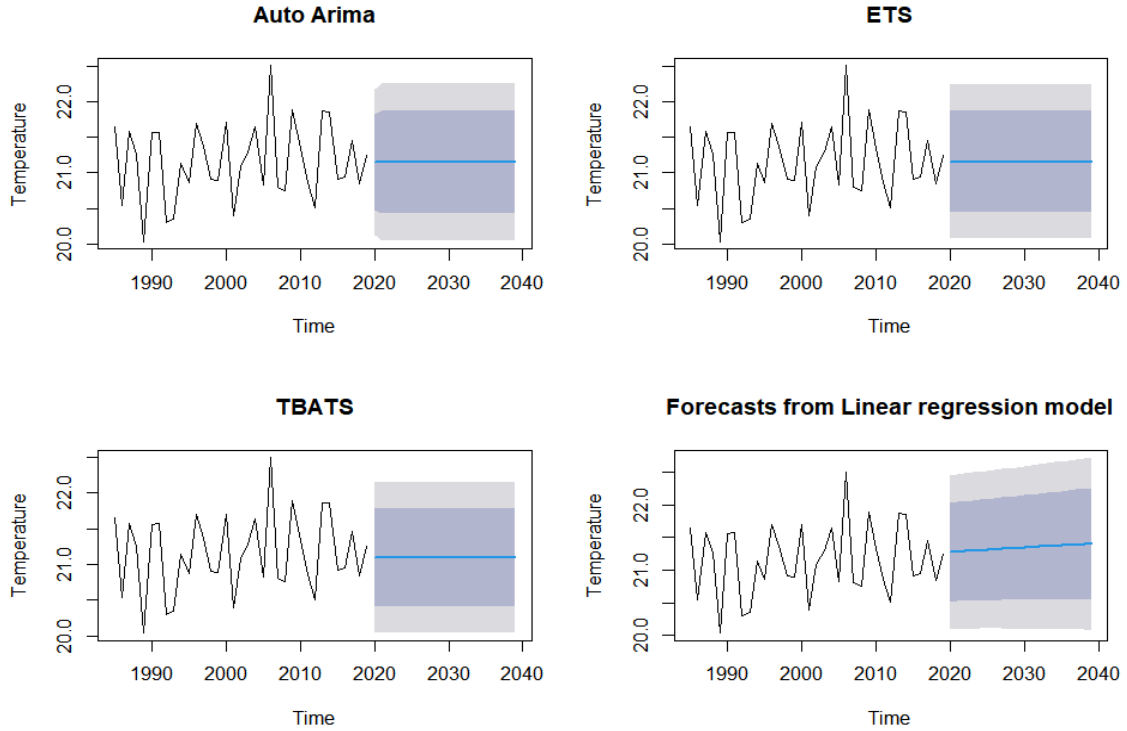

Fig. 2. Graphs showing temperature variations between 1985 and 2019 and forecast between 2020 and 2030 for Sikasso using the different models.

For the TBATS model, temperature was forecasted at the 95% confidence level and the forecast could go as high 21.72℃ as and as low as 20.41℃.

From table 7, the model that made the best forecast was the Arima model since it recorded the lowest Root Mean Square Error value of 0.507 for the location with a forecast range of 20.48℃ – 22.4℃. The average observed value was 21.27 and the forecast value is 21.40℃ with a percentage anomaly of 0.6%.

Below is a table showing the auto correlation function coefficients for Sikasso.

Table 3: Forecast coefficients for Sikasso.

SIKASSO	AIC	AICC	BIC	MEAN	R^2	SE	P value	INTERCEPT	ACF
ARIMA	58.01	58.78	62.67	21.1531	-	0.1601	-	-	0.042
ETS	86.78310	87.55730	91.44915	-	-	-	-	-	-0.225
LINEAR	-	-	-	-	-0.01359	0.189119	0.466	21.035041	-0.252
TBATS	84.80428	-	-	-	-	-	-	-	-0.223

KAYES

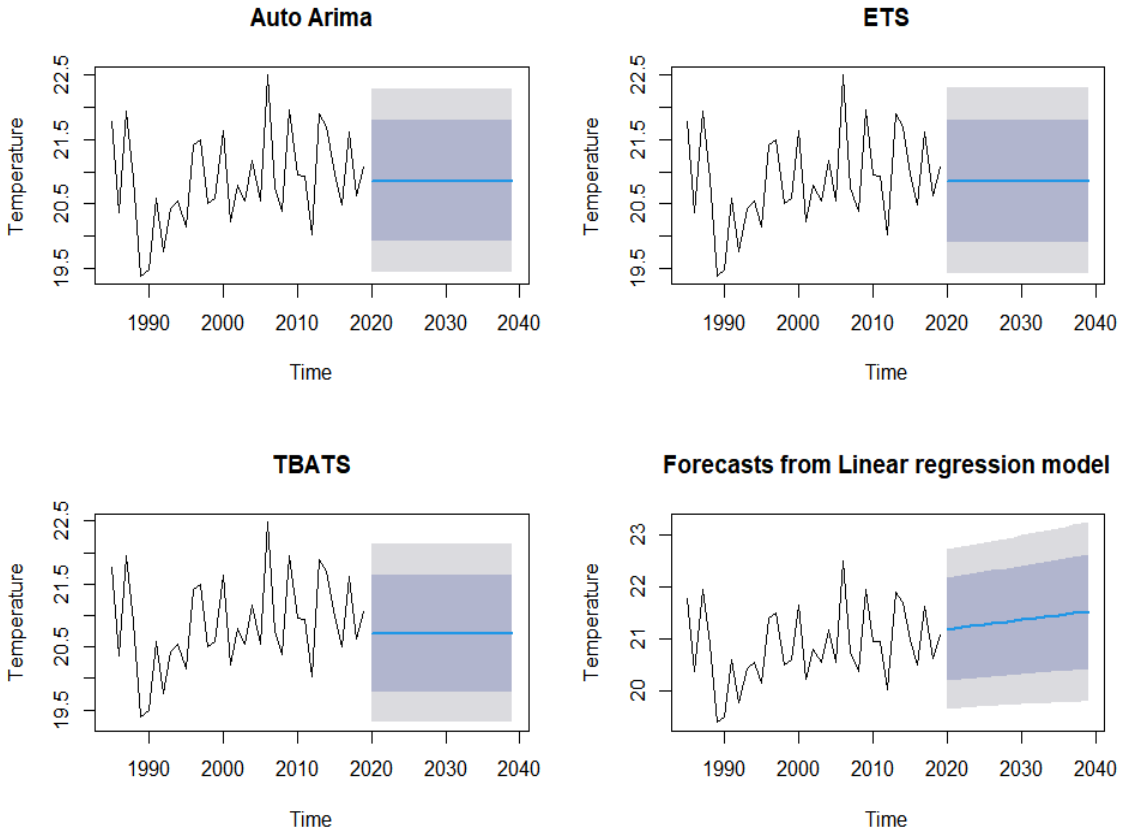

Fig 3: Graphs showing temperature variations between 1985 and 2019 and forecast between 2020 and 2030 for Kayes using the different models.

From Figure 3, average annual temperature was observed to vary over the years in Kayes with the highest value at 22.49℃ in 2006 and the lowest value of 19.38℃ in 1989. For the Arima Model, temperature was forecasted at the 95% confidence level and the forecast can go as high 21.87℃ as and as low as 20.16℃.

For the ETS model, temperature was forecasted at the 95% confidence level and the forecast could go as high 21.93℃ as and as low as 20.31℃.

For the linear regression model, temperature was forecasted at the 95% confidence level and the forecast could go as high 22.66℃ as and as low as 20.63℃.

For the TBATS model, temperature was forecasted at the 95% confidence level and the forecast could go as high 21.61℃ as and as low as 19.73℃.

From Table 7, the model that made the best forecast was the linear model since it recorded the lowest Root Mean Square Error value of 0.69 for the location with a forecast range of 21.63℃ – 22.66℃. The average observed value was 20.94℃ and the forecast value is 21.64℃ with a percentage anomaly of 3.34%.

Below is a table showing the forecast coefficients for Kayes.

Table 4: Forecast coefficients for Kayes

KAYES	AIC	AICC	BIC	MEAN	R^2	SE	P value	INTERCEPT	ACF
ARIMA	79.98	80.35	83.09	20.8588	-	0.1211	-	-	-0.0006
ETS	107.0921	107.8662	111.7581	-	-	-	-	-	-0.0006
LINEAR	-	-	-	-	0.03475	0.24668	0.1454	20.53801	-0.087
TBATS	105.7442	-	-	-	-	-	-	-	0.006

GAO

From Figure 4, average temperature was observed to vary over the years in Gao with the highest value at 25.49℃ in 2000 and the lowest value of 19.38℃ in 1997.

For the Arima Model, temperature was forecasted at the 95% confidence level and the forecast can go as high 25.50℃ as and as low as 22.48℃.

For the ETS model, temperature was forecasted at the 95% confidence level and the forecast could go as high 25.49℃ as and as low as 22.50℃.

For the linear regression model, temperature was forecasted at the 95% confidence level and the forecast could go as high 25.37℃ as and as low as 22.08℃.

For the TBATS model, temperature was forecasted at the 95% confidence level and the forecast could go as high 25.29℃ as and as low as 22.49℃.

From Table 7, the model that made the best forecast was the TBATS model since it recorded the lowest Root Mean Square Error value of 0.791 for the location with a forecast range of 22.49℃ – 25.29℃. The average observed value was 22.43℃ and the forecast value is 23.89℃ with a percentage anomaly of 6.51%.

Below is a table showing the forecast coefficients for Gao.

Table 5: Forecast coefficients for Gao.

GAO	AIC	AICC	BIC	MEAN	R^2	SE	P value	INTERCEPT	ACF
ARIMA	87.14	87.52	90.25	23.9494	-	0.1341	-	-	-0.12
ETS	114.2597	115.0339	118.9258	-	-	-	-	-	-0.12
LINEAR	-	-	-	-	-0.028	0.282073	0.8084	24.009550	-0.125
TBATS	112.0242	-	-	-	-	-	-	-	-0.125

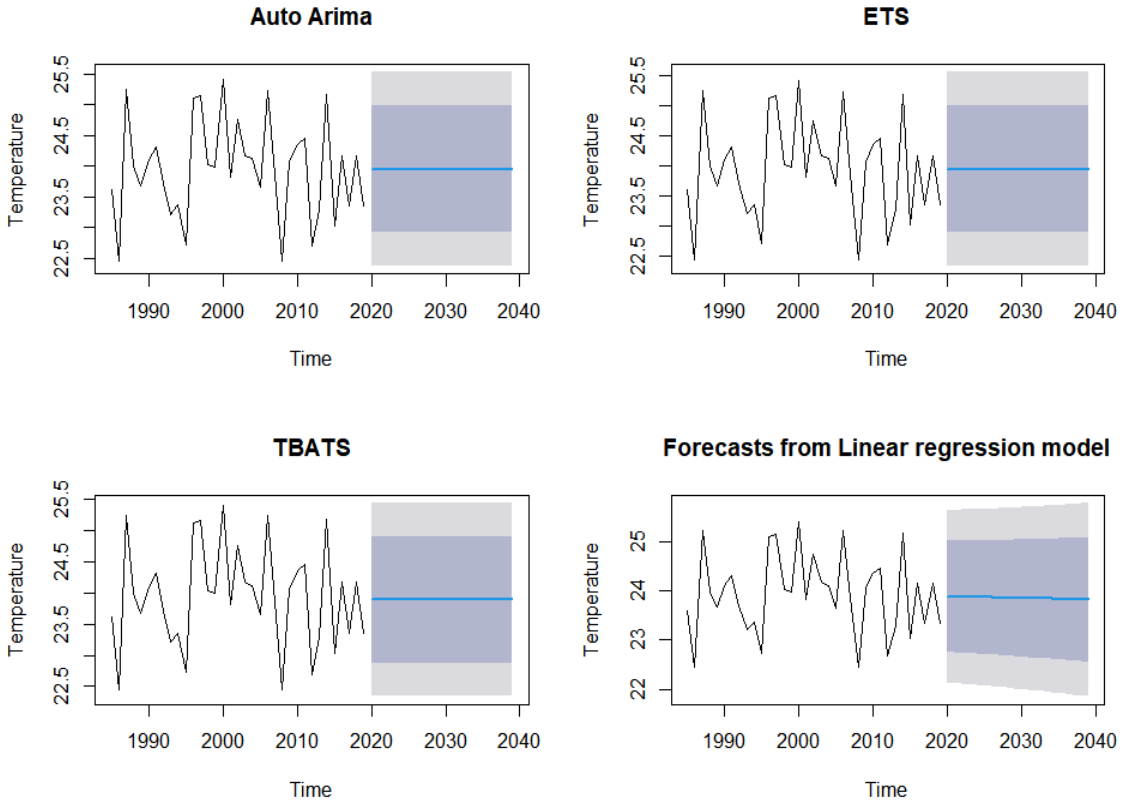

Fig. 4. Graphs showing temperature variations between 1985 and 2019 and forecast between 2020 and 2030 for Gao using the different models.

TAOUDENNI

From Figure 5, average temperature was observed to vary over the years in Taoudenni with the highest value at 21.29℃ in 1991 and the lowest value of 17.77℃ in 2008.

For the Arima Model, temperature was forecasted at the 95% confidence level and the forecast can go as high 21.25℃ as and as low as 17.97℃.

For the ETS model, temperature was forecasted at the 95% confidence level and the forecast could go as high 21.20℃ as and as low as 17.60℃.

For the Linear regression model, temperature was forecasted at the 95% confidence level and the forecast could go as high 20.64℃ as and as low as 16.82℃.

For the TBATS model, temperature was forecasted at the 95% confidence level and the forecast could go as high 21.15℃ as and as low as 17.71℃.

From Table 7, the model that made the best forecast for the location was the linear model since it recorded the lowest Root Mean Square Error value of 0.808 for the location with a forecast range of 16.822℃ – 20.64℃. The average observed value was 19.53℃ and the forecast value is 18.73℃ with a percentage anomaly of -4.1%.

Below is a table showing the forecast coefficients for Taoudenni.

Table 6: Forecast coefficients for Taoudenni.

TAOUDENNI	AIC	AICC	BIC	MEAN	R^2	SE	P value	Intercept	ACF
ARIMA	90.6	90.98	93.71	19.515		0.1409	-		0.040
ETS	117.7183	118.4925	122.384	-		-	-		0.040
LINEAR	-	-	-	-	0.060	0.8322	0.1536	19.88156	-0.023
TBATS	116.8273	-	-			0.2874	-		0.009

Fig. 5. Graphs showing temperature variations between 1985 and 2019 and forecast between 2020 and 2030 for Taoudenni using the different models.

Annual temperature variations from 1985-2019 and 10 year forecast for Segou is as shown in fig 1. Table 1 shows the Mann-Kendall trend analysis parameters for Segou and the results obtained exhibits no significant trend, making it difficult to assess the recent changes in temperature patterns in this location over the years considered. This is because the p-value of 0.293 is greater than the set alpha value of 0.05. The positive z-value of 1.05 recorded as well as the positive tau value of 0.126 becomes insignificant since there is no trend. The linear model produced the best forecast since it recorded the lowest Root Mean Square Error value of 0.69 for the location with a forecast range of 20.243℃ – 22.553℃. The average observed value was 21.06℃ and the forecast value is 21.73℃ with a percentage anomaly of 3.18%.

Annual temperature variations from 1985-2019 and 10 year forecast for Sikasso is as shown in fig 2. Table 1 shows the Mann-Kendall trend analysis parameters for Sikasso and the results obtained exhibits no significant trend, making it difficult to assess the recent changes in temperature patterns in this location over the years considered. This is because the p-value of 0.65 is greater than the set alpha value of 0.05. The positive z-value of 0.45 recorded as well as the positive tau value of 0.05 becomes insignificant since there is no trend. The ARIMA model produced the best forecast since it recorded the lowest Root Mean Square Error value of 0.51 for the location with a forecast range of 20.48℃ – 22.4℃. The average observed value was 21.27℃ and the forecast value is 21.40℃ with a percentage anomaly of 0.6%.

Table 7. Summary forecast Error Matrices for computer stimulated models for locations in Mali

COUNTRY	LOCATION	MODEL	FORECAST ERROR METRICS			
			RMSE	MAE	MPE	MAPE
MALI	SEGOU	ARIMA	0.7068015	0.5485527	-0.1025036	2.498599
		ETS	0.7068368	0.548575	-0.1019651	2.498689
		LINEAR	0.690267	0.5435422	-0.09763038	2.474713
		TBATS	0.7163979	0.5316598	0.4600906	2.407051
	SIKASSO	ARIMA	0.507526	0.4083713	-0.0391515	1.931589
		ETS	0.5359954	0.4477136	-0.0613197	2.117101
		LINEAR	0.5316043	0.4528471	-0.06303722	2.140672
		TBATS	0.5361576	0.4460023	0.1675978	2.104197
	KAYES	ARIMA	0.7163759	0.5798585	-0.1177178	2.776958
		ETS	0.7164117	0.5798236	-0.1160546	2.776747
		LINEAR	0.693391	0.5595368	-0.1099555	2.674297
		TBATS	0.7231157	0.5742113	0.3889485	2.735901
	GAO	ARIMA	0.7936096	0.6267157	-0.110006	2.620907
		ETS	0.793655	0.627	-0.09758923	2.621767
		LINEAR	0.7928921	0.6269887	-0.1098197	2.622059
		TBATS	0.7909886	0.6279222	0.1031281	2.620536
	TAOUDENNI	ARIMA	0.8338108	0.682474	-0.1832373	3.506958
		ETS	0.833853	0.6824711	-0.1796436	3.506819
		LINEAR	0.8081034	0.674337	-0.1719619	3.462911
		TBATS	0.8471683	0.7108771	-0.8564933	3.676114

Annual temperature variations from 1985-2019 and 10 year forecast for Kayes is as shown in Figure 3. Table 1 shows the Mann-Kendall trend analysis parameters for Kayes and the results obtained exhibits no significant trend, making it difficult to assess the recent changes in temperature patterns in this location over the years considered. This is because the p-value of 0.09 is greater than the set alpha value of 0.05. The positive z-value of 1.70 recorded as well as the positive tau value of 0.20 becomes insignificant since there is no trend. The linear model produced the best forecast since it recorded the lowest Root Mean Square Error value of 0.69 for the location with a forecast range of 21.63℃ – 22.66℃. The average observed value was 20.94℃ and the forecast value is 21.64℃ with a percentage anomaly of 3.34%.

Annual temperature variations from 1985-2019 and 10 year forecast for Gao is as shown in Figure 4. Table 1 shows the Mann-Kendall trend analysis parameters for Gao and the results obtained exhibits no significant trend, making it difficult to assess the recent changes in temperature patterns in this location over the years considered. This is because the p-value of 0.09 is greater than the set alpha value of 0.05. The negative z-value of 0.02 recorded as well as the negative tau value of 0.005 becomes insignificant since there is no trend. The TBATS model produced the best forecast since it recorded the lowest Root Mean Square Error value of 0.79 for the location with a forecast range of 22.49℃ – 25.29℃. The average observed value was 22.43℃ and the forecast value is 23.89℃ with a percentage anomaly of 6.51%.

Annual temperature variations from 1985-2019 and 10 year forecast for Taoudenni is as shown in Figure 5. Table 1 shows the Mann-Kendall trend analysis parameters for Taoudenni and the results obtained exhibits no significant trend, making it difficult to assess the recent changes in temperature patterns in this location over the years considered. This is because the p-value of 0.20 is greater than the set alpha value of 0.05. The negative z- value of 1.29 recorded as well as the negative tau value of 0.15 becomes insignificant since there is no trend. The linear model produced the best forecast since it recorded the lowest Root Mean Square Error value of 0.808 for the location with a forecast range of 16.822℃ – 20.64℃. The average observed value was 19.53℃ and the forecast value is 18.73℃ with a percentage anomaly of -4.1%.

CONCLUSIONS

Variations of air temperature have been observed in certain locations in Mali from 1985-2019 using satellite data from the European Centre for Medium-Range weather forecast (ECMWF) website and a 10-year forecast has been carried out using four different models (ARIMA, TBATS, ETS and the Linear model). The results reveal a continuous increase in temperature across most of the locations considered for this research. The Mann-Kendall trend test for the temperature trends at the various locations studied in the study showed that none of the locations showed a significant temperature trend. Temperature forecast results show that the linear model records the least RMSE, and is very effective in forecasting average temperature for Segou, Kayes and Taoudenni. Taking the anomaly percentage of 3.18% for the forecast point value of 21.73°C, 3.34% of the anomaly percentage for the forecast point value of 21.64°C and -4.1% of the anomaly percentage of the forecast point value of 18.73°C, using the 95% confidence interval, it is found that the RMSE It is effective.

The ARIMA model that recorded the smallest RMSE was found to be the best model for predicting Sikasso temperature. This is because it has a predicted point value of 21.40°C and an anomaly percentage of 0.6%. TBATS has the smallest high RMSE, the forecast point value is 23.89°C, and the anomaly percentage using the 95% confidence interval is 6.51%, so it is considered as the best model for temperature forecasting in this region.

Negative anomaly was recorded in Taoudenni while positive anomaly was recorded in Segou, Kayes, Sikasso and Gao. This suggests that cooler years are expected to be warmer in these regions, further suggesting that events associated with higher temperatures may increase, such as droughts.

These are in line with the Intergovernmental Panel on Climate Change projections that there will be “high likelihood of warming” ranging West Africa. This has wide-ranging implications for many economic sectors such as the health sector, aviation, agriculture, water resources, etc. Active steps by individuals, governments and companies will help mitigate the effects of climate change.

CONFLICTS OF INTEREST

The authors declare that there is no conflict of interests regarding the publication of this paper.

REFERENCES

[1] Fabbri, K. (2015). Indoor thermal comfort perception. *A Questionnaire Approach Focusing on Children; Springer: New York City, NY, USA*.

[2] Dube, T., Moyo, P., Ncube, M., & Nyathi, D. (2016). The impact of climate change on agro-ecological based livelihoods in Africa: A review. *Dube T, Moyo P, Mpofu M, Nyathi D (2016), The impact of climate change on agro-ecological based livelihoods in Africa: A review, Journal of Sustainable Development*, *9*(1), 256-267.

[3] Aune, J. B., Coulibaly, A., & Giller, K. E. (2017). Precision farming for increased land and labour productivity in semi-arid West Africa. A review. *Agronomy for sustainable development*, *37*, 1-10.

[4] Yang, K., Yu, Z., Luo, Y., Zhou, X., & Shang, C. (2019). Spatial-temporal variation of lake surface water temperature and its driving factors in Yunnan-Guizhou Plateau. *Water Resources Research*, *55*(6), 4688-4703.

[5] Aragón, F. M., Oteiza, F., & Rud, J. P. (2021). Climate change and agriculture: Subsistence farmers' response to extreme heat. *American Economic Journal: Economic Policy*, *13*(1), 1-35.

[6] Dissanayake, D. M. S. L. B., Morimoto, T., Murayama, Y., Ranagalage, M., & Handayani, H. H. (2018). Impact of urban surface characteristics and socio-economic variables on the spatial variation of land surface temperature in Lagos City, Nigeria. *Sustainability*, *11*(1), 25.

[7] Ibitoye M. O., Aderibigbe O. G., Adegboyega S. &Adebola A. (2017). Spatio temporal analysis of land surface temperature variations in the rapidly developing Akure and its environs, southwestern Nigeria using Land sat data. *Ethiopian Journal of Environmental Studies and Management* 10(3):389, DOI:10.4314/ejesm.v10i3.9.

[8] Ogunjobi, K. O., Adamu, Y., Akinsanola, A. A., & Orimoloye, I. R. (2018). Spatio-temporal analysis of land use dynamics and its potential indications on land surface temperature in Sokoto Metropolis, Nigeria. *Royal Society open science*, *5*(12), 180661.

[9] Jaseena, K. U., & Kovoor, B. C. (2022). Deterministic weather forecasting models based on intelligent predictors: A survey. *Journal of King Saud University-Computer and Information Sciences*, *34*(6), 3393-3412.

[10] Paglia, E., & Parker, C. (2021). The intergovernmental panel on climate change: guardian of climate science. *Guardians of Public Value: How Public Organisations Become and Remain Institutions*, 295-321.

[11] Daramola, M. T., Eresanya, E. O., & Erhabor, S. C. (2017). Analysis of rainfall and temperature over climatic zones in Nigeria. *J Geogr Environ Earth Sci Int*, *11*, 1-14.

[12] Yusuf, N., Okoh, D., Musa, I., Adedoja, S., & Said, R. (2017). A study of the surface air temperature variations in Nigeria. *The Open Atmospheric Science Journal*, *11*(1).

[13] Taylor, K. E., Stouffer, R. J., & Meehl, G. A. (2012). An overview of CMIP5 and the experiment design. *Bulletin of the American meteorological Society*, *93*(4), 485-498.

[14] Stoner, A. M., Hayhoe, K., Yang, X., & Wuebbles, D. J. (2013). An asynchronous regional regression model for statistical downscaling of daily climate variables. *International Journal of Climatology*, *33*(11), 2473-2494.

[15] Chai, T., & Draxler, R. R. (2014). Root mean square error (RMSE) or mean absolute error (MAE)?–Arguments against avoiding RMSE in the literature. *Geoscientific Model Development*, 7(3), 1247-1250.

Trends in Renewable Energy
OPEN ACCESS ISSN: 2376-2144
Peer-Reviewed Review Article futureenergysp.com/index.php/tre

A Review of Low Temperature Combustion Mode of Engine

Qingyang Hao

North China University of Water Resources and Electric Power, No. 36, Beihuan Road, Zhengzhou City, Henan, China

Received May 10, 2023; Accepted June 21, 2023; July 14, 2023

Since the 21st century, people's increasing attention to fuel economy and environmental issues has prompted the engine research community to continuously develop new efficient and clean combustion theories and methods. In terms of combustion technology, many researchers have proposed different new engine combustion methods, such as homogeneous charge compression ignition combustion (HCCI), premixed charge compression combustion (PCCI), and reaction controlled compression ignition (RCCI), which are the three main low-temperature combustion methods. These combustion methods are different from the premixed combustion method of the spark ignition (SI) engine represented by the traditional gasoline engine and the diffusion combustion method of the compression ignition (CI) engine represented by the traditional diesel engine. The flame temperature affects the combustion and emission process of the engine, and realizes the efficient and clean combustion of the engine. This paper first briefly describes the conventional engine combustion method, and then briefly summarizes the comparison between these three low-temperature combustion methods and their respective combustion and emission characteristics as well as advantages and disadvantages, with respect to the conventional combustion method.

Keywords: Internal combustion engine; Combustion method; Homogeneous charge compression ignition combustion (HCCI); Premixed charge compression combustion (PCCI); Reaction controlled compression ignition (RCCI)

1. Introduction

Rising global energy demand and concerns about environmental protection require engines in the automotive industry to effectively improve fuel efficiency and reduce exhaust emissions. The proportion of pollutants has met the current emission regulations and environmental protection requirements, but with the development of technology and the advancement of CO_2 regulations, ultra-low emissions or even zero emissions of harmful emissions will be required in the future. Economics and emissions are becoming more stringent, requiring new advances in alternative fuels and combustion technologies for engines to meet energy demands and regulatory requirements. In this context, the limitations of the combustion method of conventional combustion engines make it impossible to meet the requirements. To this end, many researchers have proposed a variety of new combustion methods, hoping to improve or replace traditional combustion methods to achieve the goals of high efficiency and low emissions. Such new combustion methods include homogeneous charge compression ignition (HCCI),

*Corresponding author: 18239192965@163.com

Tr Ren Energy, 2023, Vol.9, No.2, 180-191. doi: 10.17737/tre.2023.9.2.00160

premixed charge compression ignition (PCCI), and reaction controllable compression ignition (RCCI). These three low-temperature combustion methods are the most widely used.

2. Limitations of Traditional Combustion Methods

There are two main types of combustion in traditional internal combustion engines: spark ignition (SI) represented by gasoline engine and compression ignition (CI) represented by diesel engine. Spark ignition engines are difficult to obtain high thermal efficiency due to relatively low compression. Compression ignition engines are more thermally efficient than spark ignition engines, but their diffusion combustion leads to an inability to deal with the relationship between NO_x and carbon soot (soot) emissions [1].

2.1 Conventional Spark Ignition

Spark-ignition engines generally use premixed combustion, which makes the fuel and air mix uniformly in advance, fixes the mixture combustion-to-air ratio, changes the total amount of mixture entering the cylinder by adjusting the throttle opening, and controls the engine torque output to adapt to different engine operating conditions by using the volume regulation. The uniformly mixed combustible mixture is ignited by the spark plug at the end of the compression stroke, and then the flame front spreads in the homogeneous mixture. The local temperature of the flame front and its combustion products is much higher than that of other unburned mixture, and the temperature distribution in the combustion chamber is extremely uneven. Local high temperature tends to lead to the formation of NO_x in the burned zone.

2.2 Conventional Compression Ignition

The compression-ignition engine adjusts the engine's cycle fuel supply by means of a fuel regulation system using mass regulation to adapt to changes in engine operating conditions. Its mixture is formed inside the cylinder, that is, when the piston is close to the top dead center, the fuel supply and regulation system injects fuel into the cylinder at high pressure within a short crank angle to achieve fuel mixing. Combustion with air, but due to the short mixing process, the mixture in the compression ignition engine is not uniform. At the same time, the compression-ignition engine combustion process is controlled by the mixing and diffusion combustion process, the chemical reaction rate is much higher than the mixing and diffusion rate of fuel and air, and the speed of combustion is determined by the mixing and diffusion rate. Therefore, in this type of combustion, although multiple points are ignited at the same time of compression, due to the extremely uneven gas mixture concentration and temperature distribution, NO_x is generated in the local high-temperature area of the combustion chamber, and carbon particles are generated in the high-temperature anoxic area. In summary, these two traditional combustion methods are characterized by uneven temperature distribution and combustion process, and it is difficult to achieve high efficiency and low emission at the same time. Therefore, the development of new combustion methods based on the traditional combustion methods to improve the efficiency and reduce the emissions of internal combustion engines [2].

3. Low Temperature Combustion Method

High-temperature oxygen enrichment promotes NO_x generation, and reducing combustion temperature can effectively reduce NO_x emissions. However, reducing the combustion temperature will also reduce the oxidation of soot, thereby increasing soot emissions. Therefore, the combustion temperature cannot be simply lowered. But below a certain temperature level, the combustion can avoid the main NO_x and smoke generating areas [3]. The low-temperature combustion method avoids a high combustion temperature in the cylinder, and at the same time changes the oil-gas mixture before combustion, improves the uniformity of the mixture, effectively reduces the emission of NOx and PM particles, and provides higher thermal efficiency, which effectively solves the problem of traditional combustion limitations of the method. The low temperature combustion is mainly achieved by high ratio of exhaust gas recirculation (EGR). The higher ratio of EGR rate can make the total specific heat capacity of in-cylinder mixture increase, which makes the temperature of combustion lower, avoiding the area of large amount of NO_x generation and reducing NO_x emission [4-5]. Meanwhile, it changes the oil-gas mixture before combustion, changes the concentration distribution, improves the mixture uniformity, reduces the local over-concentration area, and thus reduces the carbon soot generation. But at the same time, too low combustion temperature will reduce the combustion efficiency and lead to deterioration of fuel economy. Therefore, the key to the application of low temperature combustion technology is to achieve a better combination of combustion efficiency, fuel economy and emission.

3.1 HCCI Combustion Method of Internal Combustion Engine and its Characteristics

Homogeneous Charge Compression Ignition (HCCI) combustion was originally proposed by Onishi, Noguchi and Najt in the late 1970s and early 1980s as a concept with two basic features: homogeneous mixture and compression ignition, thus combining the best performance of spark ignition and compression ignition engines. However, due to technical problems at the time, it has not been reintroduced for study until recent years. HCCI is a new combustion method for internal combustion engines after decades of research by domestic and foreign scholars [6-7]. The HCCI combustion method is based on the homogeneous charge spark ignition gasoline engine and the stratified charge compression ignition diesel engine, and the advantages of both are combined in the innovative design. HCCI looks like a combination of spark ignition and compression ignition, with the homogeneous premixed gas of spark ignition engine and compression ignition of compression ignition engine. But in terms of combustion essence, HCCI combustion method is different from the traditional SI and CI combustion methods [8-10]. The SI engine injects fuel through the intake stroke to prepare a homogeneous fuel-air mixture, and then completes the entire combustion process through flame propagation after spark ignition. The CI engine injects fuel through mass regulation, and relies on flame propagation during the deceleration period after ignition through compression combustion, relying on the diffusion of the combustible mixture during the slow combustion period. The HCCI engine is not just a simple combination of the two traditional combustion methods, *i.e.,* it is neither propagation combustion nor non-diffusion combustion. But it is the same as the SI engine, before the start of combustion, the combustion chamber is already filled with evenly mixed critical combustible gas. It also like a CI engine, after further compression by the piston compression stroke, the

temperature and pressure in the cylinder reach a certain level, and multiple ignition points are ignited in the combustion chamber at the same time. Based on the chemodynamic reaction, the HCCI combustion process consists of two stages: The initial stage of combustion is low temperature oxidation (LTO) and the second stage of combustion is high temperature oxidation(HTO) [11-16].

3.1.1 Advantages of HCCI Combustion Method

(1) High thermal efficiency

HCCI engines are generally realized by exhaust gas recirculation (EGR) technology. Through a high proportion of EGR rate, in addition to fuel and fresh charge, there is exhaust gas from the previous cycle in the combustible mixture of each cycle, changing the concentration of the mixture. At the same time, increasing the total specific heat capacity of the mixture makes the combustion temperature in the cylinder drop significantly, effectively reducing the heat transfer loss caused by heat transfer to the cylinder wall. In addition, HCCI adopts a quality adjustment similar to CI, without throttling loss. Multiple points are ignited at the same time during combustion. There is no obvious flame propagation, and heat loss is reduced. The HCCI engine has a higher compression ratio, and the continuous combustion time of compression ignition is short. So, the thermal efficiency can be further improved. Generally, the HCCI engine can use a lean mixture and get a relatively high power [17].

(2) Low NO_x and carbon soot particle emissions

The combustible mixture of the HCCI engine is mixed evenly before being compressed and ignited. At the same time, the concentration of the oil-air mixture is reduced by using EGR. Due to the homogeneous and lean fuel-air mixture, the soot emission of the HCCI engine is extremely low. In addition, the HCCI engine adopts quality adjustment control similar to CI to inject fuel, and then compresses and ignites at multiple points. The uniform mixture burns at a very fast speed, which improves the fuel utilization rate, and the thin fuel-air mixture also reduces the maximum temperature in the cylinder [18]. Therefore, while increasing the average temperature in the cylinder, the maximum temperature in the cylinder is reduced, and the NO_x emission is effectively reduced.

(3) Fuel flexibility

The HCCI engine is a fuel-flexible engine. It does not need specific fuel to perform (like traditional SI and CI engines). It can accept any type of fuel, such as high octane fuel and high propane [19].

3.1.2 Shortcomings of HCCI Combustion Method

(1) Emissions of CO and unburned hydrocarbons (UHC)

The HCCI combustion method mainly solves the emission problems of NO_x and soot particles, but it makes the CO and unburned hydrocarbon (UHC) emissions higher than the traditional combustion method. This is mainly because the high ratio EGR makes the peak in-cylinder combustion temperature lower, resulting in part of the fuel not being completely burned during the combustion process and the hydrocarbons not being completely oxidized and eventually expelled along with the burned mixture. In addition, the low temperature combustion of HCCI will increase the intensity of the cylinder wall excitation cooling effect, thus causing the HC emissions to rise [20].

(2) Difficulty in cold start of HCCI engine

Because the HCCI engine performs low-temperature lean combustion, the temperature of the cylinder wall and the mixture in the cylinder is low under cold start conditions, which may cause the engine to fail to compress normally and catch fire, affecting engine startup and combustion. Scholars have also studied a variety of solutions to this problem. One is to start through the traditional combustion mode and then switch to the HCCI combustion mode; the other is to change the intake air temperature to heat the intake air to complete the start; the third is to use variable compression ratio or variable valve control technology to increase the compression ratio, which not only improves the cold start performance of the HCCI engine, but also changes the load range.

(3) Combustion phase control

The two extremely important parameters of engine combustion are fuel injection timing and ignition timing. Since HCCI compresses and ignites at the same time, it does not control the timing of the ignition like a SI engine does with spark plug direct ignition. The ignition of HCCI engine fuel depends entirely on the temperature and pressure in the cylinder as well as the physical and chemical properties of the fuel. There is no physical mechanism that can precisely control the spontaneous combustion moment of the mixture. Therefore, it is difficult to control the combustion phase of the HCCI engine, which will affect the combustion performance of the engine. Therefore, the combustion phase control of HCCI engines has become one of the key and difficult points in the research of current HCCI combustion methods.

(4) Small operating range

Since HCCI is low-temperature lean-burn, it can only operate normally in the low-load range. And there is the possibility of misfire at low load, and at high load, it is very likely to spontaneously ignite due to compression in the cylinder, thereby causing an explosion. Therefore, HCCI engines cannot operate normally under various operating conditions as conventional SI and CI engines, which hinders the widespread use of HCCI combustion methods [21-22].

3.2 PCCI Combustion Method of Internal Combustion Engine and its Characteristics

The emergence and development of premixed charge compression ignition (PCCI) combustion is due to the fact that HCCI combustion is mainly controlled by chemical reaction kinetics, and it is difficult to control the combustion time and combustion rate in the full range of operating conditions. The premixed charge compression combustion PCCI mode engine has a larger mixture concentration range and has the potential to expand the range of clean operating conditions, which is easier to achieve than HCCI

PCCI generally adopts secondary injection or multi-stage injection, and usually injects part of the fuel to the intake pipe or cylinder in the early stage of the intake or compression process. Therefore, the fuel supply varies between 10% and 70% of the circulating oil volume, while self-injecting the cylinder near dead center under compression. The mixture before the main injection is relatively lean and cannot be ignited. After the main injection, the concentration of the mixture increases. When the mixture in the cylinder reaches the self-ignition temperature, it will cause ignition and combustion. The two main parameters affecting its performance are premixed fuel volume and main injection timing. This combustion concept for refining in-cylinder parameters is considered to be a more practical and economical approach compared to HCCI [23].

The PCCI combustion mode uses a combination of multi-stage injection strategies (such as advance or lag injection and large proportional exhaust gas recirculation EGR) to control the combustion phase and combustion rate. Depending on the injection timing, PCCI is usually divided into two types: One is achieved by early fuel injection, where fuel is injected into the cylinder at very early injection timing (90° to 120° CA before the upper stop) to obtain sufficient mixing time to form a thin and homogeneous mixture. The other is achieved by late fuel injection, where fuel is injected close to the upper stop [24].

3.2.1 Advantages of PCCI Combustion Method for Internal Combustion Engines

(1) Combustion control

PCCI mainly achieves better mixing of fuel and air before combustion compared with CI engine, so as to reduce the proportion of diffusion combustion in combustion. After simultaneous ignition at multiple points, as much fuel as possible is completely burned in the premixed combustion stage, and the diffusion combustion stage is reduced or even eliminated as far as possible. In order to achieve a better combustion effect than HCCI combustion and obtain better combustion control.

(2) Operating conditions

Different from HCCI combustion, PCCI combustion adopts a mixture that is not sufficiently homogeneous, but achieves its charge gradient in terms of temperature and concentration, so that mixtures with different concentration gradients do not burn at the same time in the cylinder, thus controlling its combustion speed and reducing the heat release rate of combustion. Therefore, PCCI combustion can be applied to medium and high loads [25].

(3) Emission performance

The combustion nature of PCCI is also low-temperature combustion. Although PCCI increases the overall combustion temperature compared with HCCI, the maximum combustion temperature is still lower than that of traditional combustion methods. Therefore, compared with HCCI, the NO_x and PM emissions of PCCI are higher, but still lower than that of traditional combustion methods. At the same time, the emission of PCCI combustion process mainly changes according to the main injection time. Early fuel injection is carried out under the condition of low in-cylinder density and temperature, which can easily lead to the increase of unburned hydrocarbon emission and deterioration of combustion efficiency [26]. When fuel injection is late, fuel injection is near top dead center, and a high proportion of EGR is added to control ignition phase and optimize mixing time, reducing mixture concentration zone to reduce soot emission under low oxygen volume fraction conditions.

3.2.2 Deficiency of PCCI Combustion Mode

(1) CO and unburned HC emissions

Shim *et al.* [27] compared engine performance and emission characteristics with HCCI, PCCI and dual-fuel PCCI combustion modes on heavy-duty diesel engines, and the results showed that the emission characteristics of CO and THC under the average indicated pressure of 0.45Mpa under various combustion modes. The emission of CO and THC of HCCI and PCCI combustion is higher than that of traditional combustion, and the emission of CO and THC of PCCI combustion is higher than that of HCCI combustion. In fact, this is one of the main reasons these advanced combustion technologies are not yet practical.

(2) Reduced thermal efficiency

The PCCI combustion method usually adopts two-stage injection or multi-stage injection. In the case of two-stage high-pressure injection, the fuel injected in the early stage can be combusted during the compression process. This injection method is more conducive to the control of the pressure rise rate and the highest combustion temperature during combustion. However, it will lead to an increase in the negative work of compression, and at the same time, the cycle combustion caused by incomplete oxidation will start earlier, thus increasing the heat transfer loss and reducing the thermal efficiency [28].

3.3 RCCI Combustion Mode and its Characteristics

RCCI also belongs to low temperature premixed combustion, which is a new low temperature combustion mode using fuel ignition activity to control combustion [29]. The biggest difference between the combustion mode of HCCI and PCCI is that RCCI combustion requires the combination of two fuels with relatively different activity and physical and chemical properties through the inlet injection and in-cylinder direct injection. Low reactive fuel (such as gasoline or alcohol) is injected in the inlet, and high reactive fuel (such as diesel) is directly injected in the combustion chamber at the end of compression stroke. Through the reactivity stratification and concentration distribution of mixtures in the cylinder, the combustion stage, heat release rate and premix ratio can be effectively controlled, so as to optimize the combustion process, improve thermal efficiency and reduce emissions [30].

3.3.1 The Advantages of RCCI Combustion Mode in Internal Combustion Engine

(1) Controlled combustion phase

The biggest problem of HCCI is that the combustion phase is not controllable. The RCCI combustion method has made a great breakthrough in this problem. RCCI controls the reaction activity of the mixture by controlling the blending ratio of two fuels with different reactivity to control the ignition moment and further control the combustion process, and also can effectively alleviate the peak pressure rise rate [31-32].

(2) Wider operating conditions

Since the RCCI combustion method has in-cylinder activity stratification, equivalence ratio and temperature stratification, the control of workpiece activity, equivalence ratio and temperature can effectively suppress engine knocking and make the working conditions of RCCI combustion wider [33].

(3) High thermal efficiency

Since the RCCI combustion working fluid is more uniformly mixed, the resulting temperature field is also uniform. So, the maximum temperature is lower, but the overall average temperature is not low. On the contrary, due to the uneven mixing of the working fluid and the large stratification range of the equivalence ratio in the traditional diesel engine combustion, the maximum combustion temperature is very high, and it is close to the cylinder wall. So, the heat transfer loss is large, but the overall average temperature is not higher than that of RCCI combustion [34].

3.3.2 Shortcomings of RCCI Combustion Method

(1) High CO, HC emissions

RCCI combustion (like other premixed combustion) has the problem of high HC and CO emissions, because the premixed gas injected into the intake port will inevitably

enter the gap area in the cylinder, such as the gap between the piston and the cylinder liner. The combustion flame is difficult to spread to the small gap area, which causes the mixture into this area can not be completely combusted [35]. Therefore, compared to the traditional combustion method, RCCI combustion of HC, CO emissions are high, which affects the combustion efficiency of RCCI combustion. The problem can be solved with two existing technologies: One is to re-introduce the exhaust gas into the cylinder secondary combustion through EGR. The second is the exhaust after-treatment catalytic oxidation.

(2) Rough working style at high load

The RCCI combustion method solves the problem of the small operating load range of the HCCI. However, although it can operate at high loads, the stability of high-load combustion is very poor [36]. Although RCCI combustion can work smoothly without using EGR at low and medium loads, it can achieve ultra-low emissions of NO_x and soot while maintaining high thermal efficiency. However, under high-load conditions, in order to maintain low emissions, the amount of fuel injected into the intake port will increase accordingly. At this time, the combustion under the compression ignition of direct-injection high-reactivity fuel in the cylinder will produce a situation similar to gasoline engine knocking. The pressure rise rate will increase, and the pressure fluctuation will also be large, resulting in rough work and unstable combustion.

4. CONCLUSIONS

The three low-temperature combustion methods of HCCI, PCCI, and RCCI are based on the traditional combustion method. Through homogeneous premixing and compression ignition in advance, the mixed state of oil and gas before combustion is changed, the temperature in the cylinder is reduced during combustion, and low-temperature combustion is realized. This combustion mode with great potential to reduce engine NO_x and soot particles can completely avoid the generation of NO_x and soot particles in the combustion path of the engine by optimizing parameters (such as EGR rate, fuel injection timing, compression ratio, and intake air temperature). At the same time, the lower combustion temperature is also conducive to reducing heat transfer loss and radiation loss, thereby improving thermal efficiency and achieving the purpose of efficient and clean combustion.

Although these three low-temperature combustion methods can achieve efficient and clean combustion of the engine to a certain extent, there are still certain difficulties in practical application. Firstly, these three low-temperature combustion methods have a narrow range of operating conditions. Although RCCI can achieve high-load operation, the work is rough and stable operation under high-load conditions is still a key problem to be solved by new combustion technologies. Secondly, although the three combustion methods have improved the emission of NO_x and soot particles, the emissions of CO and HC are still relatively high. In order to meet the increasingly stringent emission regulations, the low-temperature combustion method should continue to be studied and improved. With the continuous research and improvement of scientific researchers, new combustion methods will be continuously improved to achieve better combustion performance. Combined with new alternative combustion, it will bring great changes in the field of internal combustion engines, and meet people's requirements for internal combustion engines with high efficiency and clean combustion.

CONFLICTS OF INTEREST

The author declares that there is no conflict of interests regarding the publication of this paper.

REFERENCES

[1] Krishnasamy, A., Gupta, S. K., & Reitz, R. D. (2021). Prospective fuels for diesel low temperature combustion engine applications: A critical review. *22*(7), 2071-2106. doi: https://doi.org/10.1177/1468087420960857

[2] Gharehghani, A. (2019). Load limits of an HCCI engine fueled with natural gas, ethanol, and methanol. *Fuel, 239*, 1001-1014. doi: https://doi.org/10.1016/j.fuel.2018.11.066

[3] Vasudev, A., Mikulski, M., Balakrishnan, P. R., Storm, X., & Hunicz, J. (2022). Thermo-kinetic multi-zone modelling of low temperature combustion engines. *Progress in Energy and Combustion Science, 91*, 100998. doi: https://doi.org/10.1016/j.pecs.2022.100998

[4] Riyadi, T. W. B., Spraggon, M., Herawan, S. G., Idris, M., Paristiawan, P. A., Putra, N. R., R, M. F., Silambarasan, R., & Veza, I. (2023). Biodiesel for HCCI engine: Prospects and challenges of sustainability biodiesel for energy transition. *Results in Engineering, 17*, 100916. doi: https://doi.org/10.1016/j.rineng.2023.100916

[5] Jain, A., Singh, A. P., & Agarwal, A. K. (2017). Effect of split fuel injection and EGR on NOx and PM emission reduction in a low temperature combustion (LTC) mode diesel engine. *Energy, 122*, 249-264. doi: https://doi.org/10.1016/j.energy.2017.01.050

[6] Maurya, R. K., & Akhil, N. (2017). Comparative study of the simulation ability of various recent hydrogen combustion mechanisms in HCCI engines using stochastic reactor model. *International Journal of Hydrogen Energy, 42*(16), 11911-11925. doi: https://doi.org/10.1016/j.ijhydene.2017.02.155

[7] Djermouni, M., & Ouadha, A. (2023). Thermodynamic analysis of methanol, ammonia, and hydrogen as alternative fuels in HCCI engines. *International Journal of Thermofluids, 19*, 100372. doi: https://doi.org/10.1016/j.ijft.2023.100372

[8] Kakoee, A., Bakhshan, Y., Aval, S. M., & Gharehghani, A. (2018). An improvement of a lean burning condition of natural gas/diesel RCCI engine with a pre-chamber by using hydrogen. *Energy Conversion and Management, 166*, 489-499. doi: https://doi.org/10.1016/j.enconman.2018.04.063

[9] Duan, X., Lai, M.-C., Jansons, M., Guo, G., & Liu, J. (2021). A review of controlling strategies of the ignition timing and combustion phase in homogeneous charge compression ignition (HCCI) engine. *Fuel, 285*, 119142. doi: https://doi.org/10.1016/j.fuel.2020.119142

[10] Noguchi, M., Tanaka, Y., Tanaka, T., & Takeuchi, Y. (1979). A study on gasoline engine combustion by observation of intermediate reactive products during combustion. *SAE Transactions*, 2816-2828. https://doi.org/10.4271/790840

[11] Najt, P. M., & Foster, D. E. (1983). Compression-ignited homogeneous charge combustion. *SAE Transactions*, 964-979. https://doi.org/10.4271/830264

[12] An, Y., Jaasim, M., Raman, V., Hernández Pérez, F. E., Sim, J., Chang, J., Im, H. G., & Johansson, B. (2018). Homogeneous charge compression ignition (HCCI) and partially premixed combustion (PPC) in compression ignition engine with low octane gasoline. *Energy, 158*, 181-191. doi: https://doi.org/10.1016/j.energy.2018.06.057

[13] Mohammed Elbanna, A., Xiaobei, C., Can, Y., Elkelawy, M., Alm-Eldin Bastawissi, H., & Panchal, H. (2022). Fuel reactivity controlled compression ignition engine and potential strategies to extend the engine operating range: A comprehensive review. *Energy Conversion and Management: X, 13*, 100133. doi: https://doi.org/10.1016/j.ecmx.2021.100133

[14] Turkcan, A., Altinkurt, M. D., Coskun, G., & Canakci, M. (2018). Numerical and experimental investigations of the effects of the second injection timing and alcohol-gasoline fuel blends on combustion and emissions of an HCCI-DI engine. *Fuel, 219*, 50-61. doi: https://doi.org/10.1016/j.fuel.2018.01.061

[15] Bobi, S., Kashif, M., & Laoonual, Y. (2022). Combustion and emission control strategies for partially-premixed charge compression ignition engines: A review. *Fuel, 310*, 122272. doi: https://doi.org/10.1016/j.fuel.2021.122272

[16] Taghavifar, H., Nemati, A., & Walther, J. H. (2019). Combustion and exergy analysis of multi-component diesel-DME-methanol blends in HCCI engine. *Energy, 187*, 115951. doi: https://doi.org/10.1016/j.energy.2019.115951

[17] Sakthivel, R., Ramesh, K., Mohamed Shameer, P., & Purnachandran, R. (2019). Experimental investigation on improvement of storage stability of bio-oil derived from intermediate pyrolysis of Calophyllum inophyllum seed cake. *Journal of the Energy Institute, 92*(3), 768-782. doi: https://doi.org/10.1016/j.joei.2018.02.006

[18] Agarwal, A. K., Singh, A. P., García, A., & Monsalve-Serrano, J. (2022). Challenges and Opportunities for Application of Reactivity-Controlled Compression Ignition Combustion in Commercially Viable Transport Engines. *Progress in Energy and Combustion Science, 93*, 101028. doi: https://doi.org/10.1016/j.pecs.2022.101028

[19] Charitha, V., Thirumalini, S., Prasad, M., & Srihari, S. (2019). Investigation on performance and emissions of RCCI dual fuel combustion on diesel - bio diesel in a light duty engine. *Renewable Energy, 134*, 1081-1088. doi: https://doi.org/10.1016/j.renene.2018.09.048

[20] Geo Varuvel, E. (2023). Effect of premixed hydrogen on the performance and emission of a diesel engine fuelled with prunus amygdalus dulcis oil. *Fuel, 341*, 127576. doi: https://doi.org/10.1016/j.fuel.2023.127576

[21] Vallinayagam, R., An, Y., S.Vedharaj, Sim, J., Chang, J., & Johansson, B. (2018). Naphtha vs. dieseline – The effect of fuel properties on combustion homogeneity in transition from CI combustion towards HCCI. *Fuel, 224*, 451-460. doi: https://doi.org/10.1016/j.fuel.2018.03.123

[22] Khandal, S. V., Banapurmath, N. R., & Gaitonde, V. N. (2019). Performance studies on homogeneous charge compression ignition (HCCI) engine powered with alternative fuels. *Renewable Energy, 132*, 683-693. doi: https://doi.org/10.1016/j.renene.2018.08.035

[23] Singh, A. P., Kumar, V., & Agarwal, A. K. (2020). Evaluation of comparative engine combustion, performance and emission characteristics of low temperature

combustion (PCCI and RCCI) modes. *Applied Energy, 278*, 115644. doi: https://doi.org/10.1016/j.apenergy.2020.115644

[24] Calam, A., Solmaz, H., Yılmaz, E., & İçingür, Y. (2019). Investigation of effect of compression ratio on combustion and exhaust emissions in A HCCI engine. *Energy, 168*, 1208-1216. doi: https://doi.org/10.1016/j.energy.2018.12.023

[25] Park, H., Shim, E., & Bae, C. (2019). Injection Strategy in Natural Gas–Diesel Dual-Fuel Premixed Charge Compression Ignition Combustion under Low Load Conditions. *Engineering, 5*(3), 548-557. doi: https://doi.org/10.1016/j.eng.2019.03.005

[26] Elkelawy, M., El Shenawy, E. A., Mohamed, S. A., Elarabi, M. M., & Bastawissi, H. A.-E. (2022). Impacts of using EGR and different DI-fuels on RCCI engine emissions, performance, and combustion characteristics. *Energy Conversion and Management: X, 15*, 100236. doi: https://doi.org/10.1016/j.ecmx.2022.100236

[27] Shim, E., Park, H., & Bae, C. (2020). Comparisons of advanced combustion technologies (HCCI, PCCI, and dual-fuel PCCI) on engine performance and emission characteristics in a heavy-duty diesel engine. *Fuel, 262*, 116436. doi: https://doi.org/10.1016/j.fuel.2019.116436

[28] Pan, S., Liu, X., Cai, K., Li, X., Han, W., & Li, B. (2020). Experimental study on combustion and emission characteristics of iso-butanol/diesel and gasoline/diesel RCCI in a heavy-duty engine under low loads. *Fuel, 261*, 116434. doi: https://doi.org/10.1016/j.fuel.2019.116434

[29] Xu, G., Jia, M., Li, Y., Chang, Y., & Wang, T. (2018). Potential of reactivity controlled compression ignition (RCCI) combustion coupled with variable valve timing (VVT) strategy for meeting Euro 6 emission regulations and high fuel efficiency in a heavy-duty diesel engine. *Energy Conversion and Management, 171*, 683-698. doi: https://doi.org/10.1016/j.enconman.2018.06.034

[30] Li, X. (2019). *An Experimental Investigation on Combustion Process and Emission of RCCI Combustion Mode*. Xihua University, Master's Theses.

[31] Salahi, M. M., Esfahanian, V., Gharehghani, A., & Mirsalim, M. (2017). Investigating the reactivity controlled compression ignition (RCCI) combustion strategy in a natural gas/diesel fueled engine with a pre-chamber. *Energy Conversion and Management, 132*, 40-53. doi: https://doi.org/10.1016/j.enconman.2016.11.019

[32] Li, J., Yang, W., & Zhou, D. (2017). Review on the management of RCCI engines. *Renewable and Sustainable Energy Reviews, 69*, 65-79. doi: https://doi.org/10.1016/j.rser.2016.11.159

[33] Sattarzadeh, M., Ebrahimi, M., & Jazayeri, S. A. (2022). A detail study of a RCCI engine performance fueled with diesel fuel and natural gas blended with syngas with different compositions. *International Journal of Hydrogen Energy, 47*(36), 16283-16296. doi: https://doi.org/10.1016/j.ijhydene.2022.03.088

[34] Xu, G., Jia, M., Li, Y., Chang, Y., Liu, H., & Wang, T. (2019). Evaluation of variable compression ratio (VCR) and variable valve timing (VVT) strategies in a heavy-duty diesel engine with reactivity controlled compression ignition (RCCI) combustion under a wide load range. *Fuel, 253*, 114-128. doi: https://doi.org/10.1016/j.fuel.2019.05.020

[35] Zheng, Z., Xia, M., Liu, H., Shang, R., Ma, G., & Yao, M. (2018). Experimental study on combustion and emissions of n-butanol/biodiesel under both blended

fuel mode and dual fuel RCCI mode. *Fuel, 226*, 240-251. doi: https://doi.org/10.1016/j.fuel.2018.03.151

CALL FOR PAPERS

Trends in Renewable Energy

ISSN Print: 2376-2136 ISSN online: 2376-2144

http://futureenergysp.com/index.php/tre/

Trends in Renewable Energy (TRE) is an open accessed, peer-reviewed semi-annual journal publishing reviews and research papers in the field of renewable energy technology and science. The aim of this journal is to provide a communication platform that is run exclusively by scientists. This journal publishes original papers including but not limited to the following fields:

- ✧ Renewable energy technologies
- ✧ Catalysis for energy generation, Green chemistry, Green energy
- ✧ Bioenergy: Biofuel, Biomass, Biorefinery, Bioprocessing, Feedstock utilization, Biological waste treatment,
- ✧ Energy issues: Energy conservation, Energy delivery, Energy resources, Energy storage, Energy transformation, Smart Grid
- ✧ Environmental issues: Environmental impacts, Pollution
- ✧ Bioproducts
- ✧ Policy, etc.

We publish the following article types: peer-reviewed reviews, mini-reviews, technical notes, short-form research papers, and original research papers.

The article processing charge (APC), also known as a publication fee, is fully waived for the Trends in Renewable Energy.

Call for Editorial Board Members

We are seeking scholars active in a field of renewable energy interested in serving as volunteer Editorial Board Members.

Qualifications

Ph.D. degree in related areas, or Master's degree with a minimum of 5 years of experience. All members must have a strong record of publications or other proofs to show activities in the energy related field.

If you are interested in serving on the editorial board, please email CV to editor@futureenergysp.com.